

Bachelor's Thesis

Bifractality of fractal scale-free networks フラクタル・スケールフリー・ネットワークの二重フラクタル性

Jun Yamamoto

February, 2022

Applied Physics and Engineering Course
Department of Applied Science and Technology
School of Engineering
Hokkaido University

Bachelor's Thesis
submitted to School of Engineering,
Hokkaido University
in partial fulfillment of the requirements for the degree of
Bachelor of Engineering.

Copyright©2022 by Jun Yamamoto. All rights reserved.

Contents

1	Introduction	4
2	Fundamentals of Complex Networks	7
2.1	Definitions and Representations of Networks	7
2.1.1	Types of Networks	7
2.1.2	Representations of Networks	8
2.2	Degrees, Degree Distributions, and Degree Correlations	9
2.2.1	Degrees	10
2.2.2	Degree Distributions	10
2.2.3	Degree Correlations	12
2.3	Network Distances, Average Shortest Path Distances, and Diameters	13
2.3.1	Distances	13
2.3.2	Average Shortest Path Distances and Diameters	14
2.4	Clustering Coefficients	14
2.4.1	Local Clustering Coefficients	14
2.4.2	Global Clustering Coefficients	15
3	Properties of Real-world Networks	16
3.1	Scale-free Property	16
3.2	Small-world Property	18
3.3	Fractal Property	20
4	Models of Fractal Scale-free Networks	23
4.1	(u, v) -flower	23
4.2	Song-Havlin-Makse Model	27
4.3	General Models of Hierarchical Fractal Scale-free Networks	30
4.3.1	Deterministic Model	30
4.3.2	Stochastic Model	36
4.4	Fractal Scale-free Random Graph	39
4.4.1	Erdős-Rényi Random Graph and Its Criticality	39
4.4.2	Generalized Random Graph	41

4.4.3 Fractal Scale-free Random Graph	42
5 Multifractality	44
5.1 Multifractality of Distributed Quantities	44
5.1.1 Mass Exponents	45
5.1.2 Lipschitz-Hölder Exponents	47
5.2 Multifractality of Complex Networks	48
5.2.1 Bifractality of (u, v) -flower	49
5.2.2 Mean-Field Arguments	52
5.3 Purpose of This Work	54
6 Bifractality of Fractal Scale-free Networks	56
6.1 Deterministic Model of Hierarchical Fractal Scale-free Networks	56
6.1.1 Renormalization Scheme	56
6.1.2 Mass Exponents	59
6.1.3 Distribution of Lipschitz-Hölder Exponents	60
6.2 Stochastic Model of Hierarchical Fractal Scale-free Networks	66
6.3 Fractal Scale-free Random Graphs	70
6.3.1 Proof of Bifractality	70
6.3.2 Numerical Confirmation of Bifractality	72
6.4 Discussion	74
7 Conclusion	77
A Acknowledgements	78
A Mathematical Supplement	79
A.1 Graph Theory	79
A.2 Calculus and Set Theory	80
A.3 Metric Topology	81
A.4 Measure Theory	83
B Algorithms for Fractal and Multifractal Analyses	86
B.1 Fractal Analysis	86
B.1.1 Greedy Coloring Algorithm	86
B.1.2 Random Sequential Burning Algorithm	87
B.1.3 Compact-Box-Burning Algorithm	87
B.1.4 Maximum-Excluded-Mass-Burning Algorithm	88
B.2 Multifractal Analysis	89
B.2.1 Sandbox Algorithm	89
C The derivation of Eq.(6.28)	91

D Multifractal Analysis of the Deterministic Model of Hierarchical Fractal Scale-free Networks	93
References	98

Chapter 1

Introduction

Many real-world systems, consisting of elements and interactions between them, can be represented as networks. In a network-representation, elements and interactions are expressed as nodes and edges of a network. For example, websites and hyperlinks in the World Wide Web, papers and their citations in scientific publications, and species and prey-predator relations in food webs are depicted as nodes and edges of networks. By ignoring the details of elements and interactions and extracting how elements are connected to one another, it becomes possible to compare diverse systems from mathematical and statistical viewpoints.

Over the last two decades, we have been able to gain much insight into networks by a vast amount of studies[1–7]. The accumulated study led to identifications of important quantities such as degrees, shortest path lengths, and clustering coefficients, which dictate the overall structures of networks. For instance, it has been reported that many real-world networks share the scale-free property[8], characterizing the heterogeneous distribution of degrees and the presence of the hubs, high-degree nodes. As another common property of real-world networks, the small-world property, a property which implies the exponential relation between the number of nodes and the average shortest path length of networks, has been identified[9]. In addition to these structural properties, we have also made progress in understanding the dynamics on networks, such as diffusion[10–12], spreads of infectious diseases[13–16], synchronization[17–22], and game theory[23–26].

In 2005, Song et al. proposed that some networks display the fractal property defined by a power-law relation between the number of nodes and the average shortest path length[27]. In their study, networks were renormalized by boxes (subgraphs) of a given linear size and the renormalized networks exhibited similar structures to the original one. The fractal property is mathematically contrary to the small-world nature shared by many networks, but a number

of small-world networks are fractal at least in shorter length scale. In fact, the fractal property has been shown in the World Wide Web, actor collaboration, cellular, and protein-protein interaction networks[27]. Extensive studies related to fractality of networks have provided insight into the growth process[28], the robustness against intentional and random failures[28, 29], and the spreading[30] of the fractal networks. In recent years, the fractal analysis of complex networks has been drawing more and more attention[31–34] due to its applicability, such as the data mining tasks[35], the vulnerability measures[36], and the recommender system[37].

The heterogeneity of networks due to the scale-free property motivated the study of the *multifractality* of fractal scale-free networks[38, 39]. Originally introduced by Mandelbrot to explain the inhomogeneous distribution of the energy dissipation in turbulent flows[40], the concept of multifractality and the multifractal analysis have been studied extensively to understand quantities distributed in a heterogeneous manner, such as the critical wavefunctions at the Anderson transition[41, 42] and the growth probability distributions in the diffusion-limited-aggregation[43, 44]. In 2011, Furuya and Yakubo showed local node densities of certain fractal scale-free networks (FSFNs) and the World Wide Web exhibit multifractality[38]. In particular, they have shown that FSFNs satisfying a certain condition are *bifractal*, a special case of multifractality. Since then, many have followed suit to study the multifractality of various networks[45–53]. However, no studies so far have looked into the bifractality of a more comprehensive class of FSFNs. In addition, the relation between the bifractality and the local structures of networks as well as its implications remain unanswered.

In this work, we investigate whether broader classes of FSFNs possess the bifractality. We utilize three models, namely a general deterministic model of hierarchical FSFNs, a general stochastic model of hierarchical FSFNs, and fractal scale-free random graphs. When combined, the three models cover a quite extensive class of FSFNs. By conducting the multifractal analysis of all three models, we propose a conjecture that any FSFN exhibits bifractality, characterized by two fractalities. Moreover, we further investigate local fractal dimensions of bifractal networks to identify the relation between bifractality and local structures. The obtained results indicate that the two fractalities of a bifractal network correspond to the local fractality near the hubs and that near the non-hubs.

The organization of this work is as follows. In Sec. 2, we introduce fundamental quantities of complex networks. We then present in Sec. 3, the three important properties commonly observed in real-world networks. Sec. 4 is devoted to discussing models of FSFNs, which we will use in our work. In Sec. 5, we focus on the definition and properties of multifractality as well as the prior

research, which serves as the basis of this work. Sec. 6 presents our main results on the bifractality of FSFNs. Finally, we conclude our work in Sec. 7.

Chapter 2

Fundamentals of Complex Networks

In this chapter, we briefly introduce the fundamental concepts of complex networks. We present the basic formalism of network-representation and some of the most significant measures and metrics to quantify the structures of networks, such as degrees, distances, and clustering coefficients which have been formalized by a vast amount of previous studies[1, 2, 4–6, 54, 55].

2.1 Definitions and Representations of Networks

A network (or a graph) $G = (V, E)$ is defined by a pair of two sets V and E , where V is a non-empty set of nodes (or vertices) and E is a set of ordered pairs of elements (i, j) for $i, j \in V$. We call elements of E as edges^{*1}. The numbers of nodes and edges in a given network $G = (V, E)$ are denoted by $N = |V|$ and $M = |E|$, where the notation $|A|$ represents the cardinality of a set A .

2.1.1 Types of Networks

If the edge from node i to node j is equivalent to the edge from node j to node i , the edge is undirected. The edge is directed otherwise. Networks whose edges are undirected are called undirected networks. In contrast, networks with directed edges are referred to as directed networks. See Fig. 2.1(a) and (b). For example, coauthorships in a scientific collaboration network are usually undirected, while citations in a scientific citation network are directed. Depending on systems and purposes, we may represent a given system as an undirected or directed network. Note that directed networks can, in principle, be represented as undirected networks by removing contextual information of the systems.

^{*1}In a network-science context, edges are often called links, but we use the term *edge* throughout this thesis.

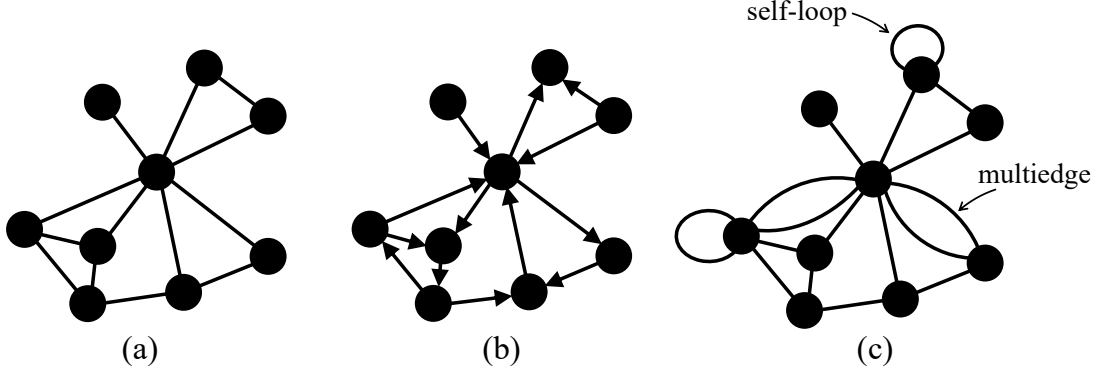


Figure 2.1: Examples of (a) a simple undirected network, (b) a simple directed network, and (c) a non-simple undirected network.

Another classification of networks is possible based on the presence of weight, a numerical attribute associated with an edge. Typically, weights on edges represent the intensity or measures of the interactions. For instance, the edges in a scientific collaboration network can be weighted with the number of collaborations between a pair of authors. The edges in a road network can be weighted by the amount of traffic.

When systems consist of two distinct types of elements and interactions exist exclusively between a pair of nodes of different types, the systems may be represented by bipartite networks. A typical example of such a system is a relation between an actor and a movie. In the corresponding bipartite network, an edge between an actor and a movie is present if the actor acts in that movie.

Throughout this thesis, we only consider undirected unweighted networks for simplicity. Furthermore, we assume that networks are simple, that is, there exist no self-loops (an edge from node i to itself) and no multiedges (more than one edges between the same node pair). Networks with multiedges are called multigraphs. An example of multigraph is shown in Fig. 2.1(c).

2.1.2 Representations of Networks

Any undirected unweighted network $G = (V, E)$ with $N = |V|$ nodes can be represented by an adjacency matrix A_{ij} of the size $N \times N$, where

$$A_{ij} = \begin{cases} 1 & \text{if } (i, j) \in E \\ 0 & \text{otherwise.} \end{cases} \quad (2.1)$$

The adjacency matrix of an undirected network is always symmetric. Hence, the number of edges M of a given network can be written in terms of its adjacency

matrix as follows;

$$M = \sum_{i < j} A_{ij} = \frac{1}{2} \sum_{i=1}^N \sum_{j=1}^N A_{ij}. \quad (2.2)$$

The representation by an adjacency matrix contains complete structural information of the network, and thus is advantageous in analytical calculation of various quantities and properties. On the contrary, an adjacency matrix is inefficient as its elements include a large number of zeros, especially when the network is sparse.

Another way to represent an undirected, unweighted network is the representation by an edge list e , in the form

$$\mathbf{e} = \begin{pmatrix} (i_1, j_1) \\ (i_2, j_2) \\ \vdots \\ (i_M, j_M) \end{pmatrix} \quad (2.3)$$

where $e_k = (i_k, j_k) \in E$. Notice that we can rewrite the edge list in one-dimensional vector of length $2M$ instead of two-dimensional matrix of size $(M, 2)$. The representation by an edge list is optimal when the network is sparse, i.e. $M \ll N^2$, because edge lists require much less memory space than adjacency matrices.

When representing a network in computers, we may also use the adjacency list F of length N

$$F = \{F_1, F_2, \dots, F_N\} \quad (2.4)$$

where

$$F_i = \{j \in V | (i, j) \in E\}. \quad (2.5)$$

This representation is optimal when we are interested in walks^{*2} of a given network.

2.2 Degrees, Degree Distributions, and Degree Correlations

One of the most important measures of networks is the degree to which a given node is connected to other nodes. This section introduces the definition and properties of such a measure.

^{*2}Refer to Definition A.1.3 in the appendix A.1.

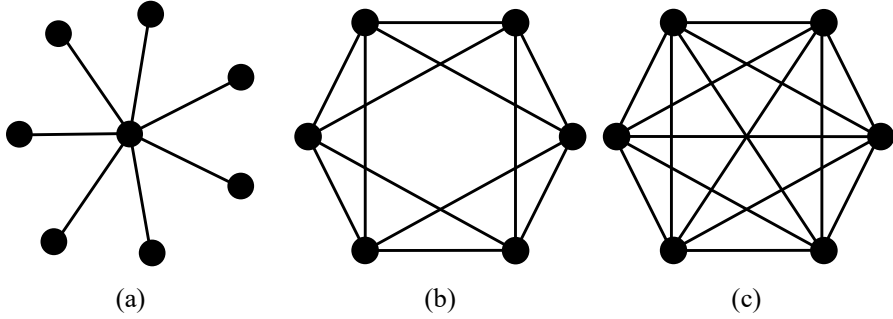


Figure 2.2: (a) The degree k_c of the central node is $k_c = 7$ while all the other nodes have the degree $k_i = 1$ ($i = 2, 3, \dots, 8$). Such a network is called a star graph. (b) and (c) are a 4-regular and complete network with 6 nodes, respectively.

2.2.1 Degrees

The degree k_i of node i is the number of edges from node i . For example, the degree of the center node in Fig. 2.2(a) is seven while those of the other nodes are one. Using the adjacency matrix, the degree of node i can be expressed as

$$k_i = \sum_{j=1}^N A_{ij}. \quad (2.6)$$

By definition of simple networks, the maximal degree of a network with N nodes is at most $N - 1$. The sum of degrees k_i over all the nodes add up to twice the number of edges, i.e.

$$\sum_{i=1}^N k_i = \sum_{i=1}^N \sum_{j=1}^N A_{ij} = 2M. \quad (2.7)$$

This is trivial because every edge in an undirected network has two ends. From the above result, the mean degree of a network \mathcal{G} is given by

$$\langle k \rangle = \frac{1}{N} \sum_{i=1}^N k_i = \frac{2M}{N}. \quad (2.8)$$

Occasionally, all the nodes in a network have the same degree k . Such a network is called a k -regular graph. Specifically, $(N - 1)$ -regular networks are complete networks, in which all nodes are adjacent to each other. See Fig. 2.2(b) and (c).

2.2.2 Degree Distributions

The degree distribution $P(k)$ of a network $\mathcal{G} = (V, E)$ is the probability that a randomly selected node $i \in V$ has degree k , or the proportion of the nodes with

degree k . By denoting the number of nodes with degree k by $N(k)$, the degree distribution is obtained as

$$P(k) = \frac{N(k)}{N} = \frac{1}{N} \sum_{i=1}^N \delta_{kk_i}, \quad (2.9)$$

where δ_{ij} is Kronecker delta, i.e. $\delta_{ij} = 1$ if $i = j$ and $\delta_{ij} = 0$ otherwise. Since the degree distribution is a probability, the sum of the degree distribution over k adds up to 1 by the normalization condition

$$\sum_{k=0}^{N-1} P(k) = 1. \quad (2.10)$$

The average degree of a network can alternatively expressed in terms of degree distribution,

$$\langle k \rangle = \sum_{k=0}^{N-1} k P(k). \quad (2.11)$$

By substituting Eq. (2.9) into Eq. (2.11), we have

$$\begin{aligned} \langle k \rangle &= \sum_{k=0}^{N-1} k \left(\frac{1}{N} \sum_{i=1}^N \delta_{kk_i} \right) \\ &= \frac{1}{N} \sum_{i=1}^N \left(\sum_{k=0}^{N-1} k \delta_{kk_i} \right) \\ &= \frac{1}{N} \sum_{i=1}^N k_i. \end{aligned} \quad (2.12)$$

Thus we can confirm Eqs. (2.8) and (2.11) are equivalent.

In addition to the average degree, the variance of degree σ_k^2 is defined as

$$\sigma_k^2 = \sum_{k=0}^{N-1} (k - \langle k \rangle)^2 P(k). \quad (2.13)$$

By definition of variances, σ_k^2 can be expressed in terms of the average degree $\langle k \rangle$ and the second-moment of the degree $\langle k^2 \rangle$ as follows:

$$\sigma_k^2 = \langle k^2 \rangle - \langle k \rangle^2, \quad (2.14)$$

where

$$\langle k^2 \rangle = \sum_{k=0}^{N-1} k^2 P(k). \quad (2.15)$$

2.2.3 Degree Correlations

In addition to the degree of a given node, the degrees of its neighbors play a significant role in networks. There often exist biases in connectivity of nodes based on their degrees. Such a bias of node connectivity is called degree correlation. When high degree nodes in a network tend to connect with each other, we call that network assortative. In contrast, a network is disassortative when high degree nodes are more likely to connect with low degree nodes. If such a bias is absent in a network, the network is said to be uncorrelated.

To determine the presence of degree correlations, we consider the conditional probability $P(k'|k)$ that an adjacent node to a k -degree node is a k' -degree node. Note that $P(k'|k)$ must be normalized for any k , i.e.

$$\sum_{k'=0}^{N-1} P(k'|k) = 1. \quad (2.16)$$

The conditional probability $P(k'|k)$ must also satisfy the so-called detailed balance condition,

$$kP(k'|k)P(k) = k'P(k|k')P(k'), \quad (2.17)$$

which expresses that the number of k -degree nodes which are adjacent to k' -degree nodes must be equal to the number of k' -degree nodes which are adjacent to k -degree nodes.

When a network is uncorrelated, the conditional probability $P(k'|k)$ is independent of k . Hence, by taking the sum of the left-hand side of Eq. (2.17) with respect to k , we get

$$\sum_k P(k'|k)P(k) = P(k'|k) \sum_k kP(k) = \langle k \rangle P(k'|k). \quad (2.18)$$

As the sum of the right-hand side of Eq. (2.17) with respect to k simplifies to $k'P(k')$ because of the normalization condition (2.16), the sum of both sides of Eq. (2.17) over k ends up in the form

$$P(k'|k) = \frac{k'P(k')}{\langle k \rangle}. \quad (2.19)$$

In contrast, if $P(k'|k)$ depends on k , the network is correlated or more specifically nearest-neighbor correlated. A simple way to observe nearest-neighbor degree correlations is to draw a scatter plot of the degrees k and k' of the terminal nodes of all the edges in a network. If there is a positive correlation between k and k' , the network is assortative. If there is a negative correlation, it is disassortative.

Average nearest-neighbor degrees $k_{\text{nn}}(k)$, the mean degrees of the neighboring nodes of a k -degree node, is defined as

$$k_{\text{nn}}(k) = \sum_{k'} k' P(k'|k). \quad (2.20)$$

In the case of uncorrelated networks, we attain

$$k_{\text{nn}}(k) = \sum_{k'} k' \cdot \frac{k' P(k')}{\langle k \rangle} = \frac{\langle k^2 \rangle}{\langle k \rangle}, \quad (2.21)$$

which is also independent of k . In contrast, the average nearest-neighbor degree $k_{\text{nn}}(k)$ depends on k for assortative and disassortative networks. $k_{\text{nn}}(k)$ is an increasing function of k in assortative networks, while it is a decreasing function of k in disassortative networks.

2.3 Network Distances, Average Shortest Path Distances, and Diameters

In general, Euclidean distances between pairs of nodes are not defined in networks³ Nonetheless, we often want to consider how "close" or how "far" a given pair of nodes is. This section introduces distances and diameters in networks.

2.3.1 Distances

To consider the distance between a pair of nodes (i, j) , we first identify the paths connecting the pair. A path \mathcal{P} between (i, j) in a network $G = (V, E)$ is an alternating sequence of nodes and edges such that no nodes are visited more than once.

$$\mathcal{P}(i, j) = (i, e_{ii'}, i', e_{i'i''}, \dots, j', e_{j'j}, j) \quad (2.22)$$

where $i, i', j', j \in V$ and $e_{ij} = (i, j) \in E$. The length of a path $\mathcal{P}(i, j)$ is the number of edges in the sequence. Node i is reachable from node j if there exists at least one path between (i, j) .

There can exist multiple paths connecting two nodes i and j . Hence, the distance l_{ij} between the pair (i, j) is defined by the length of the shortest path between (i, j) . We define the distance from node i to itself as $l_{ii} = 0$ for $\forall i \in V$. In case node i is not reachable from j , we set $l_{ij} = \infty$. As mentioned earlier, we

³Obviously, with exception of geographic networks in which every node is embedded in a Euclidean space.

will only consider unweighted undirected graphs in this work. Therefore, the distance defined above always satisfies the conditions of a metric, namely $l_{ij} \geq 0$ for $i, j \in V$ (non-negativity), $l_{ij} = 0 \Leftrightarrow i = j$ (identity of indiscernibles), $l_{ij} = l_{ji}$ (symmetry), and $l_{ij} \leq l_{ik} + l_{kj}$ (triangle inequality). Refer [56] for proof.

2.3.2 Average Shortest Path Distances and Diameters

The network distance defined above is a local measure. Instead, as we will see later, we want to extract global measures of a given connected network^{*4}. Two important global measures are the average shortest path distance and diameter.

The average shortest path distance of a network is defined as

$$\langle l \rangle = \frac{1}{N(N-1)} \sum_{i=1}^N \sum_{j \neq i} l_{ij}. \quad (2.23)$$

The diameter L of a network is the maximal distance between any pair of nodes within a network. Therefore, the diameter is given by

$$L = \max_{i \neq j} l_{ij}. \quad (2.24)$$

2.4 Clustering Coefficients

2.4.1 Local Clustering Coefficients

Local clustering coefficients quantify the degree to which neighbors of a node are connected to each other. A local clustering coefficient in a friendship network, for instance, is the quantity which represents how many friends of a person are friends to each other. Local clustering coefficient is a significant characteristic quantity in networks because it evaluates the proportion of closed paths of length 2. Mathematically, the local clustering coefficient for a given node i is defined by

$$C_i = \begin{cases} \frac{2m_i}{k_i(k_i - 1)} & \text{if } k_i > 1 \\ 0 & \text{if } k_i = 0, 1 \end{cases} \quad (2.25)$$

where m_i is the number of edges between the neighbors of node i . Note that $\frac{k_i(k_i - 1)}{2}$ is the maximal number of triangles which contain node i as one of the

^{*4}We can consider global measures only for connected networks, because l_{ij} diverges when nodes i and j are disconnected.

three vertices. Local clustering coefficients thus take the values between 0 and 1, i.e., $0 \leq C_i \leq 1$. C_i of a tree graph is zero for any node i and $C_i = 1$ ($\forall i \in V$) for complete graphs. The numerator m_i can be rewritten in terms of the adjacency matrix,

$$m_i = \sum_{j < k} a_{ij} a_{jk} a_{ki}. \quad (2.26)$$

Using the relations (2.26) and (2.6), Eq. (2.25) is expressed as

$$C_i = \frac{\sum_{j,k} a_{ij} a_{jk} a_{ki}}{\sum_{j,k} a_{ij} a_{ki} - \sum_j a_{ij}}. \quad (2.27)$$

2.4.2 Global Clustering Coefficients

Local clustering coefficients introduced in the previous section can be averaged over an entire network to characterize the network globally. The average clustering coefficient, or the global clustering coefficient, is then defined by

$$C = \frac{1}{N} \sum_{i \in V} C_i. \quad (2.28)$$

Trivially, the average clustering coefficients satisfy $0 \leq C \leq 1$ since $0 \leq C_i \leq 1$ for $\forall i \in V$.

Alternatively, transitivity T may be used as global clustering coefficient of a given network. Transitivity of the network is defined as follows:

$$T = \frac{3\Delta}{(\# \text{ of distinct paths of length 2})}. \quad (2.29)$$

where Δ is the number of triangles in a given network. Here, the number of distinct paths of length 2 means the number of sets of three nodes (u, v, w) such that there exist edges in node pairs (u, v) and (v, w) .

Chapter 3

Properties of Real-world Networks

Network science, as mentioned in Ch. 1, has been established on many empirical studies on various real-world networks. In this chapter, we introduce the three significant properties, which are commonly observed in real-world networks, and their implications[1, 2, 4–6, 54, 55]. These properties, namely the scale-free, small-world, and fractal properties, play a central role in determining the statistical properties of and dynamics on networks.

3.1 Scale-free Property

Various real-world networks possess degree distributions with power-law tails for $k \gg 1$, i.e.

$$P(k) \propto k^{-\gamma}. \quad (3.1)$$

The property that $p(k)$ behaves according to Eq. (3.1) is called the scale-free property, and a network with a power-law tail degree distribution is said to be a scale-free network.

In 1999, Barabási and Albert reported the scale-free property of the World-Wide-Web, actor collaboration network, and power-grid network[8]. See Fig. 3.1. Since then many real-world networks are shown to be scale-free. It has been found that the scale-free exponents γ of most real-world networks are generally in the range $2 < \gamma \leq 3$.

The term "scale-free" originates in the fact that there exists no characteristic scale in a power-law function. Due to the fat-tail of degree distributions, the degrees of nodes in scale-free networks are heterogeneous. While the majority of nodes have low degrees, a minority of nodes have extremely high degrees. Such a high-degree node is called a hub.

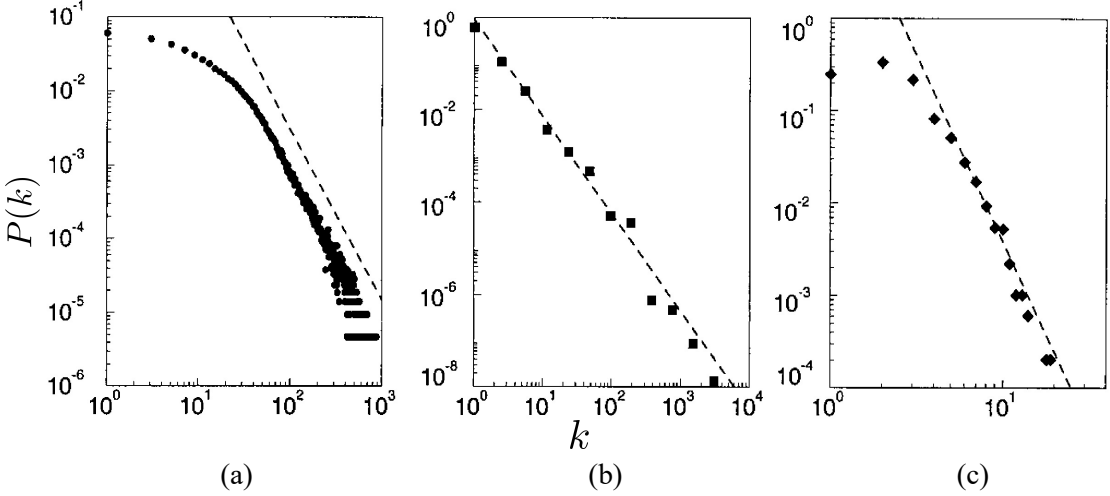


Figure 3.1: Degree Distributions of (a) actor collaboration network with $N = 212, 250$, (b) the World-Wide-Web with $N = 325, 729$, and (c) power-grid network with $N = 4, 941$. The dashed lines show the slopes of (a) $\gamma = 2.3$, (b) $\gamma = 2.1$, and (c) $\gamma = 4$. The figure is taken from [8] and slightly modified for presentation purposes.

To better understand the scale-free property, let us consider a network whose degree distribution is asymptotically given by

$$P(k) = Ck^{-\gamma} \quad \text{for } k \gg 1, \quad (3.2)$$

where C is the normalization constant and $\gamma > 1$. The condition on γ ensures that the degree distribution is normalized

$$\sum_k P(k) = 1. \quad (3.3)$$

The mean degree $\langle k \rangle$ and second moment $\langle k^2 \rangle$ are expressed as

$$\langle k \rangle = \sum_k kP(k) = \sum_k Ck^{1-\gamma} \quad (3.4)$$

and

$$\langle k^2 \rangle = \sum_k k^2 P(k) = \sum_k Ck^{2-\gamma}. \quad (3.5)$$

From Eq. (3.4) and (3.5), we observe three different regimes based on the value of γ .

1. For $1 < \gamma \leq 2$, both $\langle k \rangle$ and $\langle k^2 \rangle$ diverge in the limit of $N \rightarrow \infty$.
2. For $2 < \gamma \leq 3$, $\langle k \rangle$ is finite and $\langle k^2 \rangle$ diverges in the limit of $N \rightarrow \infty$.
3. For $\gamma > 3$, both $\langle k \rangle$ and $\langle k^2 \rangle$ are finite in the limit of $N \rightarrow \infty$.

Since most real-world networks take the scale-free exponent in the range $2 < \gamma \leq 3$, they have finite mean degree but infinite second moment. That is, though real-world networks have finite mean degrees which do not depend on samples or network sizes, the values of mean degrees are not characteristic, which is, as stated above, exactly what "scale-free" means. The heterogeneity of degrees can be also confirmed by diverging standard deviation $\sigma(k) = \sqrt{\langle k^2 \rangle - \langle k \rangle^2} \rightarrow \infty$ for $N \rightarrow \infty$. This property is a consequence of the hubs whose degrees are order of magnitude much larger than the mean degree. The presence of the hubs plays a vital role in various properties of and dynamics on scale-free networks.

Speaking of the hubs, the highest degrees k_{\max} of scale-free networks with $\gamma > 2$ are known to scale as

$$k_{\max} \sim N^{\frac{1}{\gamma-1}}. \quad (3.6)$$

Note that in the limit $\gamma \rightarrow 2$, $k_{\max} \rightarrow N$. In fact, the heterogeneity of degrees increases with decreasing scale-free exponents.

Beware that not all the real-world networks display scale-free property. Geographical networks such as railroad networks and power-grid networks ^{*1} do not exhibit scale-free property.

3.2 Small-world Property

A network is said to be small-world if it has a large clustering coefficient and short average shortest path distance relative to the number of nodes. Clustering coefficients are considered large if the clustering coefficient takes a finite value which does not depend on the network size, i.e.,

$$C \propto N^0. \quad (3.7)$$

In the case of real-world networks with fixed network sizes, clustering coefficients are considered large if the clustering coefficients of the networks are

^{*1}Attentive readers may have noticed that Barabási and Albert claimed that a power-grid network is scale-free in 1999. The later works, however, showed that the degree distribution of the power-grid network is actually exponential.

greater than those of the random graphs^{*2} with the same numbers of nodes and edges.

The average shortest path distance of a network is considered short relative to the number of nodes if it is of the equal (or lower) order than the logarithm of the number of nodes.

$$\langle l \rangle \propto \log N \quad (3.8)$$

Alternatively, if the diameter of a network satisfies

$$L \propto \log N \quad (3.9)$$

in addition to Eq. (3.7), then the network is small-world. Many real-world networks are known to be small-world[1].

The small-world property of some networks, though in a more vague manner, has been known as far back as the 1940s, as it was contained in a the preprint by de Sola Pool and Kochen^{*3} [57]. Their work inspired the widely known work by Milgram in 1967[58], which reported that any two individuals in the world are on average separated by the ‘six degrees of separation,’ i.e. the average shortest path distance in a social network is six. Though subsequent studies have suggested the different values of average shortest path distances, they nonetheless confirmed that social networks are typically small-world.

To understand the emergence of the small-world property, let us first consider a d -dimensional regular lattice of N nodes. In the lattice, the average shortest path distance behaves as $\langle l \rangle \propto N^{1/d}$ and takes a much larger value of $\langle l \rangle$ than that of a small-world network when $N \gg 1$. Motivated by the presence of shortcut edges, which connect distant nodes, in many of the real-world networks with small-world property, let us add shortcut edges in a regular lattice to transform it to be small-world.^{*4} By adding $N \log N$ shortcut edges at random, the average shortest path of the originally regular lattice becomes $\langle l \rangle \propto \log N$ [6]. At the same time, the clustering coefficient behaves as $C \sim 1/(\log N)^2$ with introduction of $N \log N$ shortcut edges, which is sufficiently larger than that corresponding value ($C \sim N^{-1}$) in random graphs, which we will explain later in Sec. 4.4.1. In short, the small-world property arises when a small number of shortcut edges are added to a regular lattice.

^{*2}A random graph is an ensemble of graphs with a fixed number of nodes N whose edges are randomly placed between any pair of nodes with a given probability p .

^{*3}Their work was not formally published until 1978.

^{*4}This is not limited to regular lattices but rather applicable to any network whose average shortest path follows power-law, $\langle l \rangle \propto N^\beta$ with $\beta > 0$.

3.3 Fractal Property

Fractal property is, in general, the property of a system in which characteristic length scale is absent[59]. In complex networks, fractal property is defined in terms of the average shortest path distance $\langle l \rangle$ or the network diameter L instead of Euclidean distance for objects embedded in Euclidean spaces. Hence, the fractal property of networks is expressed as

$$N \propto \langle l \rangle^{D_f}, \quad N \propto L^{D_f}. \quad (3.10)$$

The exponent D_f is called the fractal dimension of a network.

Notice from Eq. (3.8) that the relation between the average shortest path and the number of nodes in a small-world network is given by

$$N \propto e^{\langle l \rangle / \tilde{l}}, \quad (3.11)$$

and there clearly exists a characteristic length scale \tilde{l} . This intuitively suggests that the small-world property and the fractal property cannot coexist in the same network. As many real-world networks are small-world, it was initially believed that the fractal property does not emerge in complex networks. Song et al. reported in 2005 that some of the extensively studied networks such as the World-Wide-Web (WWW) and the protein-protein interaction network (PIN) satisfy the fractality condition in a box-covering sense[27], i.e.

$$N_B \propto l_B^{-D_f}. \quad (3.12)$$

Here, N_B is the number of boxes (subgraphs) required to cover the entire network and l_B is the box size (the diameter of each subgraph). The fractality in a box-covering sense is based on the covering of a network by the minimal set of boxes (subgraphs). As the problem of finding the true minimal covering of a given network is NP-hard[60], we numerically approximate the minimal covering in practice. So far, various algorithms to compute a box-covering of a network have been proposed[34, 35, 60–63]. Real-world networks which have been identified as fractal by the box-covering method include the WWW, PINs and metabolic networks of *H. sapiens* and *E. coli*, as well as the actor collaboration network[27, 64]. In fact, Fig. 3.2 shows that the World Wide Web is fractal in a box-covering sense, as the log-log plot of the number of boxes and the box size is linear. Most of these networks are small-world in the length scale of $l \sim \langle l \rangle$ or L but fractal in the length scale of $l \ll \langle l \rangle$ or L .

In addition to the definitions of the fractal property in the forms of Eq. (3.10) and (3.12), the fractality of networks can alternatively be defined in a cluster-growing sense as

$$\langle M_c(l_c) \rangle \propto l_c^{D_f}, \quad (3.13)$$

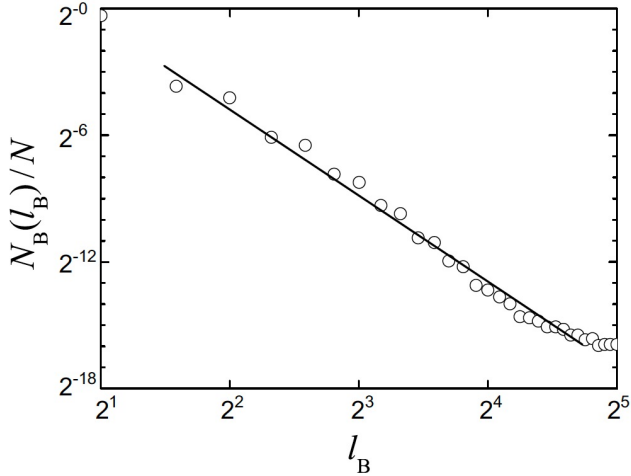


Figure 3.2: The log-log plot of the normalized number of boxes and the box size for the World-Wide-Web with $N = 325,729$. The figure is taken from [6].

where the $\langle M_c(l_c) \rangle$ is the mean number of nodes ("mass") within distance l_c from a seed, averaged over a set of randomly selected seed nodes.

It is important to note that the self-similarity and the fractal property are distinguished in complex networks. While the fractality of a network is expressed by the relations in Eq. (3.10) - (3.13), the self-similarity is defined as a property of a network which remains invariant under the following renormalization scheme:

- (1) Find an optimal box-covering of a network by boxes of size l_B .
- (2) For the optimal covering, apply a renormalization by replacing each box by a supernode. In the renormalized network, supernodes i and j are connected by a superedge if and only if there exists at least one edge that connects one of the nodes belonging to supernode i and one of the nodes belonging to supernode j .
- (3) Iterate step (1) and (2) until there remains a single supernode.

Fig. 3.3(a) shows an example of the renormalization steps with different box sizes and Fig. 3.3(b) visualizes the renormalization of the World Wide Web. Though we distinguish the concepts of fractality and self-similarity, fractal networks generally exhibit self-similarity. At the same time, as the fractal property and the self-similarity are distinct properties, the self-similarity is observed in some small-world networks, such as the Internet[64].

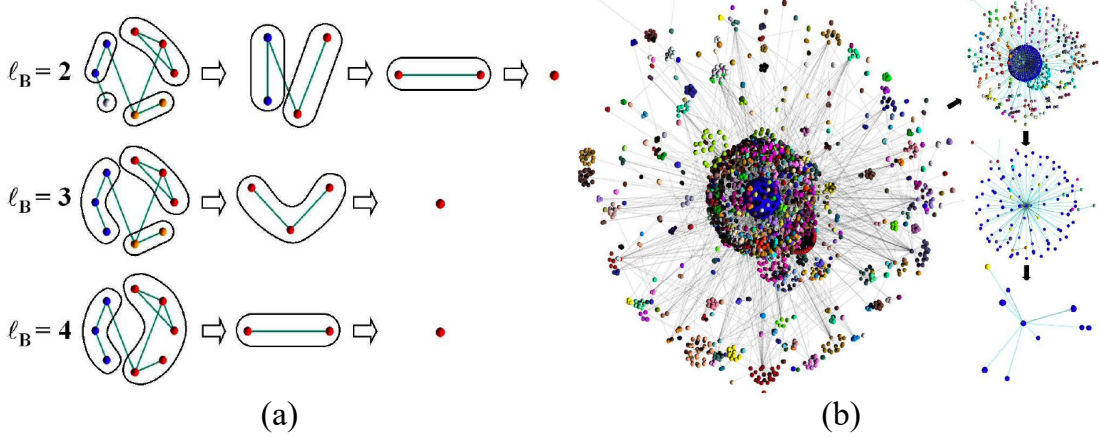


Figure 3.3: The renormalization procedure of networks. (a) Examples of the renormalization scheme in a network of eight nodes by boxes of three different sizes $l_B = 2$, $l_B = 3$, and $l_B = 4$. (b) Three renormalization steps of the World-Wide-Web by a fixed box size $l_B = 3$. The figure is taken from [27].

Interestingly, the superdegree k' of each supernode in the renormalized network scales with the largest degree k in the box as

$$k' = s(l_B)k. \quad (3.14)$$

The scaling factor s was also empirically found to scale with l_B ,

$$s(l_B) \sim l_B^{-D_k}. \quad (3.15)$$

The exponent D_k is called the degree exponent. The exponents γ , D_f , and D_k are not independent but are related to each other with the scaling relation

$$\gamma = 1 + \frac{D_f}{D_k}. \quad (3.16)$$

Chapter 4

Models of Fractal Scale-free Networks

In this chapter, we introduce some of the models of fractal scale-free networks (FSFNs), namely (u, v) -flower model[65], Song-Havlin-Makse model[28], general models of hierarchical FSFNs[66–68], and fractal scale-free random graphs[3, 69, 70]. These synthetic models enable us to study FSFNs systematically. We indeed utilize some of the these models to study the bifractality of FSFNs.

4.1 (u, v) -flower

(u, v) -flower is one of the most extensively studied models of FSFNs. Originally proposed by Rosenfeld, et al. in 2007, it is a recursive deterministic fractal scale-free networks[65]. The two parameters u and v are positive integers. Without the loss of generality, we assume $1 \leq u \leq v$. Networks are constructed as follows:

- (1) Initiate a network as a cycle graph of $w = u + v$ edges.
- (2) Replace every edge of the $(t - 1)$ -th generation network by a cycle graph of $w = u + v$ edges.
- (3) Repeat step (2) until a number of nodes reaches the target value.

Figure 4.1 shows two example networks constructed by the above procedures.

Denoting the number of edges in the t -th generation network by M_t , the increase in the number of edges from $t - 1$ to t -th generation is expressed as

$$M_t = wM_{t-1}. \quad (4.1)$$

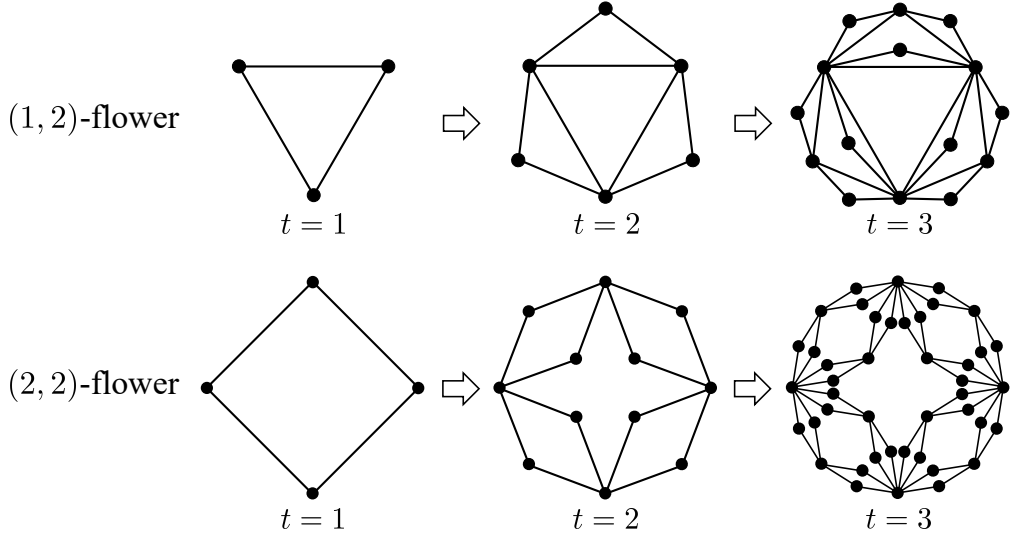


Figure 4.1: The 1st, 2nd, and 3rd generation $(1, 2)$ -flower and $(2, 2)$ -flower.

The number of edges in the 1st generation network is $M_1 = w$. By solving the recurrence relation, we obtain

$$M_t = w^t. \quad (4.2)$$

Similarly, the number N_t of nodes in the t -th generation network increases by the factor of w from the $(t-1)$ -th generation network but we must subtract the number of double-counted nodes, which is w , i.e.

$$N_t = wN_{t-1} - w. \quad (4.3)$$

Under the initial condition $N_1 = w$, Eq. (4.3) can be solved as

$$N_t = \left(\frac{w-2}{w-1} \right) w^t + \frac{w}{w-1}. \quad (4.4)$$

In the (u, v) -flower, the possible values of degrees are

$$k_n = 2^n, \quad \text{for } 1 \leq n \leq t, \quad (4.5)$$

because degrees of the nodes are multiplied by two at every generation. The number of k_n -degree nodes in the t -th generation network must be equal to the number of k_{n-1} -degree nodes in the $(t-1)$ -th generation network. The number of $k_1 = 2$ -degree nodes is equivalent to the number of newly added nodes in the final operation from $t-1$ to t -th generation. That is,

$$N_t(k_n) = \begin{cases} w^{n-1}(w-2) & \text{for } k_n = 2, \\ N_{t-1}(k_{n-1}) & \text{for } k_n > 2. \end{cases} \quad (4.6)$$

By solving the recurrence relation (4.6), we obtain

$$N_t(k_n) = \begin{cases} (w-2)w^{t-n} & \text{for } k_n < 2^t, \\ w & \text{for } k_n = 2^t. \end{cases} \quad (4.7)$$

In a sufficiently large network with $t > n \gg 1$, the degree sequence may be considered as continuous. Thus, the degree distribution $P(k)$ approximately satisfies the relation

$$|P(k)dk| = |N_t(k_n)dk_n| \quad (4.8)$$

for $k \gg 1$. From Eqs. (4.5) and (4.7), the degree distribution for $k \gg 1$ is given by

$$P(k) = \frac{(w-2)w^t}{\log 2} k^{-(\log w / \log 2 + 1)}. \quad (4.9)$$

Hence, the (u, v) -flower model exhibits the scale-free property and its scale-free exponent in terms of u and v is

$$\gamma = \frac{\log(u+v)}{\log 2} + 1. \quad (4.10)$$

Next, let us consider the diameter L_t of the t -th generation (u, v) -flower. The diameter in the case of $u = 1$ and odd v is given by

$$L_t = (v-1)t + \frac{3-v}{2}. \quad (4.11)$$

In the case of $u > 1$, the recurrence relation of the diameter is

$$L_t = uL_{t-1} + v - u. \quad (4.12)$$

Specifically, when $u + v$ is even, the diameter of the first generation is $L_1 = (u+v)/2$ and the diameter is determined as

$$L_t = \left(\frac{u+v}{2} + \frac{v-u}{u-1} \right) u^{t-1} - \frac{v-u}{u-1}. \quad (4.13)$$

Equation (4.12) cannot be solved analytically when $u + v$ is odd. It is however known that

$$L_t \sim u^t \quad (4.14)$$

for $t \gg 1$. From Eqs. (4.4) and (4.11)-(4.14), the relation between the number of nodes and the diameter in the (u, v) -flower is as follows:

$$L_t \sim \begin{cases} \frac{v-1}{\log(v+1)} \log N_t & \text{if } u = 1, \\ N_t^{-\log(u+v)/\log u} & \text{if } u \geq 2. \end{cases} \quad (4.15)$$

The above result indicates that the (u, v) -flower is small-world when $u = 1$ and fractal when $u \geq 2$. The model exhibits qualitatively different properties depending on the value of u . This difference arises from the presence of short-cut edges between hubs in the case of $u = 1$. Nevertheless, the fractal dimension of (u, v) -flower with even $u + v$ is

$$D_f^{cg} = \frac{\log(u+v)}{\log u}. \quad (4.16)$$

The above argument presents the fractal dimension in the cluster-growing sense. To determine the fractality in the box-covering sense, let us consider the box-covering scheme of (u, v) -flower. The most simple way to box-cover the t -th generation (u, v) -flower \mathcal{G}_t is probably to cover each $\mathcal{G}_{t'}$ ($1 \leq t' \leq t$) in \mathcal{G}_t by a box. We call this covering scheme the scheme I. The scheme I is unfortunately not the minimal box-covering of (u, v) -flower. Again, the proper fractal analysis in a box-covering method requires the minimal box-covering of a given network^{*1}. In the case of (u, v) -flower, the true minimal covering is unknown but the covering in the descending order of the degree sequence, as shown in Fig. 4.2(b), enables the box-covering with less boxes than the scheme I. Let us call this covering scheme the scheme II.

We now consider the box-covering of the t -th generation (u, v) -flower by the scheme II. Let the box sizes l_B be the diameter of t' -th generation network ($1 \leq t' \leq t$). Then the number $N_{b(s)}(L_{t'})$ of boxes whose centers are s -th largest hubs is equal to the number of the s -th largest hubs,

$$\begin{aligned} N_{b(s)}(L_{t'}) &= N_s - N_{s-1} \\ &= (w-2)w^{s-1}(1-\delta_{1s}) + w\delta_{1s}. \end{aligned} \quad (4.17)$$

where $1 \leq s \leq t - t'$ and $w = u + v$. The total number of boxes needed to cover the t -th generation (u, v) -flower is attained by taking the sum of $N_{b(s)}(L_{t'})$ from

^{*1}The box-covering scheme does not have to be minimal as long as it is close to minimal as to give the same scaling in fractal analysis.

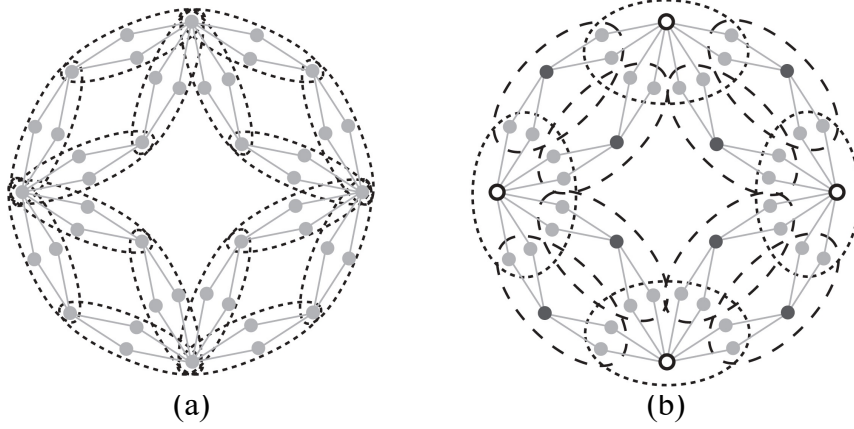


Figure 4.2: Two box-covering schemes of the 3rd generation $(2, 2)$ -flower. (a) Non-optimal covering scheme with 16 boxes. (b) Optimal covering scheme with 12 boxes. The figure is taken from [6].

$s = 1$ to $s = t - t'$, i.e.

$$\begin{aligned} N_B(L_{t'}) &= \sum_{s=1}^{t-t'} N_{b(s)}(L_{t'}) \\ &= \left(\frac{w-2}{w-1}\right) w^{t-t'} - \frac{w}{w-1}. \end{aligned} \quad (4.18)$$

In a sufficiently large generation $t \gg 1$,

$$N_B(L_{t'}) \propto w^{t-t'}. \quad (4.19)$$

By expressing t' in terms of $L_{t'}$ from Eq. (4.14), we finally obtain

$$N_B(L_{t'}) \propto L_{t'}^{-\log w / \log u}. \quad (4.20)$$

The fractal dimension in the box-covering sense is

$$D_f^{bc} = \frac{\log(u+v)}{\log u}. \quad (4.21)$$

Notice that the fractal dimension in the box-covering sense and that in the cluster-growing sense agree with each other.

4.2 Song-Havlin-Makse Model

Song et al. proposed in 2006 a simple mathematical model which incorporates the formation of fractal networks to identify the origin of fractality[28]. In this model, networks are formed by the following algorithm:

- (1) Initiate a network with a star graph with a small number of nodes. Denote the numbers of nodes and edges in the initial network by N_1 and M_1 , respectively. Since the initial network is a star graph, $M_1 = N_1 - 1$.
- (2) For every node i in the $(t - 1)$ -th generation network \mathcal{G}_{t-1} , add mk_i nodes around it and connect them to node i . Here, k_i is the degree of node i and m is an integer model parameter with $m \geq 2$.
- (3) For every edge in \mathcal{G}_{t-1} , we perform one of the two modes:
 - Mode I: with probability e , do nothing. The quantity e is the second model parameter with $0 \leq e \leq 1$.
 - Mode II: with probability $1 - e$, remove the edge. Let the two terminal nodes of the edge be i and j . Then, connect one of the newly added nodes around i and one of the newly added nodes around j by a new edge.
- (4) Repeat steps (2) and (3) until a desired number of nodes is obtained.

Figure 4.3 shows an example of networks generated by the SHM model.

Let us now calculate the properties of the SHM model. From the algorithm described above, the number N_t of nodes in the t -th generation network increases from that of the $(t - 1)$ -th generation network by

$$N_t = N_{t-1} + 2mM_{t-1}, \quad (4.22)$$

where M_{t-1} is the number of edges in the $(t - 1)$ -th generation network. Since the resulting networks of SHM model are trees, the number of edges is given by $M_{t-1} = N_{t-1} - 1$. Hence, Eq. (4.22) can be rewritten as

$$N_t = (2m + 1)N_{t-1} - 2m. \quad (4.23)$$

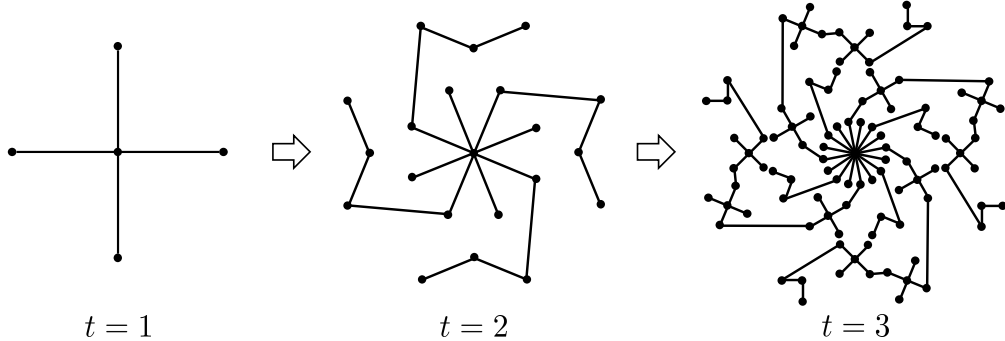


Figure 4.3: The 1st, 2nd, and 3rd generation Song-Havlin-Makse model for $m = 2$ and $e = 0$.

In a sufficiently large network with $t \gg 1$, the second term is negligible. Thus, we have

$$N_t = (2m + 1)N_{t-1}. \quad (4.24)$$

Before we proceed to the degree distribution of SHM model, let us consider the diameter of SHM model. Assuming the diameter of the $(t - 1)$ -th generation network is known as L_{t-1} , the diameter of the t -th generation network is given by

$$L_t = [e + 3(1 - e)] L_{t-1} + 2. \quad (4.25)$$

The second term on the right-hand side is the contribution from the two edges added around the two terminal nodes of the longest shortest path which gives the diameter. In a sufficiently large network with $L_t \gg 1$, the second term is negligible, and hence the diameter of the t -th generation network grows from that of the $(t - 1)$ -th generation network by a factor of $[e + 3(1 - e)]$. That is, when the number of nodes increases by the factor $(2m + 1)$ as in Eq. (4.24), the diameter grows by the factor $[e + 3(1 - e)]$. We therefore have the fractal dimension in the cluster-growing sense as

$$D_f^{cg} = \frac{\log(2m + 1)}{\log [e + 3(1 - e)]}. \quad (4.26)$$

Note that in the case of $e = 1$, the denominator becomes zero and the fractal dimension diverges. This indicates that the network is small-world, $L_t \propto \log N_t$ if $e = 1$. The parameter $e = 1$ corresponds to the condition at which two hubs are directly connected, i.e. the resulting networks are assortative. It provides us with a key insight that the disassortativity, or the repulsion of the hubs, plays an important role in the formation of fractal networks. For the sake of brevity, we do not argue the fractality in the box-covering sense here but it has been known that the fractal dimension of SHM model in the box-covering sense agrees with that in the cluster-growing sense.

Finally, let us determine the degree distribution of SHM model. The degree k of each node in the $(t - 1)$ -th generation network grows by the factor of m in the t -th generation network. The number of mk -degree nodes in the t -th generation network is hence equal to the number of k -degree nodes in the $(t - 1)$ -th generation network, i.e. $N_t(mk) = N_{t-1}(k)$. In terms of the degree distributions,

$$N_t P_t(mk) d(mk) = N_{t-1} P_{t-1}(k) dk, \quad (4.27)$$

where P_t is the degree distribution of the t -th generation network. Since the SHM model generates fractal networks in the case of $e < 1$, the formed networks

are self-similar and thus the degree distribution function retains the same form, i.e. $P_t(k) = P_{t-1}(k) = P(k)$. Assuming the degree distribution of the form $P(k) \propto k^{-\gamma}$, Eq. (4.27) gives

$$\begin{aligned} N_t(mk)^{-\gamma} d(mk) &= N_{t-1} k^{-\gamma} dk \\ \therefore N_t m^{-\gamma+1} &= N_{t-1}. \end{aligned} \quad (4.28)$$

Substituting Eq. (4.24) into Eq. (4.28), we attain

$$(2t + 1)m^{-\gamma+1} = 1. \quad (4.29)$$

We therefore have the scale-free exponent as

$$\gamma = \frac{\log(2t + 1)}{\log t} + 1. \quad (4.30)$$

4.3 General Models of Hierarchical Fractal Scale-free Networks

The models we have considered so far are two extreme cases of FSFNs: (u, v) -flower is cyclic and SHM model is tree. They fail to reproduce real-world FSFNs, such as the WWW and PINs, which consist of both cycles and trees. It is also different from real-world networks that the clustering coefficients of the FSFNs formed by these two models are always zero. In addition, the scale-free exponents, the fractal dimensions, and other structural features of FSFNs are restricted in the two models. To address these problems, Yakubo and Fujiki proposed a general model of hierarchical fractal scale-free networks (HFSFNs)[66, 67]. We introduce two versions of their model: deterministic one in Sec. 4.3.1 and stochastic one in Sec. 4.3.2.

4.3.1 Deterministic Model

In the deterministic model of HFSFNs, we need to prepare a small connected graph called a generator G and an initial graph \mathcal{G}_0 . In a generator G , we must specify two nodes as root nodes. We repeat the procedure of forming the t -th generation network \mathcal{G}_t by replacing iteratively every edge of \mathcal{G}_{t-1} with the generator G in a manner that the root nodes align with the terminal nodes of the replaced edge. See Fig. 4.4(a). For simplicity, we set \mathcal{G}_0 to be a graph which consists of a pair of nodes and an edge connecting the pair.

In order for generated networks to be scale-free and fractal, the following conditions of a generator G must be satisfied.

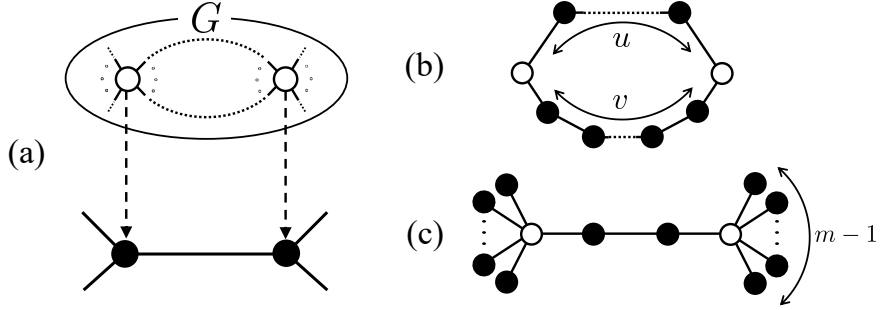


Figure 4.4: (a) The procedure of edge replacement by a generator G . A generator replaces an edge in a way that the positions of the root nodes of the generator match those of the terminal nodes of the edge. (b) The generator G_{uv} for (u,v) -flower. (c) The generator G_{shm} for Song-Havlin-Makse model. (a)-(c) White nodes represent the root nodes of generators.

- The two root nodes are symmetric to each other.
- The degree of the root node is at least 2.
- The shortest path distance between the two root nodes is longer than 1.

The first condition is, in other words, the generator structure is invariant when the two root nodes are swapped. This condition is required for the model to be deterministic. The model without the first condition is discussed in details in [66]. The second and third conditions are necessary conditions for scale-free and fractal properties, respectively. As long as the three conditions are satisfied, the generator G can be arbitrarily selected. This model encompasses (u,v) -flower and SHM model. In fact, (u,v) -flower can be constructed by choosing a cycle graph with $u+v$ nodes as a generator and assigning the two nodes which are separated by distance u . Similarly, SHM model (with parameter $e = 0$) is constructed by a generator of two connected m -edge star graphs. See Fig. 4.4(b) and (c). Figure 4.5 shows an example network generated by the deterministic model.

In the following explanation, we use symbols listed in Table 4.1. Let us now determine the numbers of edges and nodes in the t -th generation network \mathcal{G}_t . Initially, the numbers of edges and nodes are respectively $M_0 = 1$ and $N_0 = 2$. The number of edges in \mathcal{G}_t grows from that of \mathcal{G}_{t-1} by a factor of m_{gen} as each edge is replaced by G , i.e.

$$M_t = m_{\text{gen}} M_{t-1}. \quad (4.31)$$

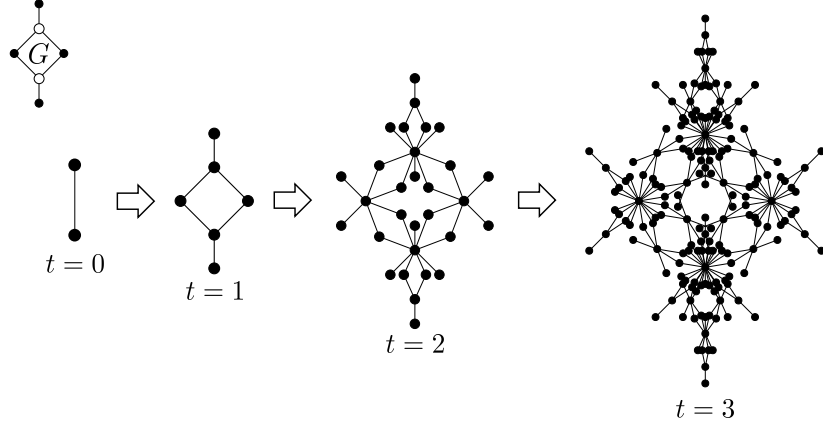


Figure 4.5: The 1st, 2nd, and 3rd generation networks formed by the deterministic model of HFSFNs.

Table 4.1: The notations for the deterministic model of HFSFNs.

n_{gen}	:	the number of nodes in G
m_{gen}	:	the number of edges in G
n_{nr}	:	the number of the non-root nodes of G $(n_{\text{nr}} = n_{\text{gen}} - 2)$
κ	:	the degree of the root node of G
k_i^{nr}	:	the degree of non-root node i of G
λ	:	the shortest path distance between the root nodes of G

By solving the recurrence relation (4.31) under the initial condition $M_0 = 1$, the number of edges in \mathcal{G}_t is given by

$$M_t = m_{\text{gen}}^t. \quad (4.32)$$

The number of nodes in \mathcal{G}_t increases as

$$N_t = N_{t-1} + n_{\text{nr}} M_{t-1}, \quad (4.33)$$

because every replacement of an edge adds n_{nr} nodes to the network. Substituting Eq. (4.32) into the recurrence relation (4.33), we attain

$$N_t - N_{t-1} = n_{\text{nr}} m_{\text{gen}}^{t-1}. \quad (4.34)$$

The number of nodes in \mathcal{G}_t is determined by solving the recurrence equation

(4.34) under the condition $N_0 = 0$, i.e.

$$\begin{aligned} N_t &= N_0 + \sum_{t'=1}^{t-1} n_{\text{nr}} m_{\text{gen}}^{t'} \\ &= 2 + n_{\text{nr}} \frac{m_{\text{gen}}^t - 1}{m_{\text{gen}} - 1}. \end{aligned} \quad (4.35)$$

When $t \gg 1$, Eq. (4.35) is approximated as

$$N_t \simeq \frac{n_{\text{nr}}}{m_{\text{gen}} - 1} m_{\text{gen}}^t. \quad (4.36)$$

From Eqs. (4.32) and (4.35), the mean degree $\langle k \rangle_t$ is given by

$$\langle k \rangle_t = \frac{2M_t}{N_t} = \frac{2m_{\text{gen}}^t(m_{\text{gen}} - 1)}{2(m_{\text{gen}} - 1) + n_{\text{nr}}(m_{\text{gen}}^t - 1)}. \quad (4.37)$$

In the limit of $t \rightarrow \infty$, the mean degree takes a finite value,

$$\langle k \rangle_\infty = \frac{2(m_{\text{gen}} - 1)}{n_{\text{nr}}}. \quad (4.38)$$

Next, let us consider the number $N_t(k)$ of nodes with a given degree k in \mathcal{G}_t . The degree of a k -degree node in \mathcal{G}_{t-1} increases to κk in \mathcal{G}_t . Introducing a function $\mathcal{N}(x)$ such that

$$\mathcal{N}(x) = \begin{cases} x & \text{if } x \in \mathbb{N} \\ 0 & \text{otherwise,} \end{cases} \quad (4.39)$$

the number $N_t(k)$ of k -degree nodes in \mathcal{G}_t is expressed by a recurrence relation

$$N_t(k) = N_{t-1}[\mathcal{N}(k/\kappa)] + M_{t-1} \sum_{i=1}^{n_{\text{nr}}} \delta_{k,k_i^{\text{nr}}}. \quad (4.40)$$

By solving Eq. (4.40) under the initial condition $N_0(k) = 2\delta_{k,1}$, we obtain

$$\begin{aligned} N_t(k) &= \sum_{t'=1}^t \left[N_{t'-1}[\mathcal{N}(k/\kappa)] + M_{t'-1} \sum_{i=1}^{n_{\text{nr}}} \delta_{k,k_i^{\text{nr}}} \right] \\ &= 2\delta_{k,\kappa^t} + \sum_{t'=1}^t \sum_{i=1}^{n_{\text{nr}}} m_{\text{gen}}^{t'-1} \delta_{k,\kappa^{t-t'} k_i^{\text{nr}}}. \end{aligned} \quad (4.41)$$

The moments of the degree can be calculated from Eq. (4.41),

$$\langle k^n \rangle_t = \frac{1}{N_t} \sum_k k^n N_t(k). \quad (4.42)$$

In fact, the second moment is obtained as

$$\langle k^2 \rangle_t = \begin{cases} \frac{(m_{\text{gen}} - 1) [2\kappa^{2t}(m_{\text{gen}} - \kappa^2) + K_2^{\text{nr}}(m_{\text{gen}}^t - \kappa^{2t})]}{(m_{\text{gen}} - \kappa^2) [2(m_{\text{gen}} - 1) + n_{\text{nr}}(m_{\text{gen}}^t - 1)]} & \text{for } m_{\text{gen}} \neq \kappa^2 \\ \frac{\kappa^{2(t-1)}(\kappa^2 - 1)(2\kappa^2 + tK_2^{\text{nr}})}{2(\kappa^2 - 1) + n_{\text{nr}}(\kappa^{2t} - 1)} & \text{for } m_{\text{gen}} = \kappa^2 \end{cases}. \quad (4.43)$$

where $K_2^{\text{nr}} = \sum_{i=1}^{n_{\text{nr}}} (k_i^{\text{nr}})^2$. For $t \rightarrow \infty$, the second moment approaches

$$\langle k^2 \rangle_\infty = \begin{cases} \frac{K_2^{\text{nr}}(m_{\text{gen}} - 1)}{n_{\text{nr}}(m_{\text{gen}} - \kappa^2)} & \text{for } m_{\text{gen}} > \kappa^2 \\ \infty & \text{for } m_{\text{gen}} \leq \kappa^2 \end{cases}. \quad (4.44)$$

Again, the degrees of nodes in \mathcal{G}_{t-1} are multiplied by a factor κ in \mathcal{G}_t . Hence the number of k -degree nodes in \mathcal{G}_{t-1} must be equal to the number of κk -degree nodes in \mathcal{G}_t if $k > \max_{i \in N_G^{\text{nr}}} [k_i^{\text{nr}}]$ where N_G^{nr} is the set of non-root nodes in G . That is,

$$N_{t-1}(k) = N_t(\kappa k) \quad (4.45)$$

for $k > \max_{i \in N_G^{\text{nr}}} [k_i^{\text{nr}}]$. Let us assume that the degree distribution asymptotically approaches $P(k)$ for $k \gg 1$ and $t \gg 1$. Then, both sides of Eq. (4.45) can be rewritten in terms of $P(k)$ as

$$N_{t-1}P(k)dk = N_tP(\kappa k)d(\kappa k) \quad (4.46)$$

for $k \gg 1$ and $t \gg 1$. Using Eq. (4.35), the relation simplifies to

$$P(k) = m_{\text{gen}}\kappa P(\kappa k). \quad (4.47)$$

Eq. (4.47) has a solution in the form $P(k) \propto k^{-\gamma}$, with

$$\gamma = \frac{\log m_{\text{gen}}}{\log \kappa} + 1. \quad (4.48)$$

Therefore, a network formed by this model is scale-free and its scale-free exponent is solely determined by the structural features of its generator G , namely the number m_{gen} of edges in G and the degree κ of the root node of G .

Finally, let us consider the diameter L_t of the t -th generation network \mathcal{G}_t . Actually, the exact form of the diameter cannot be determined because the

diameter of \mathcal{G}_t strongly depends on the detailed structure of a generator G . It is however possible to obtain the asymptotic behavior of the diameter to assess the fractality of networks. This is done by assuming that we know the diameter L_{t-1} of \mathcal{G}_{t-1} . Given L_{t-1} , the diameter L_t of \mathcal{G}_t can be estimated from the fact that the shortest path distance between the pair of nodes which gives the diameter L_{t-1} in \mathcal{G}_{t-1} grows by a factor of λ . For convenience, we denote the shortest path whose length is the diameter L_{t-1} in \mathcal{G}_{t-1} by \mathcal{P}_{t-1}^{\max} . Let us also refer to the node, which is most distant from the root node and does not belong to paths connecting the two root nodes, as the l -max node. The pair of nodes which becomes most distant in \mathcal{G}_t is then updated to the pair of the l -max nodes which belong to the generators that replace the two terminal edges of \mathcal{P}_{t-1}^{\max} . Denoting the distance between the l -max node and the root node in G by L_0 , the diameter L_t in \mathcal{G}_t is expressed in terms of L_{t-1} as

$$L_t = \lambda L_{t-1} + 2L_0. \quad (4.49)$$

In a sufficiently large network, i.e. $t \gg 1$, we have $\lambda L_{t-1} \gg 2L_0$. Thus, the diameter L_t of \mathcal{G}_t is approximated by

$$L_t \simeq \lambda L_{t-1}. \quad (4.50)$$

From Eqs. (4.35) and (4.50), the relation between the number N_t of nodes and the diameter L_t in \mathcal{G}_t is obtained as

$$N_t \propto L_t^{D_f}, \quad (4.51)$$

and the fractal dimension in a cluster-growing sense is given by

$$D_f = \frac{\log m_{\text{gen}}}{\log \lambda}. \quad (4.52)$$

This result indicates a network formed by this model is fractal, as long as the third condition for generators stated in p.30 is satisfied. If the condition is violated, i.e. $\lambda = 1$, the fractal dimension diverges and the network becomes small-world.

Local and global clustering coefficients as well as nearest-neighbor degree correlations are also exactly solvable in this model. The authors of [66] additionally present the critical exponents and the critical point of the bond-percolation transition on FSFNs generated by this model. Refer [66] for more details.

We have so far derived scale-free exponent and fractal dimension of networks generated by the deterministic model of HFSFNs. The results imply that the scale-free and fractal properties of FSFNs are solely determined by the structural features of a single generator. This hints that those of real-world FSFNs are

possibly determined only by their structural unit, or "generator." It is however unlikely that real-world FSFNs are formed by a single generator, as they appear to take much more complicated structures. In the following section, we introduce a stochastic model of HFSFNs, which extends the deterministic model.

4.3.2 Stochastic Model

While the deterministic model of HFSFNs generalizes the two representative models of FSFNs and enables the formation of networks with much diverse values of scale-free exponent and fractal dimension, real-world FSFNs are unlikely to be formed from a single generator. Thus the model is limited in its applicability to reproduce real-world FSFNs. To better simulate real-world FSFNs, we extend the deterministic model by introducing more than one generators in the network formation procedures. The stochastic model with two generators are discussed in [68].

In the stochastic model, we prepare a set $\{G_i\}_{i=1}^{N_{\text{gen}}}$ of generators and a set $\{p_i\}_{i=1}^{N_{\text{gen}}}$ of probabilities, where N_{gen} is the number of generators. The sum of the probabilities in the set must be unity, i.e.

$$\sum_{i=1}^{N_{\text{gen}}} p_i = 1. \quad (4.53)$$

We then form a network by iteratively replacing every edge of the previous generation network with one of the generators with its corresponding probability. In other words, an edge is replaced by G_i with probability p_i . Two example networks formed by the stochastic model are shown in Fig. 4.6. Let us denote the number of edges, the number of non-root nodes, the degree of the root node and the shortest path distance between the root nodes of G_i by m_i^{gen} , n_i^{nr} , κ_i , and λ_i , respectively.

We initiate a network \mathcal{G}_0 from a graph of two nodes connected by an edge. To construct the first generation network \mathcal{G}_1 , each edge in \mathcal{G}_0 is replaced by one of the generators with probabilities $\{p_i\}_{i=1}^{N_{\text{gen}}}$. Hence the expected number of edges in \mathcal{G}_1 is given by

$$M_1 = \sum_{i=1}^{N_{\text{gen}}} p_i m_i^{\text{gen}} = \bar{m}_{\text{gen}}. \quad (4.54)$$

Similarly, the expected number of edges in \mathcal{G}_2 is expressed as

$$\begin{aligned} M_2 &= \sum_{i=1}^{N_{\text{gen}}} p_i m_i^{\text{gen}} \cdot \sum_{j=1}^{N_{\text{gen}}} p_j m_j^{\text{gen}} \\ &= \bar{m}_{\text{gen}}^2. \end{aligned} \quad (4.55)$$

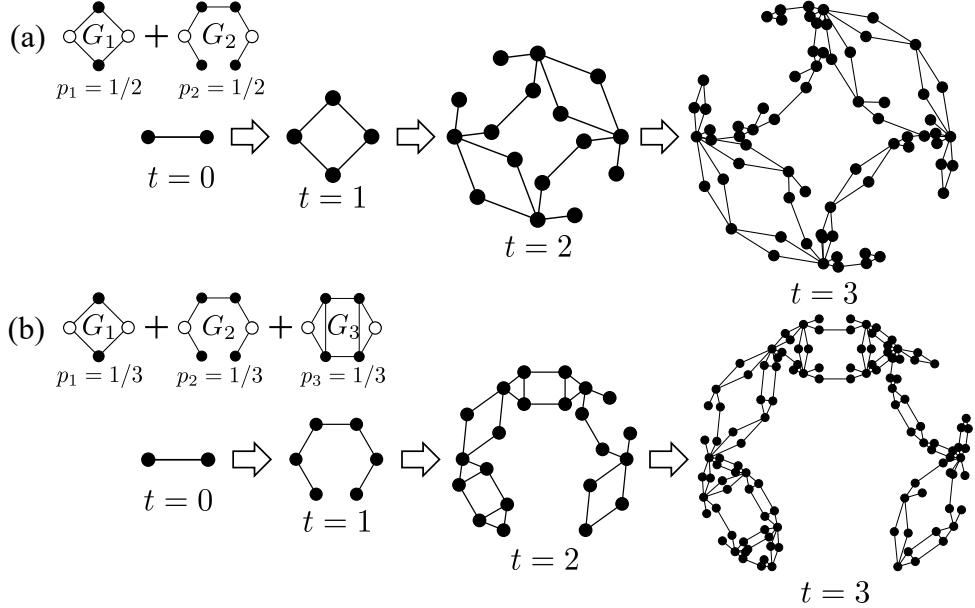


Figure 4.6: The 1st, 2nd, and 3rd generation networks formed by the stochastic model of HFSFNs with (a) two generators and (b) three generators. (a) Generators G_1 and G_2 shown in the upper left replace edges with an equal probability $p_1 = p_2 = 1/2$. (b) Generators G_1 , G_2 , and G_3 shown in the upper left replace edges with an equal probability $p_1 = p_2 = p_3 = 1/3$.

Hence, the expected number of edges in \mathcal{G}_t is attained as

$$M_t = \bar{m}_{\text{gen}}^t. \quad (4.56)$$

By analogy with the deterministic model, the number N_t of nodes, the number $N_t(k)$ of k -degree nodes, and the diameter L_t are obtained by simply replacing the structural features m_{gen} , n_{nr} , κ , and λ of G by the expected values \bar{m}_{gen} , \bar{n}_{nr} , $\bar{\kappa}$, and $\bar{\lambda}$ of $\{G_i\}_{i=1}^{N_{\text{gen}}}$,

$$\bar{m}_{\text{gen}} = \sum_{i=1}^{N_{\text{gen}}} p_i m_i^{\text{gen}}, \quad (4.57)$$

$$\bar{n}_{\text{nr}} = \sum_{i=1}^{N_{\text{gen}}} p_i m_i^{\text{nr}}, \quad (4.58)$$

$$\bar{\kappa} = \sum_{i=1}^{N_{\text{gen}}} p_i \kappa_i, \quad (4.59)$$

$$\bar{\lambda} = \sum_{i=1}^{N_{\text{gen}}} p_i \lambda_i. \quad (4.60)$$

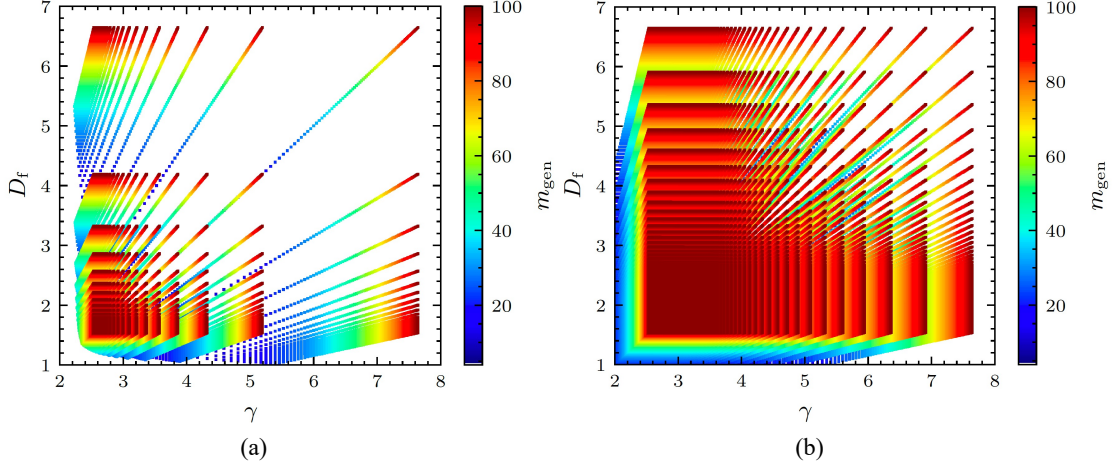


Figure 4.7: The possible values of scale-free exponent γ and fractal dimension D_f of networks generated by (a) the deterministic model and (b) the stochastic model. In both cases, κ ($\bar{\kappa}$) and λ ($\bar{\lambda}$) are shifted within the range of [2, 20]. The minimum m_{gen} for a given pair of κ and λ is given by the relation $m_{\text{gen}}^{\min} = \lambda + 2\kappa - 2$. $m_{\text{gen}}(\bar{m}_{\text{gen}})$ is shifted in the range $[m_{\text{gen}}^{\min}, 100]$.

Therefore, some of the essential quantities of \mathcal{G}_t are given by:

$$M_t = \bar{m}_{\text{gen}}^t, \quad (4.61)$$

$$N_t = 2 + \bar{n}_{\text{nr}} \frac{\bar{m}_{\text{gen}}^t - 1}{\bar{m}_{\text{gen}}^t - 1}, \quad (4.62)$$

$$\gamma = 1 + \frac{\log \bar{m}_{\text{gen}}^t}{\log \bar{\kappa}}, \quad (4.63)$$

$$D_f = \frac{\log \bar{m}_{\text{gen}}^t}{\log \bar{\lambda}}. \quad (4.64)$$

Notice that the possible values of scale-free exponent and fractal dimension can be continuously tuned, because the values of \bar{m}_{gen} , $\bar{\kappa}$, and $\bar{\lambda}$ in the stochastic model are real numbers whereas m_{gen} , κ , and λ in the deterministic model are integers. This indicates that a much broader class of FSFNs is represented by the stochastic model. In fact, Fig. 4.7 clearly shows the possible values of scale-free exponent and fractal dimension for networks generated by the stochastic model of HFSFNs cover a wider area in the γ - D_f space than those by the deterministic model.

4.4 Fractal Scale-free Random Graph

A random graph is a graph whose edges are placed randomly. Random graphs have played a significant role in the study of complex networks by providing various sets of networks to which networks of our interest can be compared. We begin this section with Erdős-Rényi random graphs (ERRGs), which is one of the earliest and simplest network models. Despite its simplicity, ERRGs involve a phase transition of connectivity, which results in a fractal network at criticality. We then introduce the generalized random graphs, whose degree distributions can be arbitrarily controlled. Finally, we describe fractal scale-free random graphs, which will appear in our main results.

4.4.1 Erdős-Rényi Random Graph and Its Criticality

Erdős-Rényi random graph (ERRG) was first introduced in the late 1950s to study graphs by the means of probability theory. In an ERRG, the number N of nodes is fixed and each pair of nodes is connected by an edge with probability p . Let us denote the ERRG model by $G_{N,p}^{\text{ER}}$. When $p = 0$, there are no edges in the network and all the nodes are isolated. When $p = 1$, all the nodes are connected to each other and the network is complete. The probability that a graph $G(N, M)$ with N nodes and M edges appears is given by

$$P(G) = p^M (1-p)^{K-M} \quad (4.65)$$

where $K = \binom{N}{2} = \frac{N(N-1)}{2}$. If we simply focus on the number M of edges in G , the probability to obtain M -edge network is

$$P(M) = K p^M (1-p)^{K-M}. \quad (4.66)$$

Using Eq. (4.66), we get the mean number $\langle M \rangle$ of edges in $G_{N,p}^{\text{ER}}$ as

$$\langle M \rangle = \sum_{m=0}^K m P(m) = pK. \quad (4.67)$$

From Eq. (4.67), the average degree $\langle k \rangle$ is attained

$$\langle k \rangle = \left\langle \frac{2M}{N} \right\rangle = \frac{2pK}{N} = p(N-1). \quad (4.68)$$

The degree distribution $P(k)$ of $G_{N,p}^{\text{ER}}$ is given by a binomial distribution

$$P(k) = \binom{N-1}{k} p^k (1-p)^{N-1-k}. \quad (4.69)$$

When the number of nodes N is sufficiently large, the degree distribution is well approximated by a Poisson distribution

$$P(k) \simeq \frac{\langle k \rangle^k e^{-\langle k \rangle}}{k!}. \quad (4.70)$$

In this sense, ERGs in the large N limit are often called Poisson random graphs. Many properties of Poisson random graphs are exactly solvable. For instance, the local clustering coefficient is obviously given by

$$C = p = \frac{\langle k \rangle}{N}, \quad (4.71)$$

and the average shortest path distance is known to be proportional to $\log N$, i.e.,

$$\langle l \rangle \propto \log N, \quad (4.72)$$

which indicates that ERGs are small-world. Refer [71] for more details.

An important feature of ERGs is a phase transition from a low-density phase to a high-density phase. While there exist numerous small components in the low-density phase, most of the nodes are contained in a single giant component in the high-density phase. The average component size $\langle S \rangle$ is in fact derived as

$$\langle S \rangle = \frac{1}{1 - \langle k \rangle + \langle k \rangle S(\langle k \rangle)} \quad (4.73)$$

by utilizing generating functions[69]. Here, S is the fraction of the giant component to the entire network. Similarly, the critical point p_c at which the mean component size diverges is also obtained from the arguments by generating functions as

$$\begin{aligned} \frac{\langle k^2 \rangle}{\langle k \rangle} &\simeq \frac{p_c N(1 + p_c N)}{p_c N} = 1 + p_c N = 2, \\ \therefore p_c &= \frac{1}{N}. \end{aligned} \quad (4.74)$$

The solid line in Fig. 4.8 shows the profile of the average component size. The divergence of the average component size can be observed at $\langle k \rangle = p_c N = 1$. We can also confirm the emergence of the giant component, because $S \rightarrow 0$ for $\langle k \rangle = p_c N < 1$ whereas $S > 0$ for $\langle k \rangle = p_c N > 1$. The universality class of percolation at ERGs is the same as that of percolation at Bethe lattice[6].

It is known from percolation theory that the giant component at the critical point possesses a fractal property[59]. The fractal dimension of the giant component of ERGs at criticality is

$$D_f = 2. \quad (4.75)$$

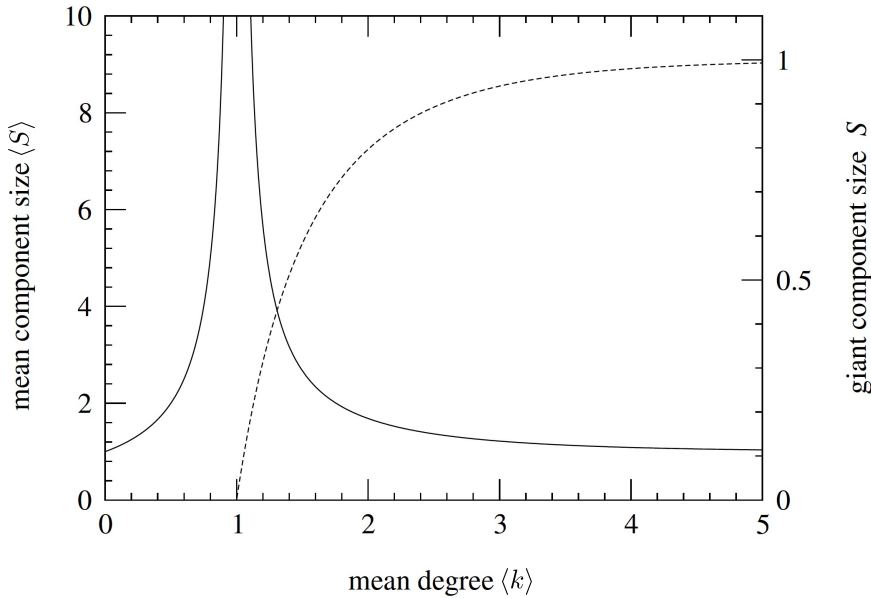


Figure 4.8: The mean component size (solid line) and the giant component size (dashed line) of Poisson random graphs. The figure is taken from [2]. The axis labels are slightly modified without changing their meanings.

4.4.2 Generalized Random Graph

While ERGs prove to be a useful model whose properties can be analytically calculated, the degree distribution in the form of binomial distribution is a significant limitation in its applicability because many real-world networks do not possess binomial degree distributions. A generalized random graph, or the configuration model, is a random graph with an arbitrary degree distribution[69]. In this model, we generate a network in the following procedures:

- (1) Initialize a network with N isolated nodes.
- (2) Prepare a degree sequence $\{k_1, k_2, \dots, k_N\}$ of length N in accordance with a given degree distribution $P(k)$. The sum of the degree sequence must be even.
- (3) Assign k_i stubs (half-edge) to each node i .
- (4) Choose two stubs randomly and connect them while avoiding the formation of multiple edges and self-loops.

The generalized random graphs have been extensively studied since the 1970s and various analytical results such as the condition for existence of a giant

component (known as the Molley-Reed criterion)[72], the expected size of the giant component[73], and the average size of non-giant components[69] have been known.

4.4.3 Fractal Scale-free Random Graph

A fractal scale-free random graph (FSFRG) is a random graph with scale-free and fractal properties. In order to form FSFRGs, we utilize the generalized random graphs introduced in Sec. 4.4.2 and the fact the giant component at the percolation transition point exhibits the fractal property. By extracting the giant components of scale-free random graphs at criticality, we can form FSFRGs characterized by the scale-free exponent γ' given by

$$\gamma' = \gamma - 1 \quad (4.76)$$

where γ is the scale-free exponent of the original scale-free random graph[70]. At the percolation transition point, the relation

$$\frac{\langle k^2 \rangle}{\langle k \rangle} = 2 \quad (4.77)$$

holds as in the case of ERRGs [see Eq. (4.74)], because generalized random graphs have no degree correlations. This implies that for obtaining an FSFRG, the original scale-free random graph needs to have a power-law degree distribution $P(k)$ satisfying Eq. (4.77). The fractal dimension D_f of a FSFRG is known as

$$D_f = \begin{cases} 2 & \text{if } \gamma \geq 4, \\ \frac{\gamma - 2}{\gamma - 3} & \text{if } 3 < \gamma < 4. \end{cases} \quad (4.78)$$

Notice that γ is the scale-free exponent of the original scale-free random graphs. In terms of the scale-free exponent γ' of a FSFRG, Eq. (4.79) is rewritten as

$$D_f = \begin{cases} 2 & \text{if } \gamma' \geq 3, \\ \frac{\gamma' - 1}{\gamma' - 2} & \text{if } 2 < \gamma' < 3. \end{cases} \quad (4.79)$$

Refer [3] for its derivation. The possible combination of scale-free exponent and fractal dimension of FSFRGs is shown in Fig. 4.9.

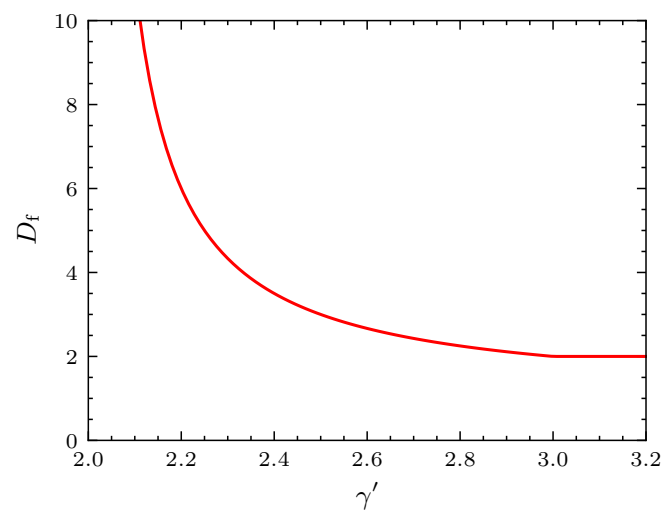


Figure 4.9: Configuration space of FSFRGs. The red line indicates the possible combination of scale-free exponent and fractal dimension.

Chapter 5

Multifractality

We have so far discussed the fractal property of networks characterized by a fractal dimension D_f . However, a fractal dimension does not suffice to describe some features of complex systems or distributions. In such a case, multifractals which involve a full spectrum of infinitely many exponents often provide well-organized descriptions.

In this chapter, we briefly introduce multifractality of distributed quantities in Euclidean spaces and in networks. We then move on to describe the multifractality of network structures. We close this chapter by stating the purposes of our work.

5.1 Multifractality of Distributed Quantities

As stated above, multifractal property is a property of systems or distributions which require an infinite number of scaling exponents for a full description. For example, let us consider the distributions of trace elements, such as gold, on the earth. Most of the trace elements are usually distributed unevenly, highly concentrated in a few "hotspots" while extremely scarce on the rest. In other words, the distributions of those trace elements are so heterogeneous that the distributions of different intensities follow different scaling from one another. Such heterogeneous distributions are not limited to trace elements but rather omnipresent in nature. To name a few, the distribution of energy dissipation in fluid turbulence[40], the growth probability distribution of diffusion-limited-aggregation[43], and the spacial distributions of the wavefunctions at the criticality of Anderson transition[74] are indeed multifractal.

Multifractal analysis is an analysis to determine the spectrum of infinitely many exponents which describe a multifractal distribution. In the following two sections, we assume a measure μ_i is distributed at a position i . The measure

satisfies the normalization condition over the space, i.e.

$$\sum_i \mu_i = 1. \quad (5.1)$$

Though the concept of multifractality was initially introduced by Mandelbrot for systems in Euclidean spaces, it has been extended to networks in which geometric supports are absent[45]. The multifractality in networks is assessed by the shortest path distances as an alternative to Euclidean distances. In addition, a measure μ_i in a network corresponds to the measure at node i . By considering so, we can treat multifractality in Euclidean spaces and that in networks equivalently. The arguments in the following sections hence stand valid for systems embedded in Euclidean spaces as well as for complex networks. However, the concept of multifractality and the multifractal analysis will be explained in Sec. 5.1.1 and 5.1.2 for systems embedded in Euclidean space because of its simplicity.

5.1.1 Mass Exponents

Similar to the ordinary fractal analysis, we will renormalize the distribution of measure μ_i and identify the self-similarity of the distribution by investigating the distribution of the renormalized measure. To renormalize the distribution, we first box-cover the distribution with a fixed box size l . See Fig. 5.1. Denote the set of boxes $b(l)$ of size l used to cover the distribution by $\mathcal{B}(l)$. Let us define a box measure as the sum of measures in a box $b(l)$ of size l , i.e.

$$\mu_{b(l)} = \sum_{i \in b(l)} \mu_i. \quad (5.2)$$

The q -th moment of the box measure is given by

$$Z_q(l) = \sum_{b(l) \in \mathcal{B}(l)} [\mu_{b(l)}]^q. \quad (5.3)$$

If the distribution is self-similar, the behavior of $Z_q(l)$ should be independent of the renormalization scale l . That is, a power-law relation

$$Z_q(l) \propto \left(\frac{l}{L}\right)^{\tau(q)} \quad (5.4)$$

stands between l and $Z_q(l)$. L is the system size. Hence, the exponent is represented by

$$\tau(q) = \lim_{l \rightarrow 0} \frac{\log Z_q(l)}{\log l}, \quad (5.5)$$

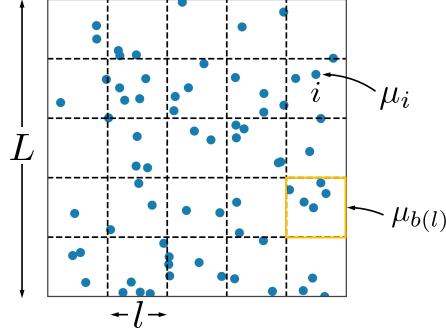


Figure 5.1: Renormalization of measures by dividing the system of size L into smaller boxes of size l .

and we call $\tau(q)$ the mass exponent. If $\tau(q)$ is nonlinear with regard to q , we say the distribution of μ_i is multifractal.

Note from Eq. (5.3) that a negative q value emphasizes smaller box measures while a positive q value intensifies larger box measures. If $q = 0$, the right-hand side of Eq. (5.3) becomes the number of boxes $b(l)$ in $\mathcal{B}(l)$. We therefore have

$$\tau(0) = -D_f, \quad (5.6)$$

because Eq. (5.4) reads $N_B \propto l^{-\tau(q)}$ and the fractal dimension is given by $N_B \propto l^{D_f}$. Furthermore, in the case of $q = 1$, we have

$$Z_1(l) = \sum_{b(l) \in \mathcal{B}(l)} \sum_{i \in b(l)} \mu_i = \sum_i \mu_i = 1. \quad (5.7)$$

Combining with Eq. (5.4), we have

$$\tau(1) = 0. \quad (5.8)$$

Let us now consider the fractal dimension of $Z_q(l)$. Assuming uniformly distributed measures on a fractal support with D_f , $Z_q(l)$ should be distributed with the same D_f independent of q . From the normalization condition (5.1) $\mu_i \propto L^{-D_f}$, and hence

$$Z_q(l) \propto \sum_{b(l) \in \mathcal{B}(l)} (l^{D_f} L^{-D_f})^q \propto \left(\frac{L}{l}\right)^{D_f} \cdot (l^{D_f} L^{-D_f})^q \propto \left(\frac{l}{L}\right)^{D_f(q-1)}. \quad (5.9)$$

Hence, the fractal dimension of $\tau(q)$ is expressed as

$$D_q = \frac{\tau(q)}{q-1}. \quad (5.10)$$

D_q is called the generalized dimension.

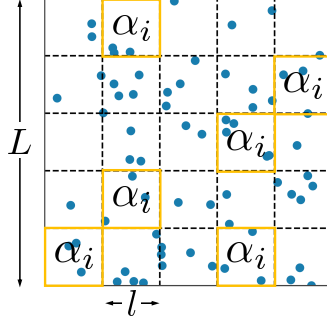


Figure 5.2: The schematic figure of multifractal spectrum. If the distribution of Lipschitz-Hölder exponent α_i is self-similar, the multifractal spectrum is defined by the fractal dimension $f(\alpha)$ of the α -distribution.

5.1.2 Lipschitz-Hölder Exponents

Consider again the box-covering $\mathcal{B}(l)$ of the distribution with box size l . If the box measure $\mu_{b(l)}$ of a box $b(l)$ scales with box size l as

$$\mu_{b(l)} \propto l^\alpha, \quad (5.11)$$

then the exponent α is expressed as

$$\alpha = \lim_{l \rightarrow 0} \frac{\log \mu_{b(l)}}{\log l}. \quad (5.12)$$

This exponent α is called the Lipschitz-Hölder exponent. This exponent quantifies the fractality of local structures. Let us consider the distribution of boxes whose Lipschitz-Hölder exponent is α_i and assume the distribution of the boxes with α_i is self-similar. Then we call the fractal dimension of the distribution of α_i the multifractal spectrum and denote it by $f(\alpha)$. See Fig. 5.2. Given the number $N(\alpha_i)$ of boxes with α_i , the multifractal spectrum is determined by

$$f(\alpha) = \lim_{L \rightarrow \infty} \frac{\log N(\alpha)}{\log L}. \quad (5.13)$$

The mass exponent $\tau(q)$ and the multifractal spectrum $f(\alpha)$ are two interdependent exponents characterizing the same distribution of μ_i . To understand the relation between $\tau(q)$ and $f(\alpha)$, let us return to the q -th moment of box measures. From Eq. (5.11), the q -th moment in Eq. (5.3) is rewritten as

$$Z_q(l) \propto \sum_{b(l) \in \mathcal{B}(l)} l^{\alpha q}. \quad (5.14)$$

Since α is a exponent which continuously changes its value depending on boxes, the summation in Eq. (5.14) can be rewritten in terms of integration by α . Consider the subset S_α of boxes with α , and let us assume the number of S_α in the range $[\alpha, \alpha + d\alpha]$ is given by $\rho(\alpha)d\alpha$. Then the number of boxes of size l contained in the subset S_α is proportional to $l^{-f(\alpha)}$ and hence the number of nodes in the interval $[\alpha, \alpha + d\alpha]$ is given as

$$N(\alpha)\rho(\alpha)d\alpha = \rho(\alpha)l^{-f(\alpha)}d\alpha. \quad (5.15)$$

By substituting the summation $\sum_{b(l) \in \mathcal{B}(l)}$ by integral $\int \rho(\alpha)l^{-f(\alpha)}d\alpha$, we get

$$Z_q(l) \propto \int \rho(\alpha)l^{\alpha q - f(\alpha)}d\alpha. \quad (5.16)$$

By solving the integral by saddle-point method, we have

$$\frac{d}{d\alpha} [\alpha q - f(\alpha)] = 0, \quad (5.17)$$

which is evaluated as

$$Z_q(l) \propto \rho[\alpha(q)]l^{\alpha q - f[\alpha(q)]}. \quad (5.18)$$

The mass exponent is then expressed as

$$\tau(q) = \alpha(q)q - f[\alpha(q)]. \quad (5.19)$$

Inversely, we have the multifractal spectrum as

$$f(\alpha) = q(\alpha)\alpha - \tau[q(\alpha)]. \quad (5.20)$$

Equations (5.19) and (5.20) imply that $q(\alpha)$ and $\alpha(q)$ are related to each other through the Legendre transformation. Hence the Lipschitz-Hölder exponent is alternatively obtained by

$$\alpha = \frac{d\tau(q)}{dq}. \quad (5.21)$$

5.2 Multifractality of Complex Networks

In the previous section, we have described multifractality of distributions rather than structures. However, networks can implicitly encompass heterogeneity, such as scale-free property, due to the absence of physical restrictions. In 2011,

Furuya and Yakubo predicted that the structures of FSFNs themselves are multifractal and demonstrated the multifractality of some of fractal scale-free networks[38].

In their work, every node in a network gives an equal measure, and the multifractal analysis of the distribution of the measure is conducted. The network is covered by overlapping boxes (subgraphs) of size l , as overlaps are unavoidable for box-covering of graphs in a manner that each box contains the maximum possible number of nodes[61]. As such, measures at each node must be normalized not by the number of nodes, but rather by the sum of the number of nodes in all the boxes, i.e.

$$\mu_i = \frac{1}{\sum_{b(l) \in \mathcal{B}(l)} \sum_{i \in b(l)}}. \quad (5.22)$$

Using the measure defined in Eq. (5.22), it is relatively simple to show that Eqs. (5.6) and (5.8).

5.2.1 Bifractality of (u, v) -flower

To confirm the multifractality of network structures, Furuya and Yakubo[38] first examined the (u, v) -flower. They assigned the equal measure in Eq. (5.22) to every node of a FSFN generated by the model. In order to cover the network, they applied the same covering scheme as the scheme II in Sec. 4.1. That is, we cover the network by boxes in the order of descending order of degrees. See Fig. 5.3(b). Furuya and Yakubo argue that it is even more important to cover a network with less boxes in the multifractal analysis than in the fractal analysis[38].

We consider covering the t -th generation (u, v) -flower by boxes of size $L_{t'}$ ($u, v : \text{even}, 1 \ll t' \ll t$). We use the same notations as those in Sec. 4.1 for the number of nodes and the diameter in the t -th generation network. The number $N_{b(s, L_{t'})}$ of boxes centered at the s -th largest hubs is equal to the number of the s -th largest hubs. Hence it is given by

$$N_{b(s, L_{t'})} = N_s - N_{s-1} \quad (5.23)$$

for $1 \leq s \leq t - t'$. The subscript $b(s, L_{t'})$ represents a box of size $L_{t'}$ centered at one of the s -th largest hubs. The number of nodes $\nu_s(L_{t'})$ in the box $b(s, L_{t'})$ is counted by taking into account the number of the t' -th generation networks connected to the hub $2^{t-t'}$, the number of t' -th generation networks connected to the s -th largest hub 2^{s-1} , and half the number of edges in the t' -th generation, $N_{t'}/2$. We thus obtain

$$\nu_s(L_{t'}) = 2^{t-t'-s} N_{t'} + 1 \simeq 2^{t-t'-s} N_{t'}. \quad (5.24)$$

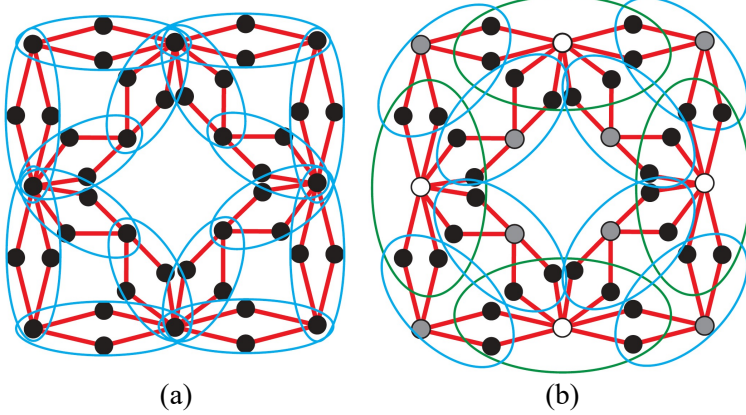


Figure 5.3: Two schemes to cover the third generation (u, v) -flower with $u = v = 2$. (a) The network is covered with the first generation (u, v) -flowers. (b) The network is covered by four subgraphs of size $l = 2$ centered at the largest hubs (green circles) and 8 subgraphs of size $l = 2$ centered at the second largest hubs (blue circles). The figure is taken from [38].

The number of nodes in all the boxes is given by

$$\sum_{b(l) \in \mathcal{B}(l)} \sum_{i \in b(l)} = \sum_{s=1}^{t-t'} N_{b(s, L_{t'})} \nu_s(L_{t'}) = \frac{w^t(w-2)}{w-1} \quad (5.25)$$

where $w = u + v$. From Eq. (5.25), the measure is defined as

$$\mu_i = \frac{w-1}{w^t(w-2)}. \quad (5.26)$$

The box measure of $b(s, L_{t'})$ is then written as

$$\mu_{b(s, L_{t'})} = \sum_{i \in b(s, L_{t'})} \mu_i = \frac{w-1}{w^t(w-2)} N_s. \quad (5.27)$$

The q -th moment of the box measure is then

$$\begin{aligned} Z_q(L_{t'}) &= \sum_{s=1}^{t-t'} N_{b(s, L_{t'})} [\mu_{b(s, L_{t'})}]^q \\ &= \frac{w^{t(1-q)}}{W_q} \left[\left(\frac{2^q}{w}\right)^{t-1} (W_q - 1) \left(\frac{L_{t'} + b}{a}\right)^{\frac{q \log w / 2}{\log u}} + \left(\frac{L_{t'} + b}{a}\right)^{\frac{(q-1) \log w}{\log u}} \right], \end{aligned} \quad (5.28)$$

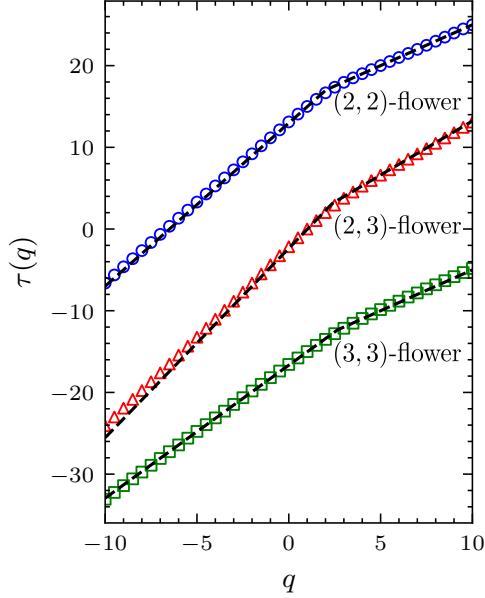


Figure 5.4: The mass exponents of $(2, 2)$ -, $(2, 3)$ -, and $(3, 3)$ -flowers. The numbers of generations of the networks are 8, 7, and 6, respectively.

where we used the following notations

$$W_q = \frac{w - 2^q}{w - 2}, \quad a = \frac{u(u - 3) + v(u + 1)}{2u(u - 1)}, \quad b = \frac{v - u}{u - 1}. \quad (5.29)$$

We therefore have the mass exponent

$$\tau(q) = \begin{cases} (q - 1) \frac{\log(u + v)}{\log u} & \text{for } q < \frac{\log(u + v)}{\log 2} \\ q \frac{\log(u + v)/2}{\log u} & \text{for } q \geq \frac{\log(u + v)}{\log 2} \end{cases}, \quad (5.30)$$

which is characterized by two distinct lines. Equation (5.30) is exact for even u and v , but it also approximates well for odd u and v . The mass exponent $\tau(q)$ obtained in Eq. (5.30) is numerically confirmed by numerical calculations based on the compact-box-covering algorithm[60] (in [38]) and the sandbox algorithm[45] (in [45] as well as by myself).

It should be noted that the multifractal analysis of the (u, v) -flower with the covering scheme in Fig. 5.3(a) will result in

$$Z_q(L_{t'}) = w^{t(1-q)} \left(\frac{L_{t'} + b}{a} \right)^{\frac{(q-1) \log w}{\log u}}, \quad (5.31)$$

which gives the mass exponent

$$\tau(q) = \frac{(q-1)\log(u+v)}{\log u}. \quad (5.32)$$

Hence, the covering scheme in Fig. 5.3(a) does not return a proper scaling for $q > \log(u+v)/\log 2$. As it is important for the fractal analysis of networks to use the minimal covering, the same is true about the multifractal analysis.

5.2.2 Mean-Field Arguments

Furuya and Yakubo[38] have generalized their argument for the (u, v) -flower by employing mean-field arguments. They considered a FSFN of N nodes with degree distribution $P(k) \propto k^{-\gamma}$. Given the minimal covering of the network with $N_{b(l)}$ boxes, the mean number of nodes $\langle \nu_l \rangle$ is^{*1}

$$\langle \nu_l \rangle = \frac{N}{N_{b(l)}}. \quad (5.33)$$

Here, the number of boxes should satisfy $N_{b(l)} \propto l^{-D_f}$ due to the fractal property. In the renormalized network whose degree distribution is $P_l(k_l)$, it is assured that $P_l(k_l) \propto k_l^{-\gamma}$ with the same scale-free exponent as that of the original network[27]. If we assume that the renormalized nodes with the same degree are statistically equivalent to each other and that the number $\nu_l(k_l)$ of nodes in a box which corresponds to the renormalized node of degree k_l has negligible fluctuations over the boxes, $\nu_l(k_l)$ is proportional to k_l and is

$$\nu_l(k_l) = \frac{\langle \nu_l \rangle}{\langle k_l \rangle} k_l. \quad (5.34)$$

The (u, v) -flower satisfies Eq. (5.34) in the thermodynamic limit $N \rightarrow \infty$.

The box measure is attained by normalizing $\nu_l(k_l)$ by the sum of all the nodes in the box (N in the original work)

$$\mu_{b(l)} = \frac{k_l}{\langle k_l \rangle N_{b(l)}}. \quad (5.35)$$

The q -th moment of the box measure is then

$$Z_q(l) = \sum_{b(l)} [\mu_{b(l)}]^q = \frac{N_{b(l)}^{1-q}}{\langle k_l \rangle^q} \sum_{k_l} k_l^q, \quad (5.36)$$

^{*1}The original argument by Furuya and Yakubo ignores the number of nodes which are covered by multiple boxes. However, the argument is valid even if we consider the multiply-covered nodes.

where we used the change of variables of the summations $\sum_{b(l)} = N_{b(l)} \sum_{k_l}$ in the second equality. Applying the continuum approximation of the degree, we rewrite the summation to the integration of degree,

$$Z_q(l) = \frac{N_{b(l)}^{1-q}}{\langle k_l \rangle^q} \int_{k_{\min}}^{k_{\max}} k_l^q P_l(k_l) dk_l \propto \frac{N_{b(l)}^{1-q}}{\langle k_l \rangle^q} \int_{k_{\min}}^{k_{\max}} k_l^{q-\gamma} dk_l. \quad (5.37)$$

The integration converges in the case of $q - \gamma < -1$, and hence we get

$$Z_q(l) \propto N_{b(l)}^{1-q} \propto l^{(q-1)D_f}. \quad (5.38)$$

Here, we used the fractal property $N_{b(l)} \propto l^{-D_f}$.

On the other hand, in the case of $q - \gamma \geq -1$, we must calculate the integration for a finite $N_{b(l)}$. In order to do so, we must first identify the maximum and minimum degrees, k_{\max} and k_{\min} . The maximum degree is obtained as follows: since $N_{b(l)}$ is finite, we have

$$\int_{k_{\max}}^{\infty} k_l^{-\gamma} dk_l = \frac{k_{\max}^{1-\gamma}}{\gamma - 1} = \frac{1}{N_{b(l)}}. \quad (5.39)$$

By solving for k_{\max} , we obtain

$$k_{\max} = \left(\frac{\gamma - 1}{N_{b(l)}} \right)^{1/(1-\gamma)}. \quad (5.40)$$

Similarly, we use

$$\int_{k_{\min}}^{\infty} k_l^{-\gamma} dk_l = \frac{k_{\min}^{1-\gamma}}{\gamma - 1} = 1 \quad (5.41)$$

to determine k_{\min} as

$$k_{\min} = (\gamma - 1)^{1/(1-\gamma)}. \quad (5.42)$$

Hence, we can express the maximum degree in terms of the minimum degree,

$$k_{\max} = k_{\min} N_{b(l)}^{1/(\gamma-1)}. \quad (5.43)$$

Using Eq. (5.43), Eq. (5.37) in the case of $q - \gamma \geq -1$ is expressed as

$$\begin{aligned} Z_q(l) &\propto \frac{N_{b(l)}^{1-q}}{\langle k_l \rangle^q} \left[\frac{k_{\max}^{q-\gamma+1}}{q - \gamma + 1} \right]_{k_{\min}}^{k_{\min} N_{b(l)}^{1/(\gamma-1)}} \\ &\propto l^{(q-1)D_f} \cdot l^{-D_f(q-\gamma+1)/(1-\gamma)} \\ &\propto l^{D_f q(\gamma-2)/(1-\gamma)}. \end{aligned} \quad (5.44)$$

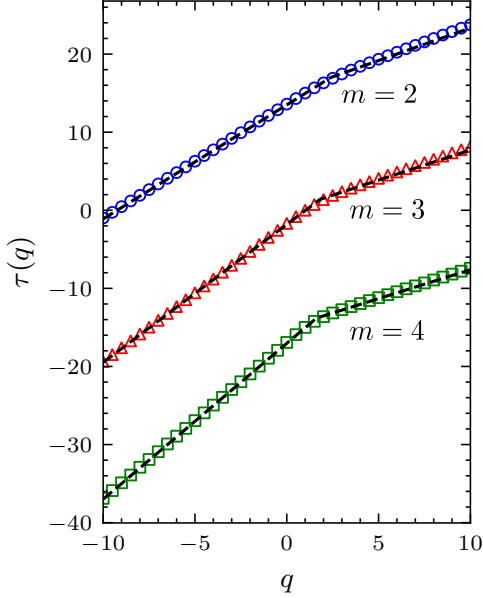


Figure 5.5: The mass exponents of Song-Havlin-Makse model with $m = 2$, $m = 3$, and $m = 4$. The numbers of generations of the networks are 7, 5, and 5, respectively.

We have used the relation $N_{b(l)} \propto l^{-D_f}$ again in the second proportionality. To summarize, we attain the mass exponent

$$\tau(q) = \begin{cases} (q-1)D_f & \text{for } q < \gamma - 1 \\ qD_f \frac{\gamma-2}{\gamma-1} & \text{for } q \geq \gamma - 1 \end{cases} \quad (5.45)$$

for a FSFN which satisfies the relation $\nu_l(k_l) \propto k_l$. When the mass exponent of a FSFN is given by Eq. (5.45), we call the FSFN bifractal. In [38], the authors presented a numerical confirmation of Eq. (5.45) for SHM model with $m = 2$.

5.3 Purpose of This Work

Ever since the publication of [38], various studies on the multifractal analysis of complex networks followed[39, 45–49, 51, 53, 75–79]. However, none has further investigated the condition for bifractality of FSFNs. As such, we do not know how general the bifractality of FSFNs is. In fact, so far only the (u, v) -flower and Song-Havlin-Makse model have been shown to be bifractal.

Furthermore, Furuya and Yakubo have not provided any discussion in [38] regarding the relation between the bifractality and the network structures. Their results indicate there exist two fractalities within the bifractal networks. However, they do not argue which subgraphs correspond to which fractalities. As an implication of the two local fractalities, the bifractal networks might have two distinct rates at which diffusion occurs. It is hence important to identify the correspondence between local structures and bifractality of a given network for application purposes.

We therefore attempt to answer the two arising questions, (1) how general among FSFNs the bifractal property is, and (2) how the bifractality relates to the subgraphs of networks. For the former, we examine three classes of FSFNs, namely the general deterministic model of HFSFNs, the general stochastic model of HFSFNs, and the fractal scale-free random graphs. For the latter, we investigate the distributions of Lipschitz-Hölder exponents within bifractal networks.

Chapter 6

Bifractality of Fractal Scale-free Networks

In the previous chapter, we have argued a specific class of fractal scale-free networks (FSFNs) and indicated the purposes of this work. In this chapter, we investigate the bifractality in broader classes of FSFNs, which are constructed by the network models discussed in Ch. 4. As we will see, the FSFNs generated by these models are bifractal. In fact, these results suggest that any FSFN displays a bifractal property.

6.1 Deterministic Model of Hierarchical Fractal Scale-free Networks

In this section, we derive analytically the bifractality of the deterministic model of hierarchical fractal scale-free networks (HFSFNs) explained in Sec. 4.3.1. To conduct the multifractal analysis of the model, we first select an appropriate renormalization (box-covering) method and then derive the necessary relation in Sec. 6.1.1. Using this relation, we determine in Sec. 6.1.2 the bifractality of networks formed by this model. We then identify the relations between local structures and two fractalities of the bifractal networks numerically in the following subsection. The last argument is supported by an analytical calculation in the (simplest) case of $(2, 2)$ -flower.

6.1.1 Renormalization Scheme

Consider renormalizing the t -th generation network \mathcal{G}_t by subgraphs with a fixed diameter in a manner which the subgraphs (supernodes) constitute the

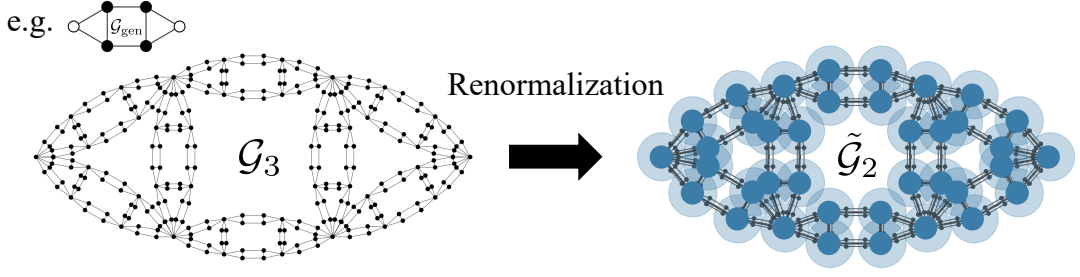


Figure 6.1: The example of renormalization for the deterministic model of fractal scale-free networks. The left figure is the third generation network constructed from the generator at the upper left. The right figure shows the renormalization scheme in which boxes constitute the network structure of the earlier generation.

t' -th generation network $\mathcal{G}_{t'}$ where $0 < t' < t$. See Fig. 6.1. The degree of supernode i in the renormalized network $\tilde{\mathcal{G}}_{t'}$ is given by

$$k_i = k_{0i}\kappa^{t'-t_i} \quad (6.1)$$

where t_i is the generation at which node i first appears in \mathcal{G}_t as a non-root node of degree k_{0i} and κ is the degree of the root node in the generator. The number of nodes $\nu(k_i)$ included in supernode i of the degree k_i in the renormalized network $\tilde{\mathcal{G}}_{t'}$ can be considered as the number of newly added nodes around the supernode i during $(t - t')$ inverse renormalization operations (i.e. operations to replace each edge with the generator) from $\tilde{\mathcal{G}}_{t'}$ to $\tilde{\mathcal{G}}_t$.

In the first operation from $\tilde{\mathcal{G}}_{t'}$ to $\tilde{\mathcal{G}}_{t'+1}$, half of edges and nodes in the generator are added to one of the terminal supernodes of the replaced edge and the other half belong to the other. Here, the partitionings of edges and nodes do not have to be exactly half, as long as the diameters of the subgraphs (subgraph i is a graph composed of nodes belonging to supernode i at the first inverse renormalization step) are the same and the topology of subgraphs with the same supernode degree is equivalent to one another. Let $m_{\text{gen}}^{\text{half}}$ and $n_{\text{gen}}^{\text{half}}$ be the numbers of edges and nodes, added to the i -th supernode in this operation. Then, the number of nodes and edges included in the i -th supernode of $\tilde{\mathcal{G}}_{t'+1}$ are given as $1 + k_i n_{\text{gen}}^{\text{half}}$ and $k_i m_{\text{gen}}^{\text{half}}$, respectively.

In the \tilde{t} -th operation ($2 \leq \tilde{t} \leq t - t'$), every edge belonging to the i -th supernode in the previous operation is replaced by the generator. Thus, the number of edges $m_i^{(\tilde{t})}$ in the i -th supernode at the \tilde{t} -th operation is expressed as

$$m_i^{(\tilde{t})} = m_{\text{gen}} m_i^{(\tilde{t}-1)}, \quad (6.2)$$

where m_{gen} is the number of edges in the generator. The number of nodes $n_i^{(\tilde{t})}$ in the i -th supernode added during the \tilde{t} -th operation is given by

$$n_i^{(\tilde{t})} = n_{\text{nr}} m_i^{(\tilde{t}-1)}, \quad (6.3)$$

where n_{nr} is the number of non-root nodes in the generator. By solving the above recurrence relations, the number of nodes belonging to the i -th supernode is calculated as

$$\begin{aligned} \nu(k_i) &= 1 + k_i \left(n_{\text{gen}}^{\text{half}} + \sum_{\tilde{t}=2}^{t-t'} n_i^{(\tilde{t})} \right) \\ &= 1 + k_i \left(n_{\text{gen}}^{\text{half}} + n_{\text{nr}} m_{\text{gen}}^{\text{half}} \sum_{\tilde{t}=2}^{t-t'} m_{\text{gen}}^{\tilde{t}-1} \right). \end{aligned} \quad (6.4)$$

In the thermodynamic limit $t \rightarrow \infty$, the first term (unity) is negligible and we obtain the relation $\nu(k_i) \propto k_i$. The index i of the above relation indicates the supernode number in the renormalized network $\tilde{\mathcal{G}}_{t'}$. In order to clarify that each supernode corresponds to a box of size $l (= L_{t-t'})$, let us relabel k_i as k_{b_l} , whose index means a box in the box-covering by boxes of size l . We thus derive the relation

$$\nu(k_{b_l}) \propto k_{b_l}. \quad (6.5)$$

This relation guarantees bifractality of deterministic HFSFNs shown in Sec. 4.3.1, because Eq. (6.4) is equivalent to Eq. (5.34).

Note that this renormalization scheme gives the fractal dimension in a box-covering sense. The number $N_b^t(t')$ of boxes in this scheme is, as stated above, equal to the number of supernodes in the renormalized network $\tilde{\mathcal{G}}_{t'}$, i.e.

$$N_b^t(t') = N_{t'} \simeq \frac{n_{\text{nr}} m_{\text{gen}}^{t'}}{m_{\text{gen}} - 1}, \quad (6.6)$$

where $N_{t'}$ is the number of nodes of the t' -th generation network in the deterministic model of HFSFNs. The second approximation is valid when the network is sufficiently large, $t \gg 1$. The box size $L_b^t(t')$ in this covering scheme is the diameter of $(t - t')$ -th generation network, i.e.

$$L_b^t(t') = L_{t-t'} \simeq \lambda^{t-t'}. \quad (6.7)$$

Taking the logarithms of Eqs. (6.6) and (6.7) and their derivatives with regard to

t' , we derive the fractal dimension

$$\begin{aligned} D_f^{bc} &= -\frac{d \log N_b^t(t')}{d \log L_b^t(t')} \\ &= -\frac{\frac{d}{dt'} \log \left(\frac{n_{nr}}{m_{gen}-1} m_{gen}^{t'} \right)}{\frac{d}{dt'} (t - t') \log \lambda} \\ &= \frac{\log m_{gen}}{\log \lambda}. \end{aligned} \quad (6.8)$$

This fractal dimension in a box-covering sense is equal to the fractal dimension in a cluster-growing sense from Sec. 4.3.1.

6.1.2 Mass Exponents

Since the scale-free exponent γ and the fractal dimension D_f of the networks generated by the deterministic model of HFSFNs are given as

$$\gamma = 1 + \frac{\log m_{gen}}{\log \kappa}, \quad D_f = \frac{\log m_{gen}}{\log \lambda} \quad (6.9)$$

respectively, the mass exponent is obtained as

$$\tau(q) = \begin{cases} (q-1) \frac{\log m_{gen}}{\log \lambda} & \text{if } q < \frac{\log m_{gen}}{\log \kappa}, \\ q \frac{\log m_{gen} - \log \kappa}{\log \lambda} & \text{if } q \geq \frac{\log m_{gen}}{\log \kappa}. \end{cases} \quad (6.10)$$

We therefore have derived the bifractality of the deterministic model of HFSFNs. Note from Eq. (6.10) that the difference in the slopes of the mass exponents in the two regions of the distortion factors is determined by the degree κ of the root nodes in a generator. When the value of κ is large, the change in slope is drastic. Since κ is a parameter which determines the scale-free property of the networks in this model, the bifractality is significantly influenced by its scale-free property. Reminding that the greater value of κ results in the smaller value of scale-free exponent γ , we can understand that the degree to which an FSFN is scale-free determines how "bifractal" it is.

In order to confirm Eq. (6.10), we numerically computed the mass exponents for networks formed from various generators by the means of the sandbox method proposed by Liu et al.[45, 52]. The algorithm used for numerical computations is explained in Appendix B.2.1.

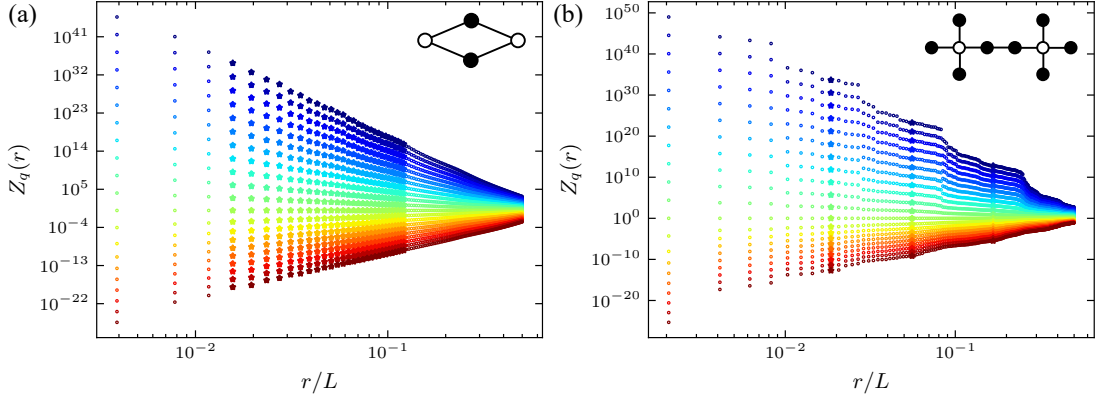


Figure 6.2: The plots of q -th moments $Z_q(r)$ for the generators at the top right corner of each figure. The circles indicate the mean $Z_q(r)$ values and the stars show the points used for fitting of $\tau(q)$. The blue points are of $q = -10.0$ and the red points are of $q = 10.0$. The colors between blue and red are of integer q values between -10.0 and 10.0 . The profiles of $Z_q(r)$ vary between generators and the right figure is one of the worst cases.

The computed q -th moment $Z_q(r)$ for two generators are shown in Fig. 6.2. The linearity of q -th moment in log-log plots strongly depends on generator structures. In fact, the partition function $Z_q(r)$ in Fig. 6.2(a) is quite linear for any q , while that in Fig. 6.2(b) contains periodic steps. Note that the scaling of the q -th moment of the networks nonetheless agrees with theory. The steps in the q -th moment worsen for HFSFNs formed from generators with more edges which are not in paths connecting the two root nodes.

The mass exponents for ten generators are shown in Fig. 6.3. Numerically computed results of mass exponents agree quite well with theoretical predictions. The detailed results for eighteen different generators are also presented in Appendix D.

6.1.3 Distribution of Lipschitz-Hölder Exponents

Now that we have confirmed the bifractality of HFSFNs formed by the deterministic model, we will look into the relation between the network structures and the bifractal property. Reminding that the Lipschitz-Hölder exponents α can be derived by

$$\alpha = \frac{d\tau(q)}{dq}, \quad (6.11)$$

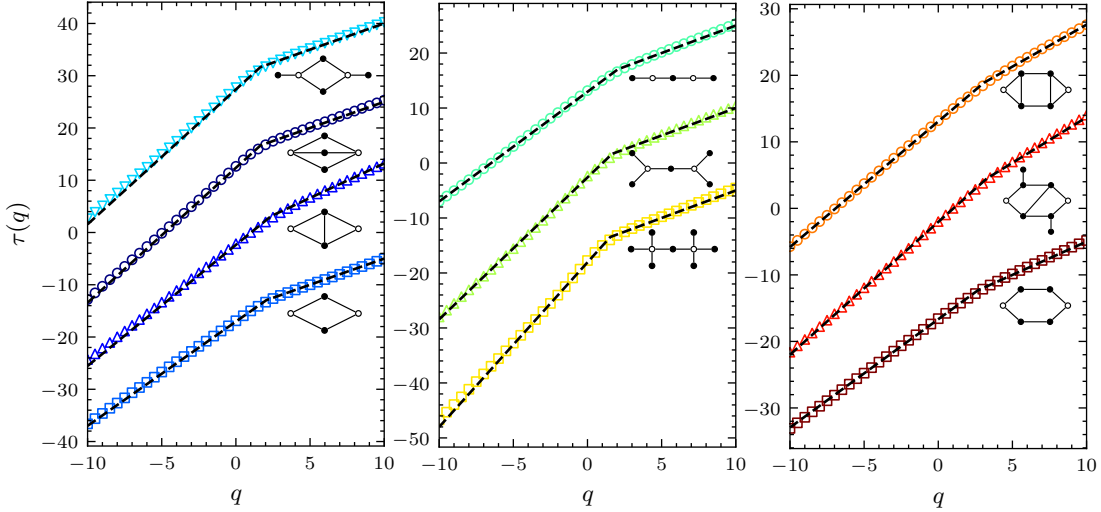


Figure 6.3: The plots of mass exponents $\tau(q)$ against distortion factor q for various generators. The dotted lines are the theoretical lines, and the symbols indicate the numerical values.

there must be two distinct values of α in bifractal networks, as we see the two distinct slopes of $\tau(q)$ for each bifractal network. We visited, in Sec. 5.1, that the Lipschitz-Hölder exponents indicate the local fractality in a cluster growing sense, i.e.

$$m(l) \propto l^\alpha \quad (6.12)$$

where $m(l)$ is the mass (the number of nodes) in a box of size l . Hence, we should be able to observe the distribution of Lipschitz-Hölder exponents^{*1} in a bifractal network by visualizing with colors the Lipschitz-Hölder exponent of the box centered at every node.

The distributions of Lipschitz-Hölder exponents can be numerically computed in a network as follows: for each node $i \in V$ of a given network,

- (1) Conduct the breadth-first-search (BFS) from node i .
- (2) Count the number of nodes $\nu_i(r)$ at distance r ($1 \leq r \leq L$) from node i .
- (3) Compute the mass of the box centered at node i for each radius r by taking the sum of $\nu_i(r')$ for $1 \leq r' \leq r$.

$$m_i(r) = \sum_{r'=1}^r \nu_i(r') \quad (6.13)$$

^{*1}It is also referred to as the node-based fractal dimension[53].

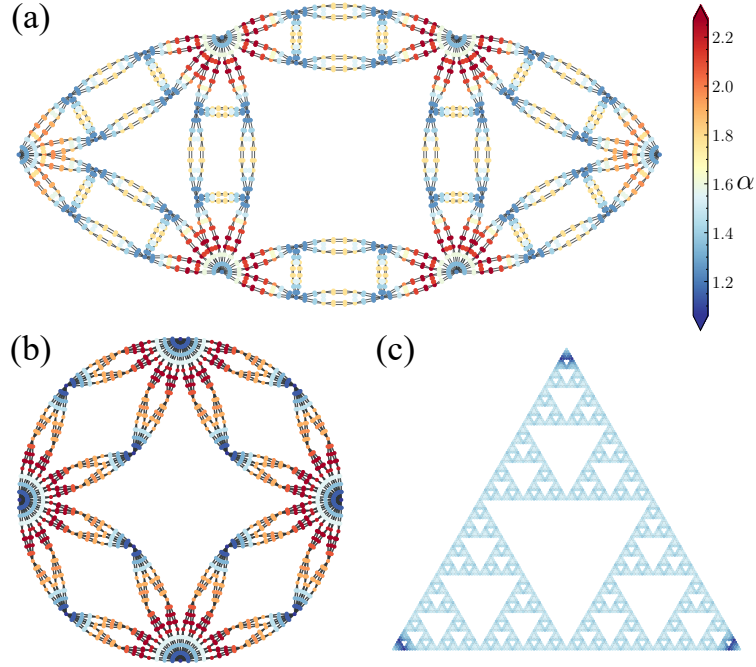


Figure 6.4: The distributions of Lipschitz-Hölder exponents in (a)-(b) bifractal and (c) unifractal networks. The color map on the right-hand side indicates the correspondence between the node colors and the Lipschitz-Hölder exponents in all the three networks. Lipschitz-Hölder exponents in (a)-(c) are numerically computed with the masses in the interval between the two radii which correspond to 5 and 20 percent of the network diameters.

- (4) Determine the Lipschitz-Hölder exponent α_i for the box centered at node i by fitting linearly logarithm of the mass $m_i(r)$ and logarithm of the radius r in the range of 5% to 20 % of the diameter.

The results of the numerical calculation are shown in Fig. 6.4. The color of each node indicates value of the Lipschitz-Hölder exponent of the box centered at that node. First thing to note from Fig. 6.4 is that the boxes centered near the hubs, in both of the bifractal networks (a) and (b), tend to have lower Lipschitz-Hölder exponents while the boxes at the regions between the hubs have higher Lipschitz-Hölder exponents. On the other hand, the Lipschitz-Hölder exponents in the Sierpinski network, a unifractal network with fixed degrees $k_i = 4$ for $\forall i \in V$ and fractal dimension $D_f = \frac{\log 3}{\log 2}$, are uniformly distributed (with exception of the three corners). The comparison of the HFSFNs and the Sierpinski network also allows us to reconfirm the bifractality, as the bifractal HFSFNs are clearly

characterized by two distinct fractalities while the unifractal Sierpinski network is characterized by single fractality.

To further our understanding of the relation between network structures and their bifractalities, let us analytically derive the two distinct Lipschitz-Hölder exponents for boxes near the hubs and the non-hubs in the (u, v) -flower. To this end, the number of nodes in a box for the box-covering scheme II explained in Sec. 4.1 shall be utilized. In this box-covering scheme, each box size is set to the diameter of the m -th generation (u, v) -flower (where $1 \leq m \leq n$), given by

$$L_m = \left(\frac{u+v}{2} + \frac{v-u}{u-1} \right) u^{m-1} - \frac{v-u}{u-1}. \quad (6.14)$$

In addition, denote ν_m the number of m -th generation (u, v) -flower,

$$\nu_m = \frac{u+v-2}{u+v-1} (u+v)^m + \frac{u+v}{u+v-1}. \quad (6.15)$$

The number of nodes $\nu_s(L_m)$ in the box of the size L_m , centered at the s -th largest hub ($1 \leq s \leq n-m$) can be added up by taking the followings into account:

- the number of the m -th generation (u, v) -flowers connected to the largest hub is 2^{n-m} ,
- the s -th largest hub has 2^{s-1} less m -th generation (u, v) -flowers connected to it, and
- only half of the nodes of each m -th generation (u, v) -flower belong to the box.

Therefore,

$$\nu_s(L_m) = 2^{n-m-s} \nu_m + 1. \quad (6.16)$$

The unity is for the hub node at the center of the box.

Since Eq. (6.14) becomes simpler in the case of $u = v$, let us consider the case of $u = v = 2$, hence

$$L_m = 2^m. \quad (6.17)$$

Similarly, Eq. (6.15) is simplified as

$$\nu_m = \frac{2^{2m+1} + 4}{3}, \quad (6.18)$$

and if m is sufficiently large, i.e. $m \gg 1$,

$$\nu_m \sim \frac{2^{2m+1}}{3}, \quad (6.19)$$

thus the number of nodes $\nu_s(L_m)$ in the box of the size L_m , centered at the s -th largest hub for $(2, 2)$ -flower is

$$\nu_s(L_m) \sim \frac{1}{3} 2^{n+m-s+1}. \quad (6.20)$$

Using Eq. (6.17), Eq. (6.20) is rewritten in terms of L_m ,

$$\nu_s(L_m) \sim \frac{1}{3} 2^{n-s+1} L_m \sim L_m \quad (6.21)$$

In the end, the Lipschitz-Hölder exponent is obtained as

$$\alpha_{\text{hub}} = 1. \quad (6.22)$$

Without the assumption that $m \gg 1$, Eq. (6.20) is as follows;

$$\nu_s(L_m) = 2^{n+m-s+1-\log_2 3} + 2^{n-m-s+2-\log_2 3} + 1. \quad (6.23)$$

Now that the Lipschitz-Hölder exponent of the box centered near the hubs is determined, next we must identify another Lipschitz-Hölder exponent of the boxes centered at the other parts of the $(2, 2)$ -flower (which we call the non-hubs). The analytical calculation of the Lipschitz-Hölder exponent of the boxes centered at the non-hubs is difficult, as the non-hub regions are hard to define. It is however reasonable to argue that the Lipschitz-Hölder exponent of the boxes at the non-hubs must be equal to the global fractal dimension $D_f = 2$ of $(2, 2)$ -flower because $(2, 2)$ -flower as a whole is, as mentioned in Sec. 4.1, characterized by $D_f = 2$. Since the majority of nodes in the network is the non-hubs, it is consistent that the fractal dimension of the entire network matches the Lipschitz-Hölder exponent of the boxes near the non-hub nodes. Thus, we can conclude

$$\alpha_{\text{non-hub}} = D_f = 2. \quad (6.24)$$

The above argument is numerically confirmed as shown in Fig. 6.5.

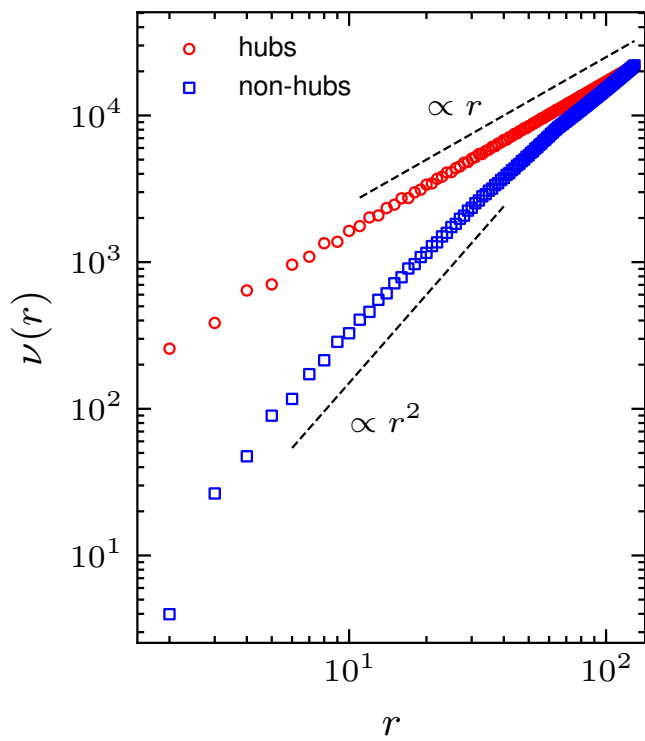


Figure 6.5: The Lipschitz-Hölder exponents of the boxes centered at the hubs (red) and the non-hubs (blue). That of the non-hubs is the average over all the non-hub nodes.

6.2 Stochastic Model of Hierarchical Fractal Scale-free Networks

We have shown, in the previous section, the bifractality of the deterministic model of HFSFNs and the relation between the bifractality and the network structures. Though the deterministic model is a model of a broad class of HFSFNs, real-world FSFNs are unlikely to be formed by the inverse renormalization based on a single generator. In fact, it is more likely that real-world FSFNs are formed iteratively by multiple structural units. In addition, fractal dimension D_f and scale-free exponents γ of a constructed network is limited because they are, as explained in Sec. 4.3.1, computed from integer m_{gen} , κ and λ . To investigate an even broader class of HFSFNs, we conducted the multifractal analysis of the stochastic model explained in Sec. 4.3.2.

We conducted the multifractal analysis of the HFSFNs generated by the stochastic model. In this analysis, we first generate a sample of fifty networks for a given set of generators and their corresponding probabilities. For each network, the sandbox algorithm is applied to compute its partition functions $Z_q(r)$. We then take the mean $\langle Z_q(r) \rangle$ of the partition functions $Z_q(r)$ for q and r . Finally we obtain the mass exponent $\tau(q)$ for the stochastic HFSFNs model.

The results of the multifractal analyses on the 5-, 6-, and 7-th generation HFSFNs with a generator pair of (2, 2)-flower and Song-Havlin-Makse model with $t = 2$ and the corresponding pair of probabilities (0.5, 0.5) are shown in Fig. 6.6. The mass exponents at $q < \gamma - 1$ agree well with the line computed from their fractal dimension and scale-free exponent. On the contrary, the mass exponents at $q > \gamma - 1$ are off from the line. Despite the shifts from the line, as the number of generation increases, the data are approaching the line. Furthermore, we can confirm that the points at which the mass exponents bend are also approaching the theoretical threshold with increasingly sharp transitions. The shifts from the theory at $q > \gamma - 1$ are likely to be caused by the finite size effects, because the hubs in the numerical calculation have not grown sufficiently. To better see this, we have shown in Fig. 6.6(b) the second derivatives of the mass exponents. The curvature of the theoretical mass exponent diverges at $q = \gamma - 1$ and remains zero at $q \neq \gamma - 1$. As the number of generation increases, i.e. the number of nodes grows, the q values which correspond to the minimum of the curvature approach the theoretical divergence point. The explanation by the finite size effect is consistent with the fact that the mass exponents aligned well at $q < \gamma - 1$ as the mass exponents at $q < \gamma - 1$ correspond to the fractality of the boxes at the non-hub nodes. The data indicate that the mass exponent in the thermodynamic limit perfectly aligns with the theoretical one and suggest that the stochastic model of HFSFNs is also bifractal.

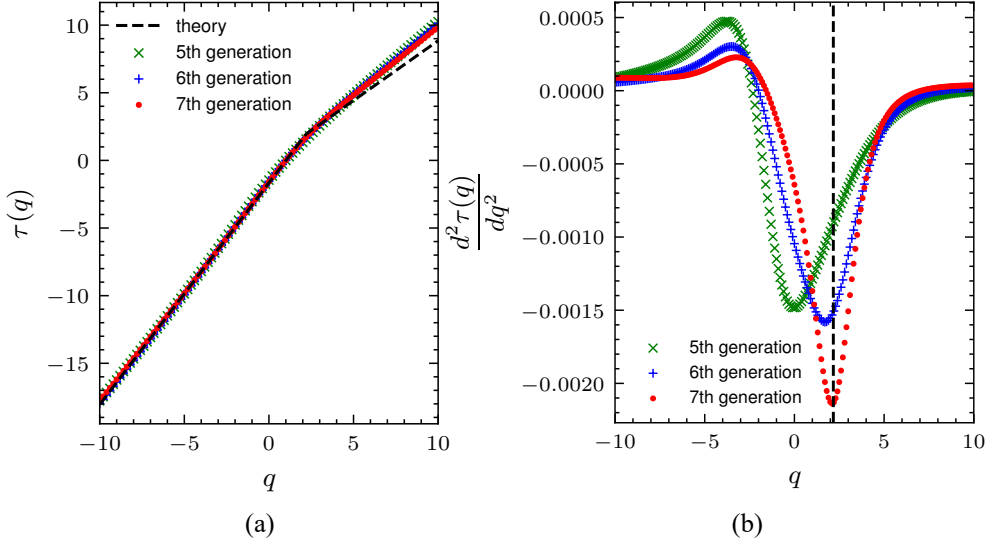


Figure 6.6: The mass exponents (left) and their second derivatives (right) for the two-generator stochastic hierarchical fractal scale-free networks of 5- (green), 6- (blue), and 7-th (red) generation. The generators of (2, 2)-flower and Song-Havlin-Makse model with $t = 2$ are selected equally with probability of 0.5. The dashed line on the left panel shows the theoretical line calculated from its fractal dimension and scale-free exponent. The dashed line on the right panel shows the theoretical point q at which the slope of its mass exponent changes.

We have additionally conducted the multifractal analyses of the stochastic HFSFNs with varying stochasticities. We used the same pair of generators as the previous result. The pairs (p, q) of probabilities were varied from $(0.1, 0.9)$, $(0.3, 0.7)$, $(0.5, 0.5)$, $(0.7, 0.3)$, to $(0.9, 0.1)$. The first probability of each pair is the probability that the generator of (2, 2)-flower replaces an edge of the previous generation. The result is shown in Fig. 6.7.

In all the five cases, the mass exponents generally agree with the theory. We notice, however, that the mass exponents at $q > \gamma - 1$ are slightly off from the theoretical lines, as was the case for Fig. 6.6. As stated before, the shifts are due to the finite size-effects. This is also supported by the fact that the mass exponent for the probability pair $(0.1, 0.9)$ matches the theoretical line best, because the networks with that probability pair most resemble (2, 2)-flower which does not have boundaries due to its loopiness and hence the finite-size effect influences our numerical calculation least.

We further investigated the bifractality of the stochastic model with three generators. The three generators employed are shown in Fig. 6.8(a). Every edge in the previous generation network is replaced by one of the three generators

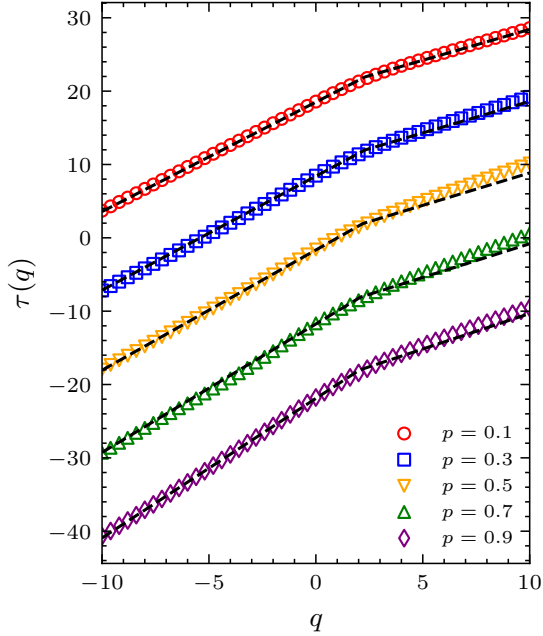


Figure 6.7: The probability dependence of the mass exponents of the stochastic model of hierarchical fractal scale-free networks. The mass exponents of HFSFNs with probability sets $(0.1, 0.9)$, $(0.3, 0.7)$, $(0.5, 0.5)$, $(0.7, 0.2)$, and $(0.9, 0.1)$ are shown by red circles, blue squares, yellow downside triangles, green upside triangles, and purple diamonds, respectively. The dashed lines are the corresponding theoretical mass exponents for each probability pair. For visualization purpose, the mass exponents are shifted vertically.

with an equal probability of $1/3$. As was the case with HFSFNs with two generators, the mass exponents of the three-generator HFSFNs obtained numerically fit the theoretical line well. In fact, the obtained result aligned better than that of the two-generator case. This appears to be a result of the choice of the three generators, because all the three generators have the same root node distance λ . Such choices of generators enable more reliable multifractal analyses even in HFSFNs of younger generations. Similar to the case of the two-generator model, the second derivatives of the mass exponents shown in Fig. 6.8(b) also supports the bifractality, as the divergence point of the curvature is approaching the theoretical one.

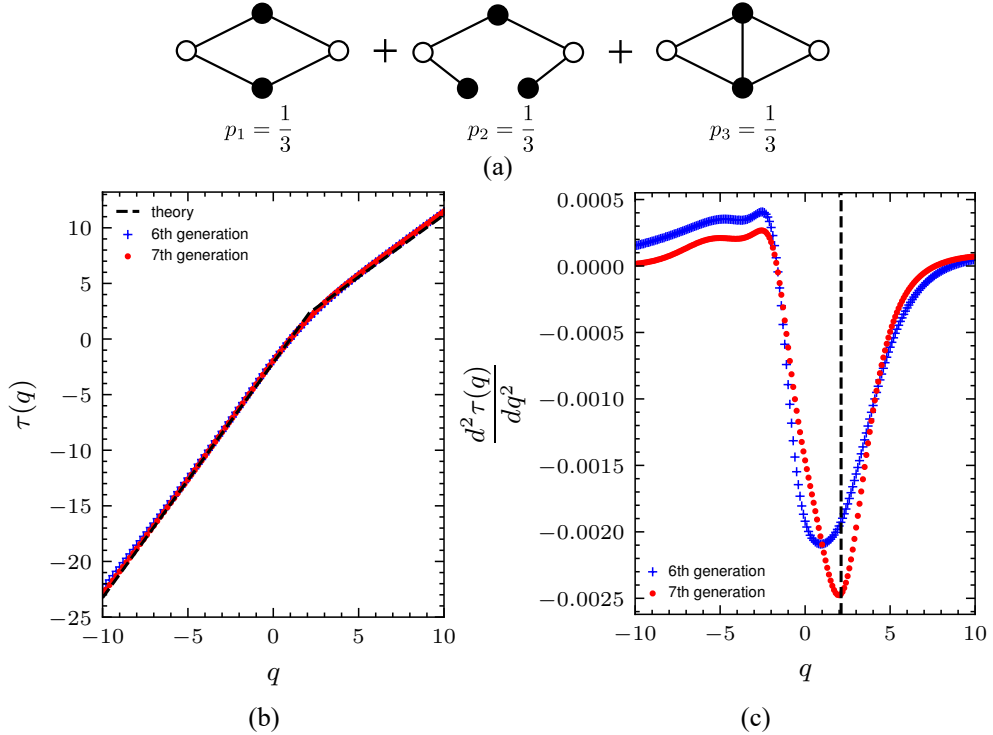


Figure 6.8: The mass exponents (b) and their second derivatives (c) for the three-generator stochastic hierarchical fractal scale-free networks of 6- (blue) and 7-th (red) generation. The generators shown in (a) are selected equally with probability of $1/3$. The dashed line on the left panel shows the theoretical line calculated from its fractal dimension and scale-free exponent. The dashed line on the right panel shows the theoretical point q at which the slope of its mass exponent changes.

6.3 Fractal Scale-free Random Graphs

We have, so far, considered fractal scale-free networks generated in hierarchical manners. Our results indicate that a broad class of hierarchically-formed FSFNs is characterized by the bifractal structures. To consider an even wider class of FSFNs, we further investigate the bifractality of fractal scale-free random graphs (FSFRGs) which are not formed hierarchically.

As we will see, our results show that FSFNs are bifractal even in the absence of hierarchy. We close this section with our conjecture that any FSFN is bifractal.

6.3.1 Proof of Bifractality

To show analytically the bifractality of the FSFRGs, let us consider an uncorrelated scale-free random graph. The conditional probability $P(k'|k, l)$ that a node at distance l from a node of degree k has degree k' is then given by

$$P(k'|k, l) = Q(k'|l) = \frac{k' P(k')}{\langle k \rangle} \quad (6.25)$$

in the uncorrelated case[80]. The average degree $\langle k \rangle_l$ of nodes at distance l is thus

$$\langle k \rangle_l = \int k' P(k'|k, l) dk' = \frac{\langle k^2 \rangle}{\langle k \rangle}. \quad (6.26)$$

Reminding that $\frac{\langle k^2 \rangle}{\langle k \rangle} = 2$ at criticality, we obtain $\langle k \rangle_l = 2$ at criticality. That is, the nodes at distance l are on average connected to two nodes, thus forming a tree graph with long chains.

To count the number of nodes within distance l from a k -degree node, we first need to identify the number $n_r(k)$ of nodes whose distances from a k -degree node (center), is exactly r . We call the set of nodes whose distance from the center is r as the r -shell of that center. If the number $n_r(k'|k)$ of k' -degree nodes in the r -shell is known, $n_r(k)$ can be solved by

$$n_r(k) = \sum_{k'} n_r(k'|k). \quad (6.27)$$

Using the relation^{*2}

$$n_r(k'|k) = \frac{kk'}{\langle k \rangle^r} \left(\langle k^2 \rangle - \langle k \rangle \right)^{r-1} P(k'), \quad (6.28)$$

^{*2}See Appendix C for its derivation.

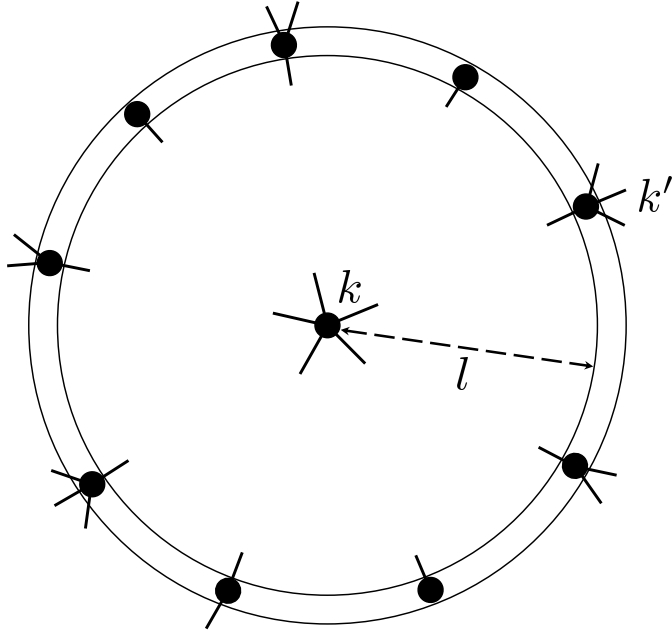


Figure 6.9: Conceptual illustration of $n_l(k')$. In this example, for $k' = 4$, $n_l(k') = 2$.

we derive

$$\begin{aligned}
 n_r(k) &= \sum_{k'} n_r(k'|k) \\
 &= \frac{k}{\langle k \rangle^r} \left(\langle k^2 \rangle - \langle k \rangle \right)^{r-1} \sum_{k'} k' P(k') \\
 &= k \left(\frac{\langle k^2 \rangle}{\langle k \rangle} - 1 \right)^{r-1}.
 \end{aligned} \tag{6.29}$$

Again, at criticality, we have $\frac{\langle k^2 \rangle}{\langle k \rangle} = 2$. Hence, we get

$$n_r(k) = k. \tag{6.30}$$

Finally, we obtain the desired relation by summing up the r -shells from $r = 1$ to $r = l$,

$$\nu_l(k) = \sum_{r=1}^l n_r(k) + 1 = kl + 1. \tag{6.31}$$

The second term (unity) is the count for the center node. In the thermodynamic limit, the unity is negligible and we obtain $\nu_l(k) \propto k$, namely Eq. (5.34).

From the above argument, if we box-cover the FSFRGs by forming boxes of size l centered at k -degree nodes, the relation $\nu(k_l) \propto k_l$ is satisfied because the k -degree nodes possess k long chains, which mean that the boxes centered at those k -degree nodes have k adjacent boxes. Since the relation $\nu(k_l) \propto k_l$ stands for FSFRGs, we have the mass exponents of FSFRGs as

$$\tau(q) = \begin{cases} (q-1)D_f & \text{if } q < \gamma' - 1, \\ qD_f \frac{\gamma' - 2}{\gamma' - 1} & \text{if } q > \gamma' - 1. \end{cases} \quad (6.32)$$

From Eq. (6.32), we also obtain

$$\alpha = \begin{cases} D_f & \text{if } q < \gamma' - 1, \\ D_f \frac{\gamma' - 2}{\gamma' - 1} & \text{if } q > \gamma' - 1. \end{cases} \quad (6.33)$$

By substituting the fractal dimension in Eq. (4.79), we have α_{\max} and α_{\min} as

$$\alpha_{\max} = \begin{cases} \frac{\gamma' - 1}{\gamma' - 2} & \text{if } 2 < \gamma' < 3, \\ 2 & \text{if } \gamma' > 3, \end{cases} \quad (6.34)$$

$$\alpha_{\min} = \begin{cases} 1 & \text{if } 2 < \gamma' < 3, \\ \frac{2(\gamma' - 2)}{\gamma' - 1} & \text{if } \gamma' > 3. \end{cases} \quad (6.35)$$

Therefore, we have shown that FSFRGs are also bifractal. Figure 6.10 shows the scale-free exponent dependence of the two Lipschitz-Hölder exponents in FSFRGs. It is important to confirm that the two exponents will converge to a single value in the limit $\gamma' \rightarrow \infty$, thus the network will be characterized by a single fractality in the absence of scale-free property.

6.3.2 Numerical Confirmation of Bifractality

Network Formation

We generated FSFRGs with a given scale-free exponent and a given fractal dimension in the following manner.

- (1) Numerically solve for d and C while satisfying the relation

$$\frac{\langle k^2 \rangle}{\langle k \rangle} = 2, \quad (6.36)$$

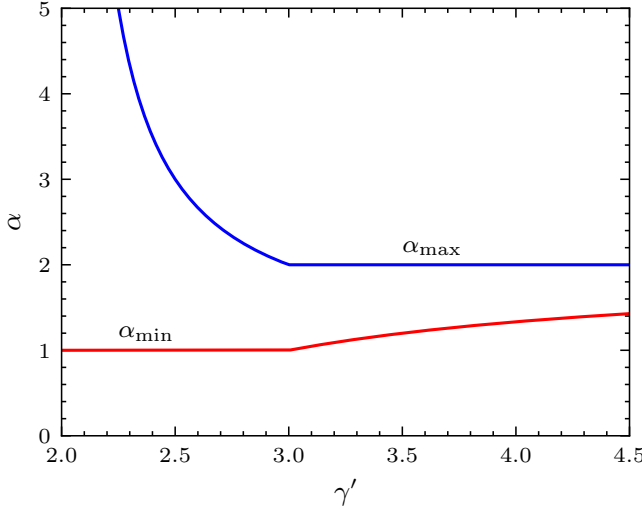


Figure 6.10: The γ' -dependence of the maximum (blue) and minimum (red) Lipschitz-Hölder exponents of FSFRGs.

with the degree distribution in the form of

$$P(k) = \frac{C}{k^\gamma + d^\gamma} \quad (6.37)$$

and the normalization condition of $P(k)$. Let us denote the critical value of d by d_c .

- (2) Generate a degree sequence which follows the distribution in Eq. (6.37) with $d = d_c$.^{*3}
- (3) Form a generalized random graph with the degree distribution (6.37).
- (4) Extract the giant component of the generated graph.

The scale-free exponent and the fractal dimension of the resulting FSFRGs are, respectively, Eq. (4.76) and (4.79) in Sec. 4.4.3. We can confirm in Fig. 6.11 that the FSFRGs generated by the above procedure do agree with the theory.

Numerical Multifractal Analysis

The multifractal analyses of FSFRGs are conducted numerically with the sand-box algorithm. Figure 6.12 shows the mass exponents and their second derivatives of FSFRGs with the scale-free exponent $\gamma = 2.75$ and the fractal dimension

^{*3}In order to generate a larger giant component, shift the parameter d to the order phase slightly, i.e. make d slightly larger than d_c .

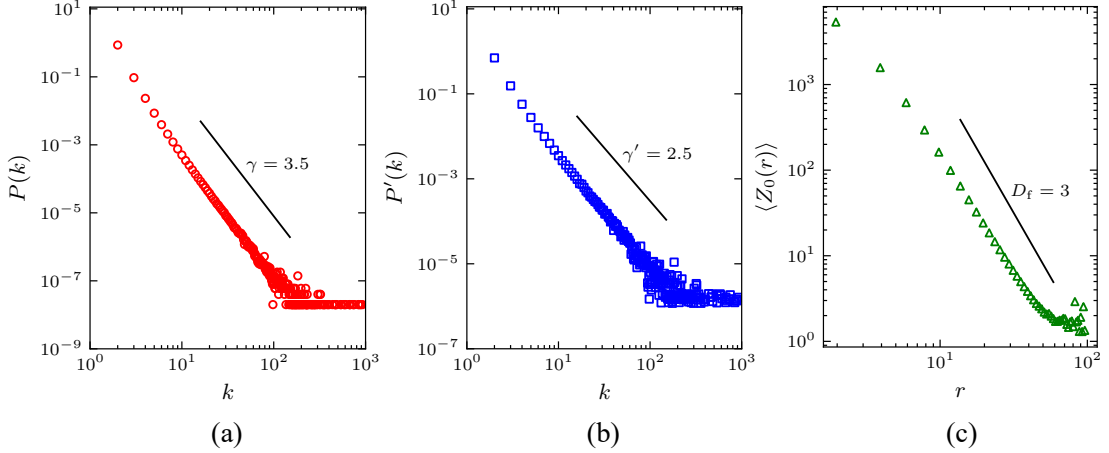


Figure 6.11: (a) The degree distribution $P(k)$ of the original scale-free random graph with 100000 nodes and scale-free exponent $\gamma = 3.5$, (b) the degree distribution $P'(k)$ and (c) the partition function $Z_0(r)$ of the FSFRG. The line in each panel shows the theoretical slope of each plot.

$D_f = \frac{7}{3} \approx 2.33$. The data are calculated from the mean partition functions of fifty sample networks. Similar to the results for the stochastic model of HFSFNs, the numerical results in the range $q < \gamma - 1$ aligned well while the numerical results in the range $q > \gamma - 1$ shifted slightly from the theoretical slope. Nonetheless, the numerical results are approaching the theoretical line with increasing network sizes. From Fig. 6.12(b), the transition of the slopes occurs more steeply for the larger FSFRGs and the transition points are also approaching the theoretical one. The results suggest that the numerical results coincide with the theoretical prediction in the thermodynamic limit. The results show in Fig. 6.12 support the analytical result in Sec. 6.3.1. We can therefore conclude that FSFRGs are also bifractal.

6.4 Discussion

We have so far conducted the multifractal analysis of FSFNs of the three different types of models. As was the case for the networks generated by (u, v) -flower and Song-Havlin-Makse model in the prior work by Furuya and Yakubo, the networks formed by a general deterministic model of FSFNs have been shown analytically to possess the bifractality. In addition, the networks generated by a general stochastic model and a non-hierarchical model of FSFNs display the bifractal structures.

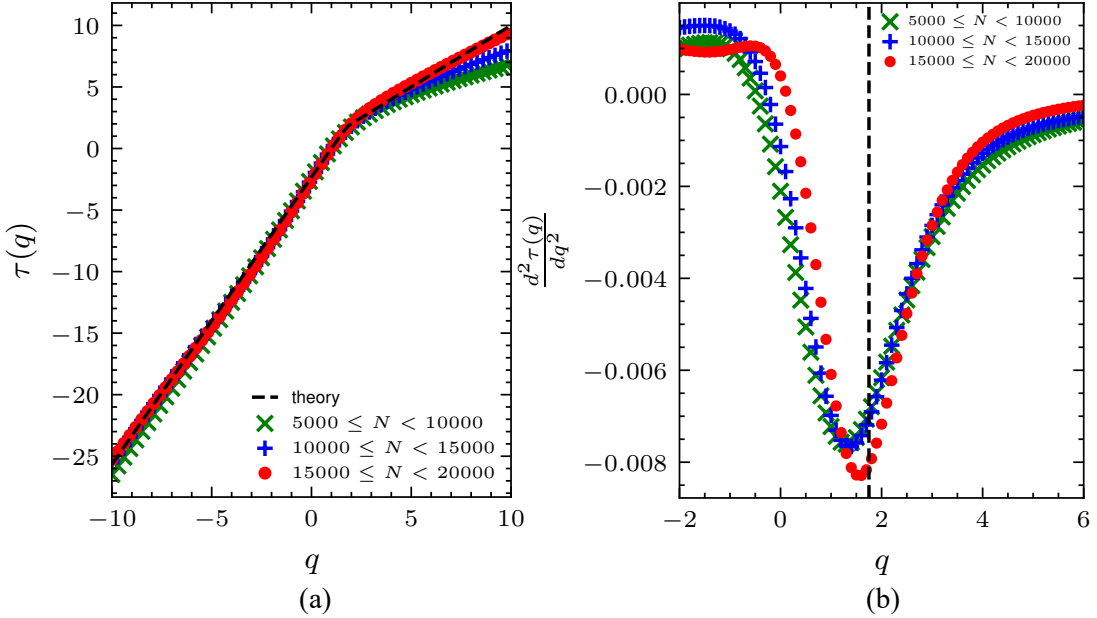


Figure 6.12: The mass exponents (a) and their second derivatives (B) of FSFRGs with scale-free exponent $\gamma = 2.75$ and fractal dimension $D_f = 7/3$ for varying network sizes. The green, blue, and red points are the mass exponents of the FSFRGs for $5000 \leq N < 10000$, $10000 \leq N < 15000$ and $15000 \leq N < 20000$. The dashed line in (a) is the theoretical mass exponent in Eq. (6.32). The dashed line in (b) is the theoretical threshold at which the slopes of the mass exponent change.

The bifractality of these FSFNs relates to the local structures as follows: one of the two fractalities corresponds to the fractality of the subgraphs near the hubs and the other corresponds to that of the subgraphs distant from the hubs. To be precise, the bifractality of FSFNs is exact in the thermodynamic limit of $N \rightarrow \infty$. Thus, in the thermodynamic limit, one of the two fractalities, namely the minimum Lipschitz-Hölder exponent is distributed on the subgraphs centered at the hubs of infinite degrees (infinite hubs), while the other, namely the maximum Lipschitz-Hölder exponent is distributed on the subgraphs centered at the finite-degree nodes which are infinitely distant from the infinite hubs.

The three models cover a quite diverse class of FSFNs, hierarchical and non-hierarchical ones. Hence, we conjecture that any FSFN exhibit the bifractality, with the same correspondence between the bifractality and the local structures of FSFNs as those of the three models. This hints that the diffusion on any FSFN is characterized by two anomalous diffusions, one for the hubs and the other for

the non-hubs. Further investigation into the dynamics on the bifractal networks is necessary to reveal the implications of the bifractality.

Chapter 7

Conclusion

This work attempted to clarify whether a more comprehensive class of FSFNs is characterized by the bifractality proposed by Furuya and Yakubo, and how the bifractality relates to the local structures of FSFNs.

In order to achieve our goals, we conducted the multifractal analysis of FSFNs generated by the three types of models: the general deterministic and stochastic models of hierarchical FSFNs and fractal scale-free random graphs. The three models cover an extensively wide range of FSFNs and the three models likely simulate the ways by which real-world FSFNs are formed. We found that the FSFNs formed by the three models all display the bifractal property and the bifractality correspond to the two distinct fractalities of the near-hub and near-non-hub structures. The fact that all three models form the bifractal FSFNs indicates that neither the presence of multiple generators nor the hierarchy removes the bifractality of FSFNs. That is, the bifractality of FSFNs is a much more widely existent property.

From the above results, we proposed a conjecture that any FSFN takes the bifractal structure characterized by two distinct fractalities of the hubs and non-hubs. This implies that the dynamics on FSFNs, for example, can consist of two distinctive ones near the hubs and the non-hubs. For instance, if we consider a diffusion in FSFNs, there may exist two anomalous diffusions whose mean square distance differ qualitatively near the hubs and near the non-hubs. Such an implication can possibly influence various dynamics on real-world FSFNs such as the World Wide Web and protein-protein interaction networks. It is important that we further investigate the relation between the bifractality of FSFNs and its dynamics.

Acknowledgements

Foremost, I would like to express my sincere gratitude to my supervisor, Prof. Kousuke Yakubo for his invaluable advice, support, and patience during my study. His guidance helped me in all the time of research and study, and his immense knowledge and enthusiasm have continuously encouraged me to pursue my research. My gratitude extends to Assoc. Prof. Yasuhiro Asano and Asst. Prof. Hideaki Obuse for their consultation throughout my study. I would also like to thank Dr. Shougo Mizutaka and Dr. Yuka Fujiki for all their insightful comments and suggestions. My sincere thanks goes to Ms. Kyoko Togashi for her assistance in daily life and her travel arrangements. I also thank my lab mates in Laboratory of Condensed Matter Physics for their kind help and support they have offered me at the lab. Finally, I am deeply grateful to my parents and my sister for their financial and emotional support.

Appendix A

Mathematical Supplement

A.1 Graph Theory

Definition A.1.1 (Undirected graph). A graph $G = (\mathcal{V}, \mathcal{E})$ is a set of two sets, $\mathcal{V} \neq \emptyset$ and \mathcal{E} . The elements of $\mathcal{V} = \{v_1, v_2, \dots, v_N\}$ are distinct ($v_i \neq v_j$ for $1 \leq i < j \leq N$) and are called vertices. The elements of $\mathcal{E} = \{e_1, e_2, \dots, e_M\}$ are distinct unordered pairs of distinct elements of N , i.e. $e_k = (i, j)$ for $i, j \in \mathcal{V}$ and $i \neq j$.

Definition A.1.2 (Subgraph). A subgraph of a graph $G = (\mathcal{V}, \mathcal{E})$ is a graph $G' = (\mathcal{V}', \mathcal{E}')$ where $\mathcal{V}' \subseteq \mathcal{V}$ and $\mathcal{E}' \subseteq \mathcal{E}$. If a subgraph G' contains all the edges in G connecting all the nodes in \mathcal{V}' , then G' is said to be *induced by* \mathcal{V}' and denoted as $G' = G[\mathcal{V}']$.

Definition A.1.3 (Walk). A walk $W(i, j)$ from node i to node j is an alternating sequence $W = (i, e_1, v_1, e_2, v_2, \dots, e_l, v_l, j)$ of nodes and edges that begins with i and ends with j , where $e_n = (v_{n-1}, v_n)$ for $n = 1, 2, \dots, l$. The length of a walk is defined by the number of edges in the sequence.

Definition A.1.4 (Trail). A trail from node i to node j is a walk from node i to node j in which no edge is repeated.

Definition A.1.5 (Path). A path from node i to node j is a walk from node i to node j in which no vertex is visited more than once.

Definition A.1.6 (Geodesic). A geodesic (shortest path) from node i to node j is a walk with minimal length from node i to node j .

Definition A.1.7 (Circuit). A circuit is a closed trail whose initial and final vertices coincide.

Definition A.1.8 (Cycle). A cycle is a closed walk $W = (v_0, v_1, v_2, \dots, v_l)$ in which $v_0 = v_l$, $l \geq 3$, and $v_i \neq v_j$ for $0 < i < j < l$. A cycle of length k is called k -cycle and is denoted by \mathbb{C}_k .

Definition A.1.9 (Connectedness). Two nodes i and j in a graph \mathcal{G} are connected if and only if there exists a path between nodes i and j . A graph is connected if all pairs of nodes are connected.

Definition A.1.10 (Tree). A tree is a connected acyclic graph. Alternatively, a tree is a connected graph with $M = N - 1$.

A.2 Calculus and Set Theory

Definition A.2.1 (upper bound). A set $A \subset \mathbb{R}$ is said to be *upper bounded* if there exists a number $c \in \mathbb{R}$ such that $a \leq c$ for all $a \in A$.

Proposition A.2.2. *If A is upper bounded, there exists $\alpha \in \mathbb{R}$ such that:*

- (i) $a \leq \alpha$ for $\forall a \in A$,
- (ii) *there exists $a_\varepsilon \in A$ such that $a_\varepsilon > \alpha - \varepsilon$ for $\forall \varepsilon > 0$.*

Definition A.2.3 (supremum). The smallest number which bounds a set $A \subset \mathbb{R}$ is called the *supremum* of A and denoted by $\sup_{a \in A} a$.

$$\sup A = \min\{c \in \mathbb{R} \mid \forall a \in A (a \leq c)\} \quad (\text{A.2.1})$$

Definition A.2.4 (lower bound). A set $A \subset \mathbb{R}$ is said to be *lower bounded* if there exists a number $c \in \mathbb{R}$ such that $a \geq c$ for all $a \in A$.

Proposition A.2.5. *If A is lower bounded, there exists $\alpha \in \mathbb{R}$ such that:*

- (i) $a \geq \alpha$ for $\forall a \in A$,
- (ii) *there exists $a_\varepsilon \in A$ such that $a_\varepsilon < \alpha + \varepsilon$ for $\forall \varepsilon > 0$.*

Definition A.2.6 (infimum). The greatest number which bounds a set $A \subset \mathbb{R}$ is called the *infimum* of A and denoted by $\inf_{a \in A} a$.

$$\inf A = \max\{c \in \mathbb{R} \mid \forall a \in A (c \leq a)\} \quad (\text{A.2.2})$$

Definition A.2.7 (limit superior). The *limit superior* of a sequence $\{a_n\}$ is defined by

$$\overline{\lim}_{n \rightarrow \infty} a_n := \lim_{n \rightarrow \infty} \left(\sup_{m \geq n} a_m \right). \quad (\text{A.2.3})$$

Definition A.2.8 (limit inferior). The *limit inferior* of a sequence $\{a_n\}$ is defined by

$$\lim_{n \rightarrow \infty} a_n := \lim_{n \rightarrow \infty} \left(\inf_{m \geq n} a_m \right). \quad (\text{A.2.4})$$

Definition A.2.9 (closure). The *closure* \overline{A} of a set A is the intersection of all the closed sets containing A .

Definition A.2.10 (interior). The *interior* $\text{int}A$ of a set A is the union of all the open sets contained in A .

Definition A.2.11 (boundary). The *boundary* $\text{Bd}A$ of a set A is defined by

$$\text{Bd}A = \overline{A} \setminus \text{int}A. \quad (\text{A.2.5})$$

Definition A.2.12 (dense). A set A is *dense* in B if $B \subset \overline{A}$, i.e. if there exist points of A arbitrarily close to every point in B .

Definition A.2.13 (compact). The *compact* set A is any collection of open sets which covers A has a finite subcollection that also covers A .

A.3 Metric Topology

Definition A.3.1 (metric space). A *metric space* is a pair of a set S and a function $\rho : S \times S \rightarrow [0, \infty)$ satisfying the following conditions:

- (i) $\rho(x, y) = 0 \iff x = y$
- (ii) $\rho(x, y) = \rho(y, x)$
- (iii) $\rho(x, z) \leq \rho(x, y) + \rho(y, z)$

for $x, y, z \in S$. The function ρ is called a *metric*.

For the following, let S be a metric space.

Definition A.3.2 (diameter). Let $A \subset S$. The *diameter* of A is then defined by

$$\text{diam } A = \sup\{\rho(x, y) \mid x, y \in A\}. \quad (\text{A.3.6})$$

Definition A.3.3 (distance). Let $A, B \subset S$ such that $A \neq \emptyset, B \neq \emptyset$. The distance between the two sets A and B is defined by

$$\text{dist}(A, B) = \inf\{\rho(x, y) \mid x \in A, y \in B\}. \quad (\text{A.3.7})$$

Definition A.3.4 (open ball). The *open ball* of center $x \in S$ and radius $r > 0$ is defined by

$$B(x, r) = \{y \in S \mid \rho(x, y) < r\}. \quad (\text{A.3.8})$$

Definition A.3.5 (closed ball). The *closed ball* of center $x \in S$ and radius $r > 0$ is defined by

$$\overline{B}(x, r) = \{y \in S \mid \rho(x, y) \leq r\}. \quad (\text{A.3.9})$$

Definition A.3.6 (δ -neighborhood). The δ -neighborhood A_δ of a set $A \subset S$ is the set of points within distance δ from A .

$$A_\delta = \{y \in S \mid \text{dist}(x, y) < \delta, \exists x \in A\} \quad (\text{A.3.10})$$

Definition A.3.7 (neighborhood). A set $A \subset S$ is a *neighborhood* of a point $x \in S$ if there exists some ball $B(x, r)$ centered at x and contained in A .

Definition A.3.8 (cover). A family \mathcal{U} of subsets of S *covers* a set $A \subset S$ if and only if A is contained in the union of \mathcal{U} , i.e.

$$A \subset \bigcup_i U_i \quad (\text{A.3.11})$$

for $U_i \in \mathcal{U}$.

Definition A.3.9 (δ -cover). A δ -cover of a set $A \subset S$ is a cover \mathcal{U} such that $0 < |U_i| \leq \delta$ for $\forall i$. We denote the number of elements in a δ -cover of A by $N_\delta(A)$.

Definition A.3.10 (hyperspace). The *hyperspace* $\mathbb{H}(S)$ for S is the collection of all nonempty compact subsets of S .

Definition A.3.11 (upper and lower box-counting dimensions). The *upper and lower box-counting dimensions* of a set $A \subset \mathbb{H}(S)$ are defined by

$$\underline{\dim}_B A = \lim_{\delta \rightarrow 0} \frac{\log N_\delta(A)}{-\log \delta}, \quad (\text{A.3.12})$$

$$\overline{\dim}_B A = \lim_{\delta \rightarrow 0} \frac{\log N_\delta(A)}{-\log \delta}. \quad (\text{A.3.13})$$

Definition A.3.12 (box-counting dimension). The *box-counting dimension* of a set $A \subset \mathbb{H}(S)$ is defined by

$$\dim_B A = \lim_{\delta \rightarrow 0} \frac{\log N_\delta(A)}{-\log \delta} \quad (\text{A.3.14})$$

if and only if the limit exists, i.e., $\underline{\dim}_B A = \overline{\dim}_B A$.

Definition A.3.12 is equivalent for any of the following:

- δ -cover of A with the smallest number of sets of diameter at most δ
- δ -cover of A with the smallest number of closed balls of radius δ
- δ -cover of A with the largest number of disjoint balls of radius δ with centers in A

A.4 Measure Theory

Definition A.4.1 (f -field). A collection \mathcal{A} of subsets of X is called f -field of X if the following conditions are satisfied:

- (i) $\emptyset \in \mathcal{A}$
- (ii) If $A \in \mathcal{A}$, then $A^c (= X \setminus A) \in \mathcal{A}$.
- (iii) If $A \in \mathcal{A}$ and $B \in \mathcal{A}$, then $A \cup B \in \mathcal{A}$

Definition A.4.2 (σ -field). A collection \mathcal{A} of subsets of X is called σ -field if \mathcal{A} is f -field of X such that if $A_i \in \mathcal{A}$ ($i \geq 1$), then $\bigcup_{i=1}^{\infty} A_i \in \mathcal{A}$.

Definition A.4.3 (measurable space). A pair (X, \mathcal{F}) of a set X and a σ -filed \mathcal{F} on X is called a *measurable space*.

Definition A.4.4 (measure). A set function μ on a σ -filed \mathcal{F} is a *measure* on (X, \mathcal{F}) if and only if

- (i) $\mu(\emptyset) = 0$, $0 \leq \mu(A) \leq \infty$ for $A \in \mathcal{F}$ (non-negativity)
- (ii) If $A_i \in \mathcal{F}$ ($i = 1, 2, \dots$) and $A_i \cap A_j = \emptyset$ ($i \neq j$), then

$$\mu\left(\bigcup_{i=1}^{\infty} A_i\right) = \sum_{i=1}^{\infty} \mu(A_i). \quad (\text{A.4.15})$$

Definition A.4.5 (measure space). A tuple (X, \mathcal{F}, μ) of a set X , a σ -filed \mathcal{F} on X , and a measure μ is called a *measure space*.

Proposition A.4.6. A measure space (X, \mathcal{F}, μ) possesses the following properties:

- (i) If $A_i, A_j \in \mathcal{F}$ and $A_i \subset A_j$, then $\mu(A_i) \leq \mu(A_j)$.

(ii) If $A_i \in \mathcal{F}$ ($1 \leq i \leq n$) and $A_i \cap A_j = \emptyset$ ($i \neq j$), then

$$\mu \left(\bigcup_{i=1}^n A_i \right) = \sum_{i=1}^n \mu(A_i). \quad (\text{A.4.16})$$

(iii) For $A_i \in \mathcal{F}$ ($i = 1, 2, \dots$),

$$\mu \left(\bigcup_{i=1}^{\infty} A_i \right) \leq \sum_{i=1}^{\infty} \mu(A_i). \quad (\text{A.4.17})$$

(iv) If $A_i \in \mathcal{F}$ ($i = 1, 2, \dots$) and $A_i \subset A_{i+1}$ ($i \geq 1$), then

$$\lim_{i \rightarrow \infty} \mu(A_i) = \mu \left(\bigcup_{i=1}^{\infty} A_i \right) \quad (\text{A.4.18})$$

(v) If $A_i \in \mathcal{F}$ ($i = 1, 2, \dots$), $\mu(A_i) < \infty$, and $A_i \supset A_{i+1}$ ($i \geq 1$), then

$$\lim_{i \rightarrow \infty} \mu(A_i) = \mu \left(\bigcap_{i=1}^{\infty} A_i \right) \quad (\text{A.4.19})$$

Definition A.4.7 (s -dimensional Hausdorff outer measure). Let us \mathcal{U}_δ be a δ -cover of a set A and define

$$\overline{\mathcal{H}}_\delta^s(A) = \inf_{\mathcal{U}_\delta} \sum_{U_i \in \mathcal{U}} (\text{diam } U_i)^s, \quad (\text{A.4.20})$$

where \mathcal{U}_δ is the set of all countable δ -covers \mathcal{U} of the set A . Then, the s -dimensional Hausdorff outer measure of a set A is defined by

$$\overline{\mathcal{H}}^s(A) = \lim_{\delta \rightarrow 0} \overline{\mathcal{H}}_\delta^s(A) = \sup_{\delta > 0} \overline{\mathcal{H}}_\delta^s(A). \quad (\text{A.4.21})$$

Proposition A.4.8. Let S and T be metric spaces with a metric ρ . Let $A \subset S$ and $f : A \rightarrow T$ be a Hölder mapping such that

$$\rho(f(x), f(y)) \leq c\rho(x, y)^\alpha \quad (\text{A.4.22})$$

for $x, y \in A$, constant $\alpha > 0$ and $c > 0$. Then,

$$\overline{\mathcal{H}}^{s/\alpha}(f(A)) \leq c^{s/\alpha} \overline{\mathcal{H}}^s(A). \quad (\text{A.4.23})$$

If f is a Lipschitz mapping ($\alpha = 1$), then

$$\overline{\mathcal{H}}^s(f(A)) \leq c^s \overline{\mathcal{H}}^s(A). \quad (\text{A.4.24})$$

Definition A.4.9 (Hausdorff dimension). Let S be a metric space and $A \subset S$, and suppose $\sup \emptyset = 0$. The Hausdorff dimension is defined by

$$\dim_H A = \inf \left\{ s \geq 0 \mid \overline{\mathcal{H}}^s(A) = 0 \right\} = \sup \left\{ s \mid \overline{\mathcal{H}}^s(A) = \infty \right\}. \quad (\text{A.4.25})$$

That is,

$$\overline{\mathcal{H}}^s(A) = \begin{cases} 0 & \text{if } s > \dim_H A \\ \infty & \text{if } 0 \leq s \leq \dim_H A \end{cases}. \quad (\text{A.4.26})$$

Appendix B

Algorithms for Fractal and Multifractal Analyses

In this chapter, we summarize some of the algorithms for fractal and multifractal analyses of complex networks. Sec.B.1 is devoted to introduce the algorithms for fractal analysis, namely the greedy coloring, random sequential burning, compact-box-burning, and maximum-excluded-mass-burning algorithms. Sec.B.2 introduces the sandbox algorithm for multifractal analysis, which we used in our main results.

B.1 Fractal Analysis

B.1.1 Greedy Coloring Algorithm

The greedy coloring algorithm is inspired by the fact that the problem of the box-covering of a graph can be mapped to the graph coloring problem^{*1}. To approximate the optimal box-covering of a graph G with an arbitrary box size l_B , the greedy coloring algorithm utilizes a dual network G' , whose nodes are connected if the shortest path distance in G is longer than or equal to l_B . We then conduct a graph coloring procedure, in which every node of G' is assigned a color while no adjacent nodes are labeled with identical color. The colors of nodes in G' will correspond to the boxes in G .

A simple implementation of the greedy coloring algorithm provided in [60] is as follows:

- (1) Prepare a two dimensional array c_{il_B} of size N by l_B^{\max} , which we store the colors of each node for each box size. l_B^{\max} denotes the maximum box size,

^{*1}The graph coloring problem is known to be NP hard[60].

which will be the diameter of a given network G .

- (2) Assign integer id numbers from 1 to N to all the nodes in the network G .
- (3) For each l_B , set color 0 for the node whose id number is 1.
- (4) From the id number 2 to N , repeat the following procedures:
 - (a) Compute the shortest path distance l_{ij} from the node whose id is i to all the nodes whose id is $j < i$.
 - (b) Repeat for each box size l_B from 1 to l_B^{\max} ,
 - (i) From all the unused colors $c_{jl_{ij}}$ for $j < i$ and $l_{ij} \geq l_B$, select one color and assign the color as c_{il_B} .

B.1.2 Random Sequential Burning Algorithm

The random sequential burning algorithm is one of the simplest box-covering algorithms proposed by Kim et al. in [61]. Though the algorithm fails to box-cover a given network with less boxes than the other algorithms[60], it returns a proper fractal scaling.

The procedures of the random sequential burning algorithm are as follows:

- (1) Mark all the nodes in a given network G as not burned.
- (2) Randomly select a seed node i from unburned nodes.
- (3) Conduct the breadth-first-search within the network to search for all the nodes j whose shortest path distance from the seed node i is less than l_B , i.e. $l_{ij} < l_B$.
- (4) Add all the nodes found in Step (3) to a new box and mark them as burned.
- (5) Repeat steps (2)-(4) until all the nodes are burned.

B.1.3 Compact-Box-Burning Algorithm

Originally proposed by Song et al. in [60], the compact-box-burning (CBB) algorithm is one of the most widely used algorithms for fractal analysis of networks. The central idea behind the CBB algorithm is to take the union of balls*2 for all the unburned nodes.

The steps of the CBB algorithm are as follows:

*2A ball $b(l_B)$ of size l_B is defined by a set of all the nodes whose shortest path distance from one another is less than l_B .

- (1) Generate a set C of all the unburned nodes. Let us call C the candidate set.
- (2) Select a random node i from the candidate set C and remove i from C .
- (3) Remove from C all nodes j whose shortest path distance from i is greater than or equal to l_B , i.e. $l_{ij} \geq l_B$.
- (4) Repeat steps (2) and (3) until the candidate set becomes empty.

B.1.4 Maximum-Excluded-Mass-Burning Algorithm

The algorithms we have so far introduced all result in disconnected boxes. That is, not all the nodes in a given box are connected to each other. Song et al. proposed the Maximum-Excluded-Mass-Burning (MEMB) algorithm to avoid disconnected boxes[60]. In the MEMB algorithm, the definition of a box is slightly modified as a set of nodes within a radius r_B from a center node. For consistency with the other algorithms, the box size of such a radius-based algorithm is defined as $l_B = 2r_B + 1$. The excluded mass which appears in the name of the MEMB algorithm is defined by the number of unburned nodes j whose shortest path distance from the center node i is $l_{ij} < r_B$.

The MEMB algorithm consists of two parts: the first part for selecting center nodes and the second part for assigning nodes to boxes. The procedures for the first part of the MEMB algorithm are as follows:

- (1) Set all the nodes in a given network as unburned and non-center.
- (2) Compute the excluded mass for each non-center node and select the node i with the maximum excluded mass as a new center.
- (3) Mark all nodes whose distance from the center node i is less than r_B as burned.
- (4) Repeat steps (2) and (3) until all the nodes are either burned or centers.

If we want only the number of boxes, we can simply finish the algorithm with the first part, as the number of center nodes is equivalent to the number of boxes.

The second part consists of the following steps:

- (1) For each center node, assign a box number from 1 to N_B , where N_B is the number of boxes.
- (2) Compute the so called central distance, which is defined by the shortest path distance from the nearest center, for each node.

- (3) Sort the non-center nodes in a list with an ascending order of central distances.
- (4) Assign to each non-center node i the box number of its neighbor with the shortest central distance. If there exist more than one nodes with the shortest central distance, select one of those at random. Remove the node i from the list.
- (5) Repeat step (4) until the list from step (3) is empty.

B.2 Multifractal Analysis

B.2.1 Sandbox Algorithm

Here, we introduce the sandbox algorithm which we used to numerically confirm our analytical form of mass exponents. The sandbox algorithm for the multifractal analysis in complex networks first appear in [45]. The improved version of the algorithm appears in [52]. The sandbox algorithm utilizes boxes of radius r centered at \tilde{N} randomly selected nodes. The "mass", or the sum of measures, of each box is computed and the mean mass at each radius r is used to calculate the mass exponents. The q -th moment $Z_q(r)$ required to compute the mass exponent is

$$Z_q(r) = \sum_{b_i \in \mathcal{B}(r)} \mu_{b_i}^q(r) \propto r^{\tau(q)}, \quad (\text{B.2.1})$$

where $\mathcal{B}(r)$ is a set of all the boxes which cover the given network and b_i is its element. For $r \ll L$, $Z_q(r)$ is approximated by

$$Z_q(r) \sim \langle \mu^{q-1}(r) \rangle = \frac{1}{\tilde{N}} \sum_{i=1}^{\tilde{N}} \left(\frac{M_i(r)}{N} \right)^{q-1}, \quad (\text{B.2.2})$$

where $M_i(r)$ denotes the mass of the box at the i -th center with radius r , i.e.

$$M_i(r) = \sum_{j=1}^N H(r - l_{ij}). \quad (\text{B.2.3})$$

l_{ij} is the distance between nodes i and j and $H(x)$ is the heaviside step function. Then, the mass exponent is obtained as follows:

$$\tau(q) = \frac{\log Z_q(r)}{\log r}. \quad (\text{B.2.4})$$

The procedures of the sandbox algorithm are as follows:

- (1) Randomly select a set of center nodes from a given network. The number of center nodes \tilde{N} is at most N .
- (2) Conduct the breadth-first search (BFS) from a center node until the maximum radius $r_{\max} (= \lceil L/2 \rceil)$ is reached. Store the number $n_i(r)$ of nodes at each distance $r (< r_{\max})$ from a center i .
- (3) Compute the mass of a subgraph of radius r , centered at node i by

$$M_i(r) = \sum_{r=0}^{r_{\max}} n_i(r). \quad (\text{B.2.5})$$

- (4) For each distortion factor q , calculate $[M_i(r)/N]^{q-1} (= [\mu_i(r)]^{q-1})$ of the mass.
- (5) Repeat steps (2)-(4) for all the center nodes.
- (6) Take the mean value $\left\langle [\mu_i(r)]^{q-1} \right\rangle_{i=1}^{\tilde{N}}$ of the $(q-1)$ -th powered mass.
- (7) Compute the mass exponent $\tau(q)$ for each q by conducting a linear regression of $\log \left\langle [\mu_i(r)]^{q-1} \right\rangle_{i=1}^{\tilde{N}}$ with regard to $\log r$.

Appendix C

The derivation of Eq.(6.28)

In Sec.6.3.1, we have used the relation Eq.(6.28). In this section, we show the derivation of the relation.

Let us begin from the case of $r = 1$. The number $n_1(k'|k)$ can be expressed as

$$n_1(k) = kP(k'|k) \quad (\text{C.0.1})$$

where $P(k'|k)$ is the conditional probability which describes the nearest-neighbor degree correlation. As we are concerned with uncorrelated networks, we have

$$P(k'|k) = \frac{k'P(k')}{\langle k \rangle}. \quad (\text{C.0.2})$$

By substituting Eq.(C.0.2) into (C.0.1), we obtain

$$n_1(k'|k) = \frac{kk'P(k')}{\langle k \rangle}. \quad (\text{C.0.3})$$

Next, let us consider the case of $r = 2$. $n_2(k'|k)$ is the count of nodes of degree k'' in the 1-shell which are connected to k' -degree nodes in the 2-shell, i.e.

$$\begin{aligned} n_2(k'|k) &= \sum_{k''} (k'' - 1)n_1(k''|k)P(k'|k'') \\ &= \sum_{k''} (k'' - 1) \frac{kk''P(k'')}{\langle k \rangle} \cdot \frac{k'P(k')}{\langle k \rangle} \\ &= \frac{kk'P(k')}{\langle k \rangle^2} \sum_{k''} k''(k'' - 1)P(k'') \\ &= \frac{kk'P(k')}{\langle k \rangle^2} (\langle k^2 \rangle - \langle k \rangle). \end{aligned} \quad (\text{C.0.4})$$

In the second line of (C.0.4), we substituted Eq.(C.0.2) and (C.0.3).

Similarly, for $3 \leq r \leq l$, we iteratively calculate

$$n_r(k'|k) = \sum_{k''} (k'' - 1) n_{r-1}(k''|k) P(k'|k'') \quad (\text{C.0.5})$$

using $n_2(k'|k)$. In the end, we attain

$$n_r(k'|k) = \frac{k k' P(k')}{\langle k \rangle^r} \left(\langle k^2 \rangle - \langle k \rangle \right)^{r-1}, \quad (\text{C.0.6})$$

and we have derived Eq.(6.28).

Appendix D

Multifractal Analysis of the Deterministic Model of Hierarchical Fractal Scale-free Networks

In this chapter, we report the numerical results of the multifractal analysis of the deterministic model of hierarchical fractal scale-free networks. We conducted the multifractal analyses of eighteen kinds of HFSFNs formed by the generators summarized in Table D.1. We present the q -th moments $Z_q(r)$, mass exponents $\tau(q)$, and the generalized dimensions D_q for all eighteen networks in Fig. D.1-D.3.

Table D.1: List of Generators

ID	structure	m_{gen}	κ	λ	γ	$D_f (= \alpha_0)$	α_{\min}
(a)	A diamond-shaped graph with two internal nodes and four boundary nodes.	4	2	2	3	2	1
(b)	A pentagonal graph with one internal node and five boundary nodes.	5	2	2	$1 + \frac{\log 5}{\log 2}$	$\frac{\log 5}{\log 2}$	$\frac{\log 5}{\log 2} - 1$
(c)	A hexagonal graph with two internal nodes and six boundary nodes.	6	2	3	$1 + \frac{\log 6}{\log 2}$	$\frac{\log 6}{\log 3}$	1
(d)	A linear chain of 5 nodes.	5	2	3	$1 + \frac{\log 5}{\log 2}$	$\frac{\log 5}{\log 3}$	$\frac{\log 5 - \log 2}{\log 3}$
(e)	A graph with 7 nodes arranged in a central horizontal chain with two vertical connections.	7	3	3	$1 + \frac{\log 7}{\log 3}$	$\frac{\log 7}{\log 3}$	$\frac{\log 7}{\log 3} - 1$
(f)	A graph with 9 nodes arranged in a central horizontal chain with three vertical connections.	9	4	3	$1 + \frac{\log 3}{\log 2}$	2	$2 \left(1 - \frac{\log 2}{\log 3} \right)$
(g)	A diamond-shaped graph with two internal nodes and four boundary nodes, similar to (a).	5	2	2	$1 + \frac{\log 5}{\log 2}$	$\frac{\log 5}{\log 2}$	$\frac{\log 5}{\log 2} - 1$
(h)	A graph with 6 nodes arranged in a central horizontal chain with two vertical connections.	6	3	2	$1 + \frac{\log 6}{\log 3}$	$\frac{\log 6}{\log 2}$	1
(i)	A diamond-shaped graph with two internal nodes and four boundary nodes, similar to (a).	6	3	2	$1 + \frac{\log 6}{\log 3}$	$\frac{\log 6}{\log 2}$	1
(j)	A pentagonal graph with one internal node and five boundary nodes, similar to (b).	7	2	2	$1 + \frac{\log 7}{\log 2}$	$\frac{\log 7}{\log 2}$	$\frac{\log 7}{\log 2} - 1$
(k)	A graph with 8 nodes arranged in a central horizontal chain with three vertical connections.	8	2	3	4	$\frac{3 \log 2}{\log 3}$	$\frac{2 \log 2}{\log 3}$
(l)	A graph with 9 nodes arranged in a central horizontal chain with three vertical connections.	9	2	3	$1 + \frac{2 \log 3}{\log 2}$	2	$2 - \frac{\log 2}{\log 3}$
(m)	A linear chain of 4 nodes.	4	2	2	3	2	1
(n)	A graph with 6 nodes arranged in a central horizontal chain with two vertical connections.	6	3	2	$1 + \frac{\log 6}{\log 3}$	$\frac{\log 6}{\log 2}$	1
(o)	A graph with 8 nodes arranged in a central horizontal chain with four vertical connections.	8	4	2	$\frac{5}{2}$	3	1
(p)	A diamond-shaped graph with two internal nodes and four boundary nodes, similar to (a).	6	2	2	$1 + \frac{\log 6}{\log 2}$	$\frac{\log 6}{\log 2}$	$\frac{\log 6}{\log 2} - 1$
(q)	A graph with 8 nodes arranged in a central horizontal chain with three vertical connections.	8	3	2	$1 + \frac{3 \log 2}{\log 3}$	3	$3 - \frac{\log 3}{\log 2}$
(r)	A graph with 8 nodes arranged in a central horizontal chain with four vertical connections.	8	4	2	$\frac{5}{2}$	3	1

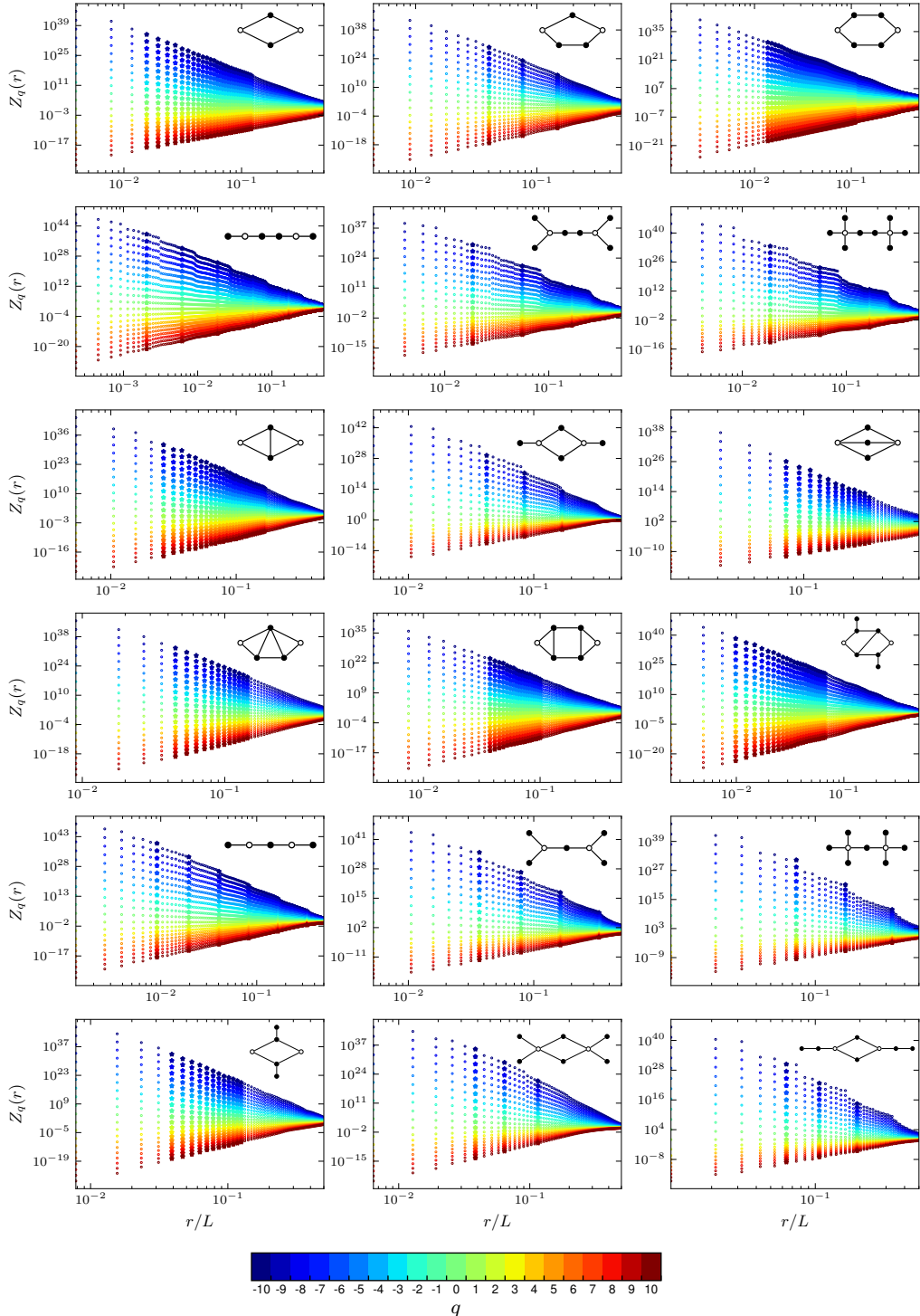


Figure D.1: The q -th moments of various HFSFNs.

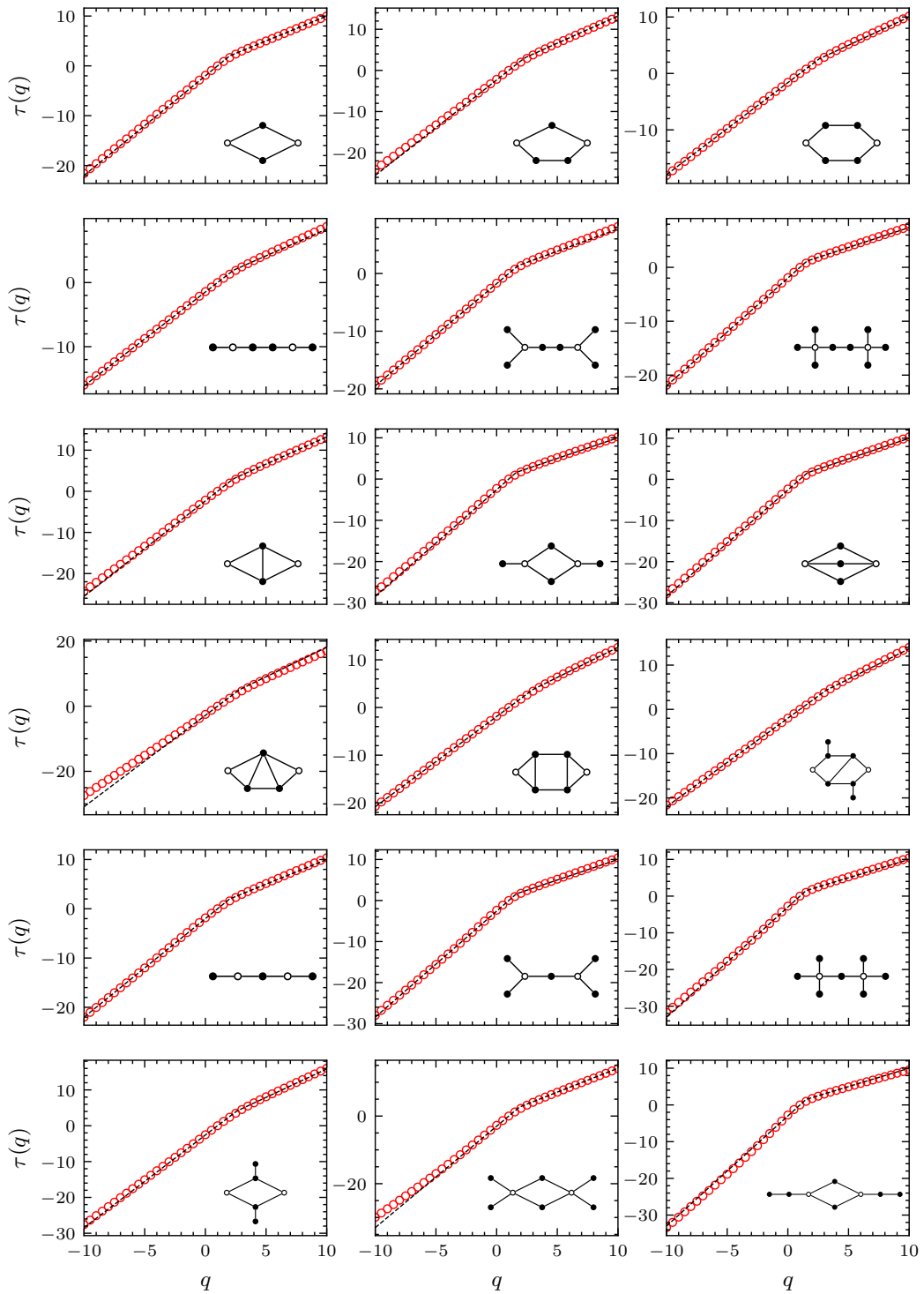


Figure D.2: The mass exponents $\tau(q)$ of various HFSFNs.

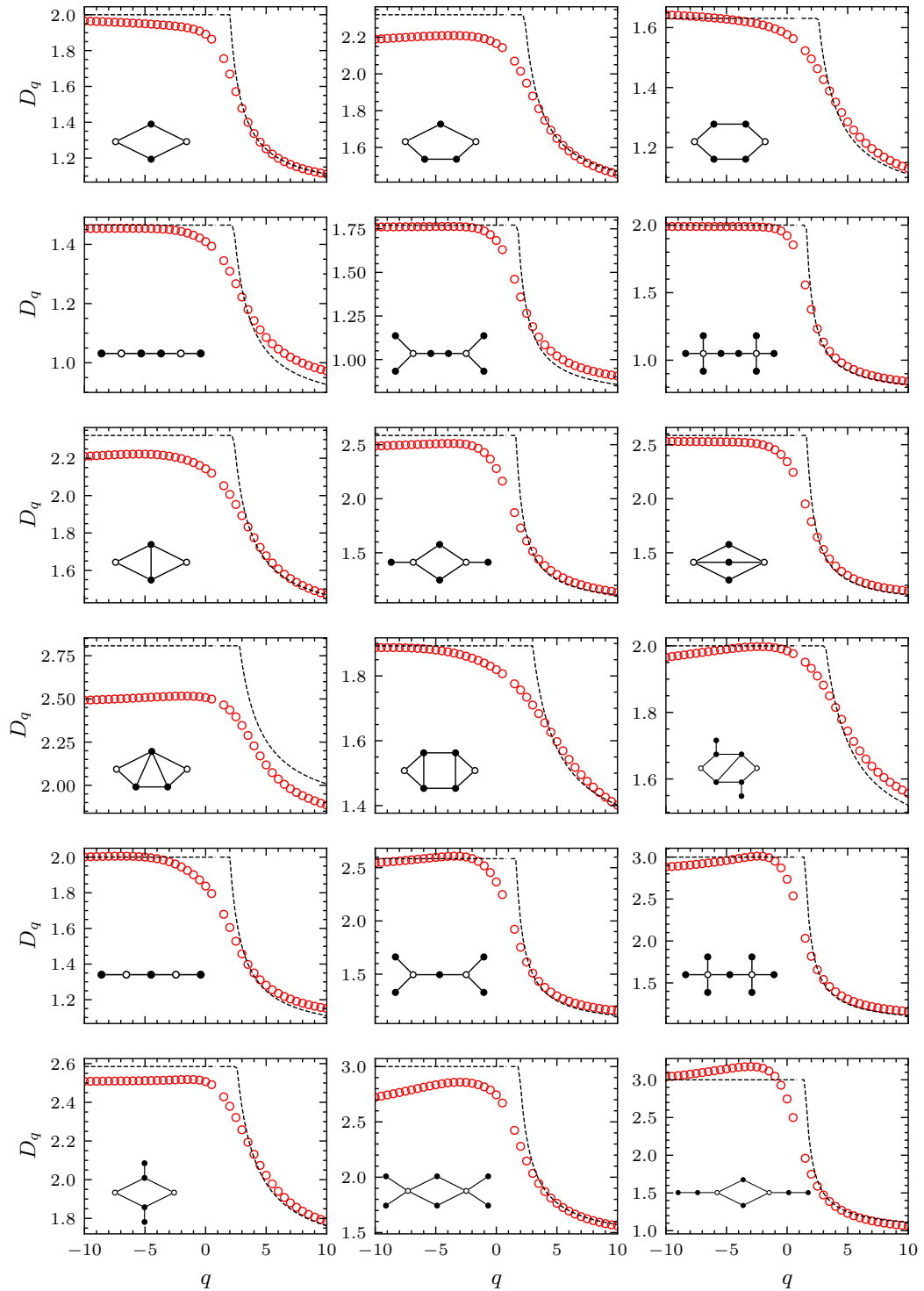


Figure D.3: The generalized dimension D_q of various HFSFNs.

References

- [1] R. Albert and A.-L. Barabási, Rev. Mod. Phys. **74**, 47 (2002).
- [2] M. E. J. Newman, SIAM Rev. **45**, 167 (2003).
- [3] *Handbook of graphs and networks: from the genome to the internet*, 1st ed (Wiley-VCH, Weinheim, 2003).
- [4] R. Cohen and S. Havlin, *Complex networks: structure, robustness and function* (Cambridge University Press, Cambridge, 2010).
- [5] 増田直紀, 今野紀雄, *複雑ネットワーク: 基礎から応用まで*, Japanese (近代科学社, 東京, 2010).
- [6] 矢久保考介, *複雑ネットワークとその構造*, Japanese (共立出版, 東京, 2013).
- [7] M. Newman, *Networks*, 2nd ed. (Oxford University Press, London, England, July 2018).
- [8] A.-L. Barabási and R. Albert, Science **286**, 509 (1999).
- [9] D. J. Watts and S. H. Strogatz, Nature **393**, 440 (1998).
- [10] S. Banerjee, S. B. Mallick, and I. Bose, Int. J. Mod. Phys. C **15**, 1075 (2004).
- [11] E. M. Bollt and D. ben-Avraham, arXiv:0409465 (2004).
- [12] I. Simonsen, K. Astrup Eriksen, S. Maslov, and K. Sneppen, Phys. A **336**, 163 (2004).
- [13] R. Pastor-Satorras and A. Vespignani, Phys. Rev. E **63**, 066117 (2001).
- [14] V. M. Eguíluz and K. Klemm, Phys. Rev. Lett. **89**, 108701 (2002).
- [15] M. Boguñá and R. Pastor-Satorras, Phys. Rev. E **66**, 047104 (2002).
- [16] M. Boguñá, R. Pastor-Satorras, and A. Vespignani, Phys. Rev. Lett. **90**, 028701 (2003).
- [17] A. Arenas, A. Díaz-Guilera, and C. J. Pérez-Vicente, Phys. Rev. Lett. **96**, 114102 (2006).
- [18] A. Arenas and A. Díaz-Guilera, Eur. Phys. J. Spec. Top. **143**, 19 (2007).

- [19] A. Arenas, A. Díaz-Guilera, J. Kurths, Y. Moreno, and C. Zhou, Phys. Rep. **469**, 93 (2008).
- [20] J. Gómez-Gardeñes, Y. Moreno, and A. Arenas, Phys. Rev. Lett. **98**, 034101 (2007).
- [21] G. X. Qi, H. B. Huang, L. Chen, H. J. Wang, and C. K. Shen, Europhys. Lett. **82**, 38003 (2008).
- [22] F. Dörfler and F. Bullo, Automatica **50**, 1539 (2014).
- [23] F. C. Santos and J. M. Pacheco, Phys. Rev. Lett. **95**, 098104 (2005).
- [24] F. C. Santos, J. M. Pacheco, and T. Lenaerts, PNAS **103**, 3490 (2006).
- [25] G. Szabó and G. Fáth, Phys. Rep. **446**, 97 (2007).
- [26] F. C. Santos and J. M. Pacheco, J. Evol. Bio. **19**, 726 (2006).
- [27] C. Song, S. Havlin, and H. A. Makse, Nature **433**, 392 (2005).
- [28] C. Song, S. Havlin, and H. A. Makse, Nat. Phys. **2**, 275 (2006).
- [29] T. Hasegawa and K. Nemoto, Phys. Rev. E **88**, 062807 (2013).
- [30] M. Á. Serrano, D. Krioukov, and M. Boguñá, Phys. Rev. Lett. **106**, 048701 (2011).
- [31] H. D. Rozenfeld, L. K. Gallos, C. Song, and H. A. Makse, arXiv:0808.2206 (2008).
- [32] E. Rosenberg, *Fractal dimensions of networks* (Springer International Publishing, Cham, 2020).
- [33] T. Wen and K. H. Cheong, Inf. Fusion **73**, 87 (2021).
- [34] P. T. Kovács, M. Nagy, and R. Molontay, Appl. Netw. Sci. **6**, 73 (2021).
- [35] T. Akiba, K. Nakamura, and T. Takaguchi, arXiv:1609.07994 (2016).
- [36] L. Gou, B. Wei, R. Sadiq, Y. Sadiq, and Y. Deng, PLoS One **11**, e0146896 (2016).
- [37] T. Wen, S. Duan, and W. Jiang, Commun. Nonlinear Sci. **78**, 104867 (2019).
- [38] S. Furuya and K. Yakubo, Phys. Rev. E **84**, 036118 (2011).
- [39] D.-L. Wang, Z.-G. Yu, and V. Anh, Chin. Phys. B **21**, 080504 (2012).
- [40] B. B. Mandelbrot, J. Fluid Mech. **62**, 331 (1974).
- [41] G. Paladin and A. Vulpiani, Phys. Rep. **156**, 147 (1987).
- [42] T. Nakayama and K. Yakubo, *Fractal concepts in condensed matter physics*, Vol. 140, Springer Series in Solid-State Sciences (Springer Berlin Heidelberg, Berlin, Heidelberg, 2003).

- [43] P. Meakin, H. E. Stanley, A. Coniglio, and T. A. Witten, Phys. Rev. A **32**, 2364 (1985).
- [44] H. E. Stanley and P. Meakin, Nature **335**, 405 (1988).
- [45] J.-L. Liu, Z.-G. Yu, and V. Anh, Chaos **25**, 023103 (2015).
- [46] E. Maiorino, L. Livi, A. Giuliani, A. Sadeghian, and A. Rizzi, Phys. A **428**, 302 (2015).
- [47] Y.-Q. Song, J.-L. Liu, Z.-G. Yu, and B.-G. Li, Sci. Rep. **5**, 17628 (2015).
- [48] S. Rendón de la Torre, J. Kalda, R. Kitt, and J. Engelbrecht, Eur. Phys. J. B **90**, 234 (2017).
- [49] E. Rosenberg, Phys. Lett. A **381**, 2222 (2017).
- [50] Y. Xue and P. Bogdan, Sci. Rep. **7**, 7487 (2017).
- [51] E. Rosenberg, Phys. A **511**, 1 (2018).
- [52] Y. Ding, J.-L. Liu, X. Li, Y.-C. Tian, and Z.-G. Yu, Phys. Rev. E **103**, 043303 (2021).
- [53] X. Xiao, H. Chen, and P. Bogdan, Sci. Rep. **11**, 22964 (2021).
- [54] A.-L. Barabási and M. Pósfai, *Network science* (Cambridge University Press, Cambridge, United Kingdom, 2016).
- [55] V. Latora, V. Nicosia, and G. Russo, *Complex networks: principles, methods and applications* (Cambridge University Press, Cambridge, 2017).
- [56] G. Chartrand and P. Zhang, *A first course in graph theory*, Dover books on mathematics (Dover Publications, 2012).
- [57] I. de Sola Pool and M. Kochen, Soc. Networks **1**, 5 (1978).
- [58] S. Milgram, Psychology Today **2**, 61 (1967).
- [59] *Fractals and disordered systems*, edited by A. Bunde and S. Havlin (Springer Berlin Heidelberg, 1996).
- [60] C. Song, L. K. Gallos, S. Havlin, and H. A. Makse, J. Stat. Mech. **2007**, P03006 (2007).
- [61] J. S. Kim, K.-I. Goh, B. Kahng, and D. Kim, Chaos **17**, 026116 (2007).
- [62] L. Gao, Y. Hu, and Z. Di, Phys. Rev. E **78**, 046109 (2008).
- [63] C. M. Schneider, T. A. Kesselring, J. S. Andrade, and H. J. Herrmann, Phys. Rev. E **86**, 016707 (2012).
- [64] L. K. Gallos, C. Song, and H. A. Makse, Phys. A **386**, 686 (2007).
- [65] H. D. Rozenfeld, S. Havlin, and D. ben-Avraham, New J. Phys. **9**, 175 (2007).

- [66] K. Yakubo and Y. Fujiki, arXiv:2109.00703 (2021).
- [67] 北原 岳哉, “フラクタル・スケールフリー・ネットワークに対する一般的な数理モデル”, Japanese, 卒業論文 (北海道大学工学部, 2020).
- [68] 宮崎 平太, “一般化フラクタル・スケールフリー・ネットワークに対する2ジエネレーター・モデル”, Japanese, 修士論文 (北海道大学大学院工学院, 2021).
- [69] M. E. J. Newman, S. H. Strogatz, and D. J. Watts, Phys. Rev. E **64**, 026118 (2001).
- [70] P. Bialas and A. K. Ole, Phys. Rev. E **77**, 036124 (2008).
- [71] B. Bollobás, *Random graphs*, 2nd ed., Cambridge Studies in Advanced Mathematics (Cambridge University Press, 2001).
- [72] M. Molloy and B. Reed, Random Struct. Algor. **6**, 161 (1995).
- [73] M. Molloy and B. Reed, Comb. Prob. Comput. **7**, 295 (1998).
- [74] M. Janssen, Phys. Rep. **295**, 1 (1998).
- [75] B.-G. Li, Z.-G. Yu, and Y. Zhou, J. Stat. Mech. **2014**, P02020 (2014).
- [76] P. Pavón-Domínguez, A. B. Ariza-Villaverde, A. Rincón-Casado, E. Gutiérrez de Ravé, and F. J. Jiménez-Hornero, Comp. Environ. Urban **64**, 229 (2017).
- [77] H. Zhang, D. Wei, Y. Hu, X. Lan, and Y. Deng, Commun. Nonlinear Sci. **35**, 97 (2016).
- [78] W. Zheng, Z. Zhang, and Y. Deng, Europhys. Lett. **119**, 66006 (2017).
- [79] J.-L. Liu, J. Wang, Z.-G. Yu, and X.-H. Xie, Sci. Rep. **7**, 45588 (2017).
- [80] Y. Fujiki and K. Yakubo, Phys. Rev. E **101**, 032308 (2020).